AMMRC TR 80-18

CONSERVATION

CERAMIC LIFE PREDICTION PARAMETERS

REPORT FOR THE PERIOD
JANUARY 1, 1977—MARCH 31, 1980

R. K. Govila
Ceramic Materials Department
Scientific Research Staff
Ford Motor Company
Dearborn, Michigan

Date Published—May, 1980

Prepared for
ARMY MATERIALS AND MECHANICS RESEARCH CENTER
Watertown, Massachusetts 02172

Contract No. DAAG-46-77-C-0028

U. S. DEPARTMENT OF ENERGY

Division of Transportation Energy Conservation

The findings in this report are not to be construed as an official Department of the Army unless so designated by other authorized documents.

Mention of any trade names or manufacturers in this report shall not be construed as advertising nor as an official indorsement or approval of such products or companies by the United States Government.

Available from

National Technical Information Service
U.S. Department of Commerce
5285 Port Royal Road
Springfield, Virginia 22161

Price: Printed Copy
Microfiche

CERAMIC LIFE PREDICTION PARAMETERS

REPORT FOR THE PERIOD
JANUARY 1, 1977—MARCH 31, 1980

R. K. Govila
Ceramic Materials Department
Scientific Research Staff
Ford Motor Company
Dearborn, Michigan

Date Published—May, 1980

Prepared for
ARMY MATERIALS AND MECHANICS RESEARCH CENTER
Watertown, Massachusetts 02172

Contract No. DAAG-46-77-C-0028

U.S. DEPARTMENT OF ENERGY

Office of the Assistant Secretary for Conservation and Solar Applications
Division of Transportation Energy Conservation

FOREWORD

This report presents the complete work done during the period January 1, 1977-March 31, 1980, Phase I part of the program, "Methodology For Ceramic Life Prediction," initiated by the Energy Research and Development Administration (ERDA), now Department of Energy (DOE), and monitored by the Army Materials and Mechanics Research Center, under Contract Number DAAG-46-77-C-0028. This work was necessary in formulating a methodology for ceramic life prediction using the material property characterization data so that ceramic materials can be used safely in high temperature structural applications.

The principal investigator of this program was Dr. R. K. Govila, Ford Motor Company, and the technical monitor was Dr. E. M. Lenoe, AMMRC. The author is thankful to R. Elder for doing the tensile stress rupture testing, and to R. Goss for doing SEM work. Thanks are due to Drs. E. M. Lenoe and R. N. Katz, AMMRC for suggestions from time-to-time in carrying out the program. Finally, it is a pleasure to thank Mr. A. F. McLean, Manager, Ceramic Materials Department, Ford Motor Company, for careful reading and constructive criticism of the report.

ABSTRACT

This program consisted of a basic study using two potential high temperature ceramic materials, hot-pressed silicon nitride, NC-132 (NORTON), and hot-pressed silicon nitride made with 3.5 wt. percent MgO (Ford material) to establish a statistical strength data base for fast fracture as well as for the presence of subcritical crack growth. The Weibull characteristic strength and modulus were determined. Among the fracture mechanics approach, the primary experimental techniques were double-torsion and indentation-induced flaw methods to determine the relationship between crack velocity, V, and stress intensity, K, during subcritical crack growth for NC-132 Si_3N_4.

The subcritical crack growth exponent 'n' was determined using flexural stress and strain rate methods and stress rupture methods, and showed a wide scatter in magnitude. When all the relevant life prediction parameters such as inherent flaw size, strength, critical stress intensity factor, and K-V relationship for slow crack growth are known, an estimate of time-to-failure for a given applied stress, temperature and environment can be made using the numerical relationships outlined by Evans and Wiederhorn earlier. Care should be taken in selecting the appropriate parameters since these parameters are a function of evaluation technique, otherwise the predicted time-to-failure will show a large variation.

Uniaxial tensile stress-rupture testing of NC-132 Si_3N_4 was investigated at 1000°, 1200°, and 1300°C, in air at various applied stress levels and the corresponding times-to-failure were measured. All of these data are used to assess parameters for use in confirmation studies of ceramic component life prediction experiments.

TABLE OF CONTENTS

1. INTRODUCTION

The use of ceramic materials for structural, high temperature, engineering components is being investigated for a number of applications, in particular, heat engines such as the gas turbine and diesel. There are at least two unusual characteristics with respect to the strength of brittle ceramics. The first is that the material is inductile (macroscopically) and its strength is controlled by the largest inherent microcrack or flaw in a given stress field; also, because there is typically a distribution of such flaws, there is a resulting scatter in material strength. The second is that inherent flaws within the material can exhibit the phenomenon of slow (subcritical) crack growth (SCG) under load at high temperature, implying that the strength is time dependent. As a result, one of the most critical factors in the structural application of ceramics is the ability to predict the reliability of a ceramic component as well as its useful life. The useful life of a component under an applied stress is usually referred to as "Lifetime Reliability" and basically involves determining statistical times to failure at a given temperature.

In the past, lack of sufficient data on high strength ceramics has been a major problem in designing turbine engine ceramic components subjected to high temperature deformation. Therefore, this program consisted of a basic study using two potential high temperature, high strength ceramic materials, namely, hot-pressed silicon nitride NC-132 (NORTON) and hot-pressed silicon nitride made with 3.5 wt. percent MgO (Ford material known as FHPSN) to generate a statistical data base for a detailed strength characterization especially related to fast fracture and to the presence of SCG. These materials are judged to be fairly representative of future sintered silicon nitrides now under development for complex-shaped engine components.

An overall idealized program to develop ceramic life prediction methodology is shown in the form of a flow chart in Fig. 1, and entails material characterization including the two parameter Weibull (volume) and fracture mechanics approaches. It further entails the development of a theoretical analysis to predict lifetime reliability and its application to selected examples for correlation. If a correlation does not occur, then the approaches should be re-examined including materials characterization (raw data and data representation), development of theoretical analysis, and the validity of testing models. The items marked with a plus in Fig. 1 are being investigated under Contract No. DAAG-46-77-C-0028 for Norton NC-132 hot-pressed silicon nitride, which is probably the most mature turbine ceramic currently commercially available.

In this study, an effort has been made to determine NC-132 Si_3N_4 parameters usually associated with life prediction. In particular, the various material parameters are:

(i) Single value Weibull characteristic strength, σ_o, and modulus, m.

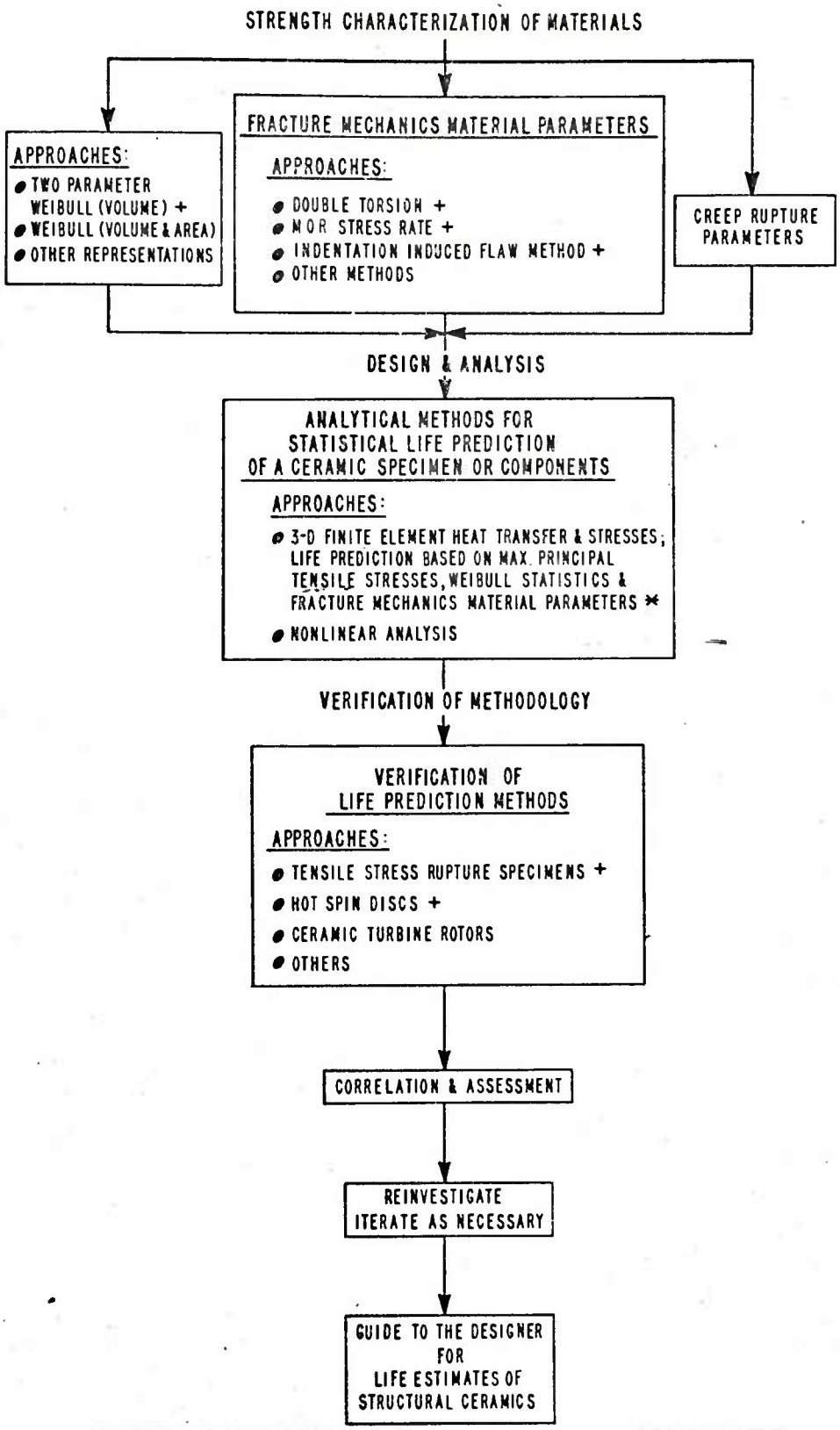

Fig. 1 Ceramic Life Prediction Methodology

+ - CURRENTLY FUNDED UNDER DOE CONTRACT DAAG 46-77-C-0028
✱ - PERFORMED UNDER CONTRACT DAAG 46-71-C-0162

(ii) Estimate of inherent flaw size, a_o, critical stress intensity factor, K_{IC}, for catastrophic failure and variation of stress intensity factor, K_I, with temperature.

(iii) Crack velocity, V, and the corresponding stress intensity, K_I, for SCG and the associated parameters A and n.

Furthermore, it should be noted that the parameters K, V, and n can be determined by several different methods as illustrated in this study, and the quantitative values obtained often differ considerably resulting in a wide scatter in predicted life. Therefore, care should be taken in choosing the appropriate data base in order to determine the ceramic component life.

Finally, a significant and unique part of this investigation involved the design, fabrication, and testing of a large number of tensile specimens in uniaxial tensile stress-rupture mode at various applied stresses in the temperature range 1000°-1300°C. Such results can be used as a first measure for verification of the analytically obtained life prediction estimates.

It is pointed out that the focus of the current program was the accumulation of the experimental data which is a long-lead item. It cannot be over-emphasized that a large, sound data base is needed as the "hard evidence" to form and validate any guidelines for a ceramic life prediction methodology. Furthermore, validation has been sought for more than one type of stress field. This study uses tensile stress-rupture testing with every effort for a uniaxial stress field. Parallel work now underway will entail spinning discs with a biaxial stress field, more representative of a ceramic turbine rotor.

2. FLEXURAL STRENGTH, STRESS RATE AND STRESS RUPTURE MEASUREMENTS

Considerable time, care and effort have been spent in obtaining a statistical strength data base for NC-132 Si_3N_4 and 3.5% MgO FHPSN. All measurements were made using the 1/4-point, 4-point bend test because of simplicity and relatively inexpensive nature of the test compared to other tests, such as uniaxial tension. Flexural strengths were measured as a function of temperature (20-1400°C) and stressing rate. Limited flexural stress rupture measurements were also made.

2.1 Materials, Specimen Preparation, and Testing

Three 6 in. x 6 in. billets of hot-pressed silicon nitride, commercially known as NC-132, were obtained from the Norton Co., two of which were 1 in. thick and the third one was 0.75 in. thick. Test specimens (MOR) of dimensions 1.25 in. long x 0.25 in. wide x 0.125 in. thick were cut such that the tensile face was perpendicular to the hot-pressing direction (strong direction) as shown in Fig. A_1, appendix. The machining process is described in Table A-1, appendix. The Ford HPSN MOR test specimens were cut from the tapered hubs of duodensity Si_3N_4 rotors, representative of those fabricated during 1977. They were fabricated using Kawacki Beryllium Company CP85 Si_3N_4 powder and 3.5 wt. percent MgO as a sintering aid. The mixture was hot-pressed at a pressure of 1000 psi and at a temperature of 1700°C with a hold of 3 hrs., following a standardized procedure. Material for this program came from good quality hubs of rotors which had been rejected due to defects within the RBSN Si_3N_4 blade zone and which were therefore unacceptable for rig or engine testing. After removal of the blade material, standard MOR bars were cut from the remaining 3.5 percent MgO FHPSN hub material in a similar fashion to that shown in Fig. A_1. For most of the test temperatures, bars cut from 6 rotors were used. Specimens from a seventh rotor were added for the 1204°C tests.

All specimens were tested in four-point bending in an Instron machine (model 1125) using a specially built self-aligning ceramic fixture, Fig. A_2, appendix, made from hot-pressed SiC. The outer and inner knife edges were 0.75 in. and 0.38 in. span, respectively. The high temperature bend tests were conducted in air in an Instron machine equipped with a rapid temperature furnace (CM Inc., High Temperature Furnaces, Bloomfield, N.J.). Initially, bend bar specimens of both types of material (hot-pressed silicon nitride NC-132 and 3.5% MgO FHPSN) were tested in bending at a crosshead speed of 0.02 in./min. (0.5 mm/min). Bend bar (MOR) specimens were also tested at higher temperatures using three additional crosshead speeds as shown in Tables 1 and 2 for both types of material, NC-132 and FHPSN, respectively.

2.2 Results and Discussion

Flexural Strength Measurements

In order to generate a statistical data base, a large number of MOR bend bar specimens (425 for NC-132 Si_3N_4 and 349 for 3.5% MgO FHPSN) were tested in bending as a function of temperature and machine head speed. Complete raw data for the two materials are given in the Appendix (Tables A-2 and A-3). Assuming a two-parameter Weibull distribution to be representative of the test results, a maximum likelihood

TABLE 1

(MOR) STRESS DATA OF NORTON NC-132 HPSN

Temp.	Head Speed mm/min	Avg. Stress Rate MPa/min	Characteristic (MOR) Strength MPa	Weibull Modulus m	No. Of Samples
Room	0.5	1,873	787 (748-828)	6.5 (4.9-8.0)	30
704°C	0.5	2,093	730 (685-778)	8.0 (5.1-10.3)	15
	0.0005	1.8	731 (607-901)	6.0 (2.1-8.7)	5
871°C	5.0	19,737	728 (708-750)	11.6 (8.7-14.1)	30
	0.5	2,003	759 (732-788)	9.2 (6.9-11.2)	30
	0.005	21.9	727 (697-759)	7.9 (5.9-9.7)	30
	0.0005	1.8	818 (719-947)	8.5 (3.1-12.5)	5
1038°C	5.0	17,100	725 (697-754)	12.6 (8.1-16.4)	15
	0.5	1,880	725 (711-740)	16.5 (12.4-20.2)	30
	0.005	22.5	679 (664-695)	14.5 (10.8-17.7)	30
	0.0005	1.5	666 (596-756)	9.9 (3.6-14.5)	5
1204°C	5.0	18,117	665 (648-683)	13.0 (9.8-15.9)	30
	0.5	1,837	688 (680-697)	25.8 (19.4-31.5)	30
	0.05	163	609 (593-626)	12.2 (9.2-14.9)	30
	0.005	21.1	545 (533-556)	16.0 (12.0-19.5)	30
	0.0005	.8	484 (421-566)	8.0 (2.9-11.7)	5
1371°C	5.0	11,910	411 (402-421)	14.3 (10.7-17.5)	30
	0.5	959	363 (347-381)	7.0 (5.2-8.5)	30
	0.05	91.0	313 (299-327)	11.2 (7.2-14.6)	15

Note: Numbers in parenthesis represent 90% confidence bands

TABLE 2

(MOR) STRESS DATA OF FORD 3.5%MgO HPSN

Temp.	Head Speed mm/min	Avg. Stress Rate MPa/min	Characteristic (MOR) Strength MPa	Weibull Modulus m	No. Of Samples
Room	0.5	1,973	668 (646-691)	10.0 (7.5-12.2)	30
704°C	0.5	1,857	697 (662-735)	6.4 (4.8-7.8)	30
871°C	0.5	1,766	591 (552-634)	4.8 (3.6-5.9)	30
	0.05	207	599 (556-647)	6.7 (4.3-8.7)	15
	0.005	20	579 (544-617)	5.3 (4.0-6.5)	30
1038°C	0.5	1,708	548 (529-569)	9.2 (6.9-11.2)	30
	0.05	198	596 (572-621)	15.9 (8.8-21.5)	10
	0.005	19	531 (517-546)	12.4 (9.3-15.1)	30
1204°C	0.5	1,576	481 (455-509)	5.5 (4.2-6.6)	35
	0.05	172	439 (412-467)	4.9 (3.8-5.9)	35
	0.005	17.5	368 (356-381)	9.0 (6.9-10.8)	35
1371°C	5.0	7,224	324 (276-388)	6.9 (2.5-10.2)	5
	0.5	558	254 (244-266)	7.9 (5.9-9.7)	29
	0.05	43	213 (194-236)	12.0 (4.3-17.6)	5

Note: Numbers in parenthesis represent 90% confidence bands

estimator (MLE) method of statistical analysis was used to determine the Weibull modulus, m, and the characteristic (MOR) strength, σ_θ, using a Fortran computer program [1]. The characteristic (MOR) strength, σ_θ, refers to that value of fracture strength at which 63.2 percent of the population (specimens) will fail and the Weibull modulus, m, is a measure of shape and distribution of flaws in the material. The flexural strength results as a function of temperature and stressing rate are shown in Tables 1 and 2 for both materials.

Flexural Stress Rate

The presence of subcritical crack growth (SCG) in ceramic materials is believed to be described by the functional relationship between crack velocity, V, and stress intensity factor, K_I, as follows:

$$V = A\, K_I^n \tag{1}$$

where A and n are constants. Flexural stress rate testing [2,3] is one simple method for determining the exponent 'n', and utilizes the material's fracture strength as a function of stressing rate as shown below for a given temperature and environment:

$$\log \sigma_F = \log D + \frac{1}{n+1} \log \dot{\sigma}_F \tag{2}$$

where σ_F is the fracture stress at a stressing rate $\dot{\sigma}_F$ and D is a constant. A log-log plot of σ_F vs stressing rate $\dot{\sigma}_F$ would yield a linear relationship (straight line) and from the slope of the plot, the parameter 'n' can be determined. The temperature dependence of the fracture stress for uncracked (virgin) samples of NC-132 Si_3N_4 as a function of stressing rate on a log-log scale is shown in Fig. 2. Up to about 1040°C, the fracture stress, σ_F, is almost independent of the stressing rate $\dot{\sigma}_F$, suggesting no evidence of SCG. At higher temperatures, the log-log plot showed a clear deviation from the horizontal line indicating presence of SCG, and at 1204 and 1371°C the values of 'n' were 19.1 and 17.2, respectively. Typical fracture surfaces at 1204°C corresponding to the three stress rates (inclined portion of log-log plot) are shown in Fig. 3, and only at the lowest stress rate was the presence of SCG observed, Fig. 3a. Metallographic examination of fracture surfaces for specimens tested at 1371°C (Fig. 2) showed the presence of SCG. It should be noted that the curves at 1204°C and 1371°C are essentially parallel, and the value of 'n' is independent of temperature in the range 1200-1400°C for a given environment. Similar behavior has been observed by Lange [3] in HS-130 Si_3N_4 (specimen configuration, weak direction, Fig. A_1 in appendix), and the values of 'n' determined were 12.7, 10.6, and 11.2 at 1200, 1300, and 1400°C, respectively.

The 3.5% MgO FHPSN material showed similar stress rate dependence, Fig. 4, as the NC-132 Si_3N_4, and the values of 'n' were found to be 15.8 and 11.2 at 1204 and 1371°C, respectively. Examination of the fracture faces of test specimen revealed significant presence of SCG at temperatures of 1200°C.

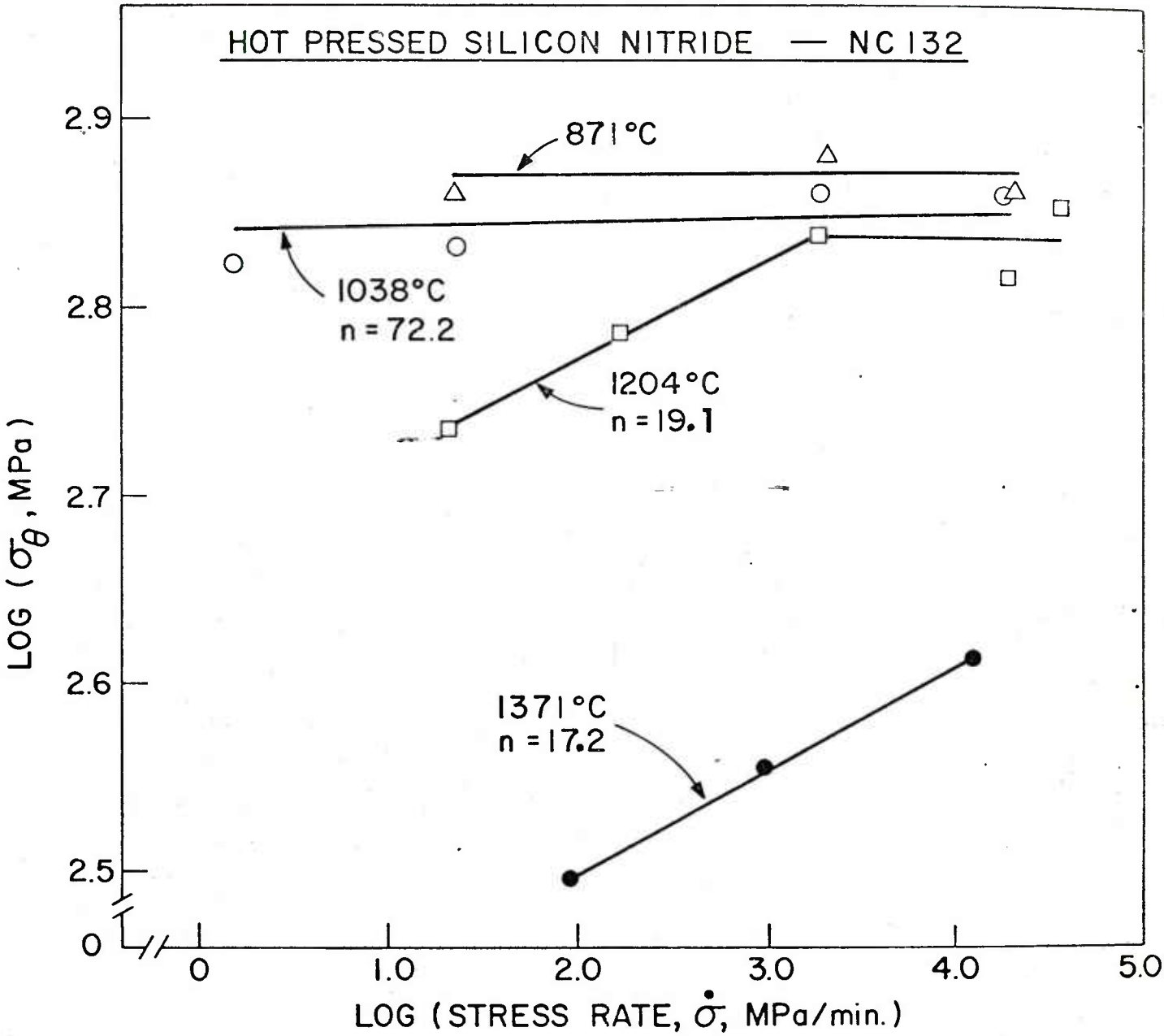

Fig. 2 Log-log plots of flexural strength vs stressing rate at various temperatures for NC-132 Si_3N_4. Data presented in this figure were obtained by R. M. Williams, Ford Motor Company.

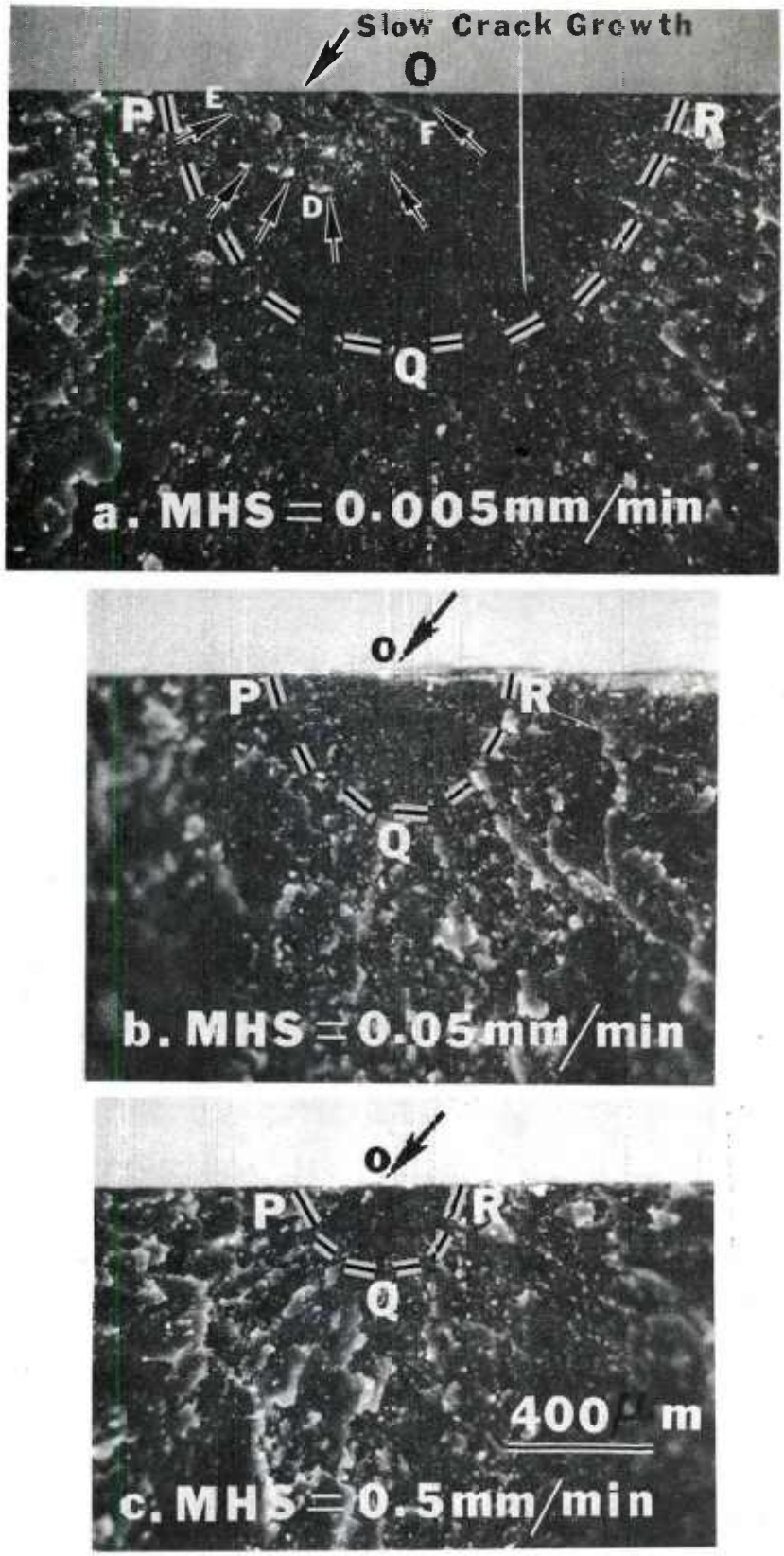

Fig. 3 Typical fracture surface appearance as seen in uncracked NC-132 Si_3N_4 flexural specimens tested in air at 1204°C as a function of stressing rate (or machine head speed, MHS). Arrow indicates the failure initiation site. PQR is approximately the semi-circular mirror region. Note the presence of slow crack growth, region EDF, was noticed only at extremely slow stress rates. Micrographs taken in plane polarized light and equal magnification.

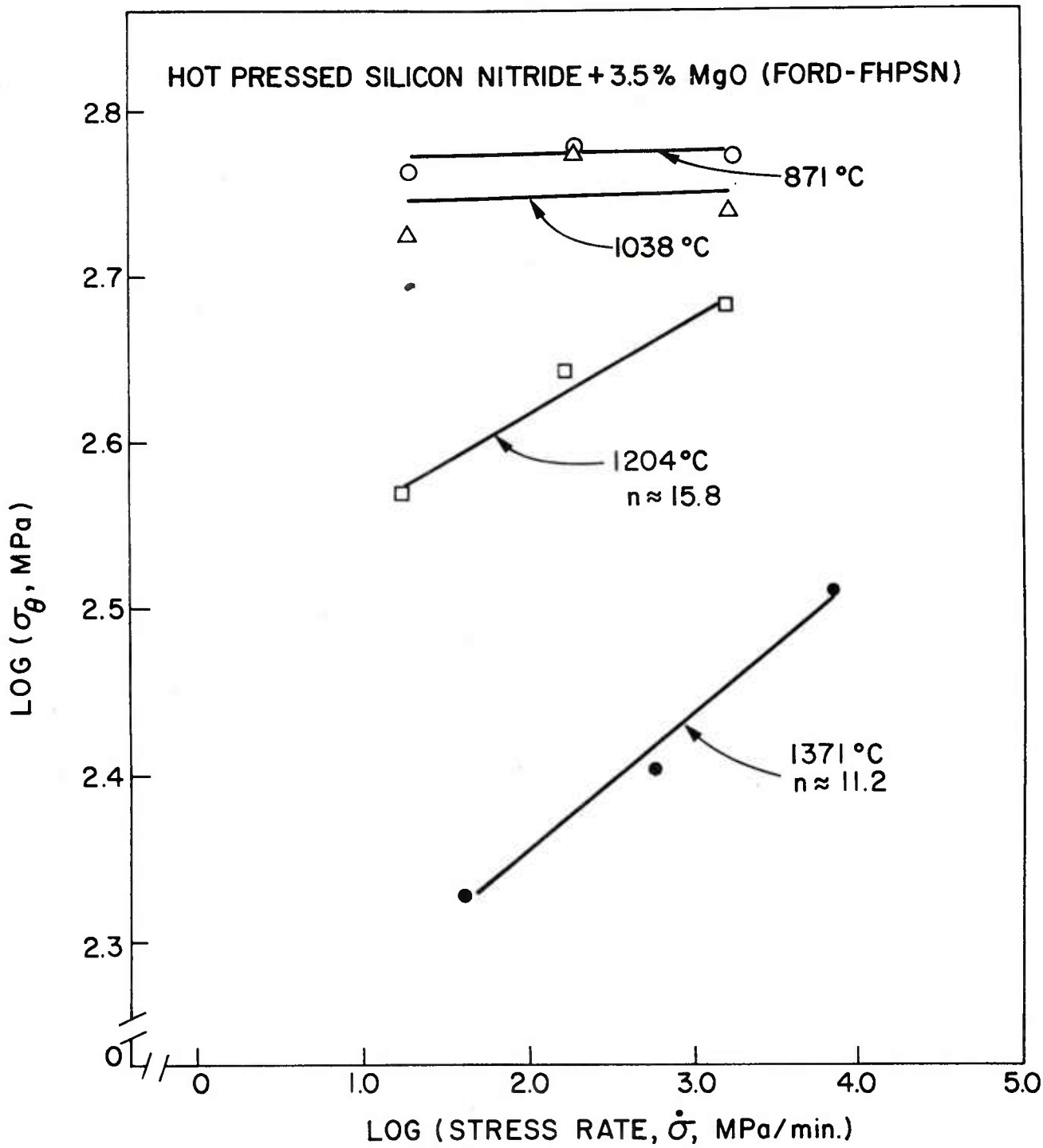

Fig. 4 Log-log plots of flexural strength vs stressing rate at various temperatures for 3.5% MgO + Si_3N_4 (FHPSN) material. Part of the data presented in this figure was obtained by R. M. Williams, Ford Motor Company.

TABLE 3

MOR (FOUR-POINT BENDING) STRESS RUPTURE DATA AT 1204°C FOR HOT-PRESSED SILICON NITRIDE, NC-132

Specimen	Applied Stress		Time to Failure, Hrs.
	MN/m^2	~ PSI	
NC-132-A_1	415	60,187	17.97
-A_2	"	"	1.15
-A_3	"	"	4.16
-A_4	"	"	1.75
-A_5	"	"	0.55
NC-132-B_1	415	60,187	2.42
-B_2	"	"	0.75
-B_3	"	"	1.33
-B_4	"	"	2.16
-B_5	"	"	0.58
NC-132-C_1	298	43,200	12
-C_2	"	"	46
-C_3	"	"	195
-C_4	"	"	46
-C_5	"	"	148
-C_6	"	"	59

TABLE 3

MOR (FOUR-POINT BENDING) STRESS RUPTURE DATA AT 1204°C FOR HOT-PRESSED SILICON NITRIDE, NC-132

Specimen	Applied Stress		Time to Failure, Hrs.
	MN/m^2	~ PSI	
NC-132-A_1	415	60,187	17.97
-A_2	"	"	1.15
-A_3	"	"	4.16
-A_4	"	"	1.75
-A_5	"	"	0.55
NC-132-B_1	415	60,187	2.42
-B_2	"	"	0.75
-B_3	"	"	1.33
-B_4	"	"	2.16
-B_5	"	"	0.58
NC-132-C_1	298	43,200	12
-C_2	"	"	46
-C_3	"	"	195
-C_4	"	"	46
-C_5	"	"	148
-C_6	"	"	59

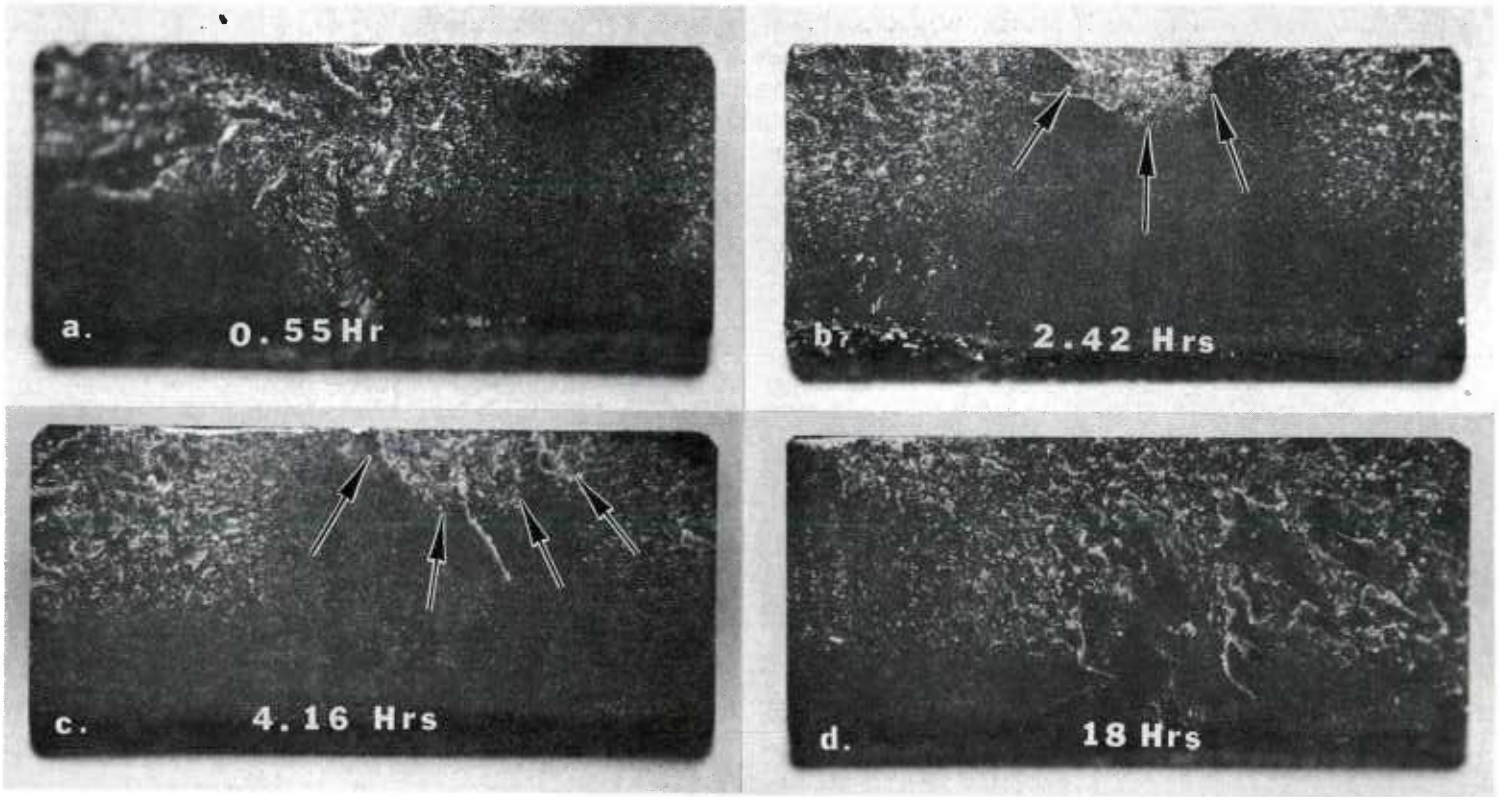

Fig. 5 Typical fracture surfaces of flexural stress rupture specimens of NC-132 Si_3N_4 tested at 1204°C in air at a constant applied stress of ~ 415 MPa. Arrows in (b) and (c) indicate the region of slow crack growth. In the above micrographs, complete cross-section of the test (failure) specimen is shown. Micrographs taken in plane polarized light.

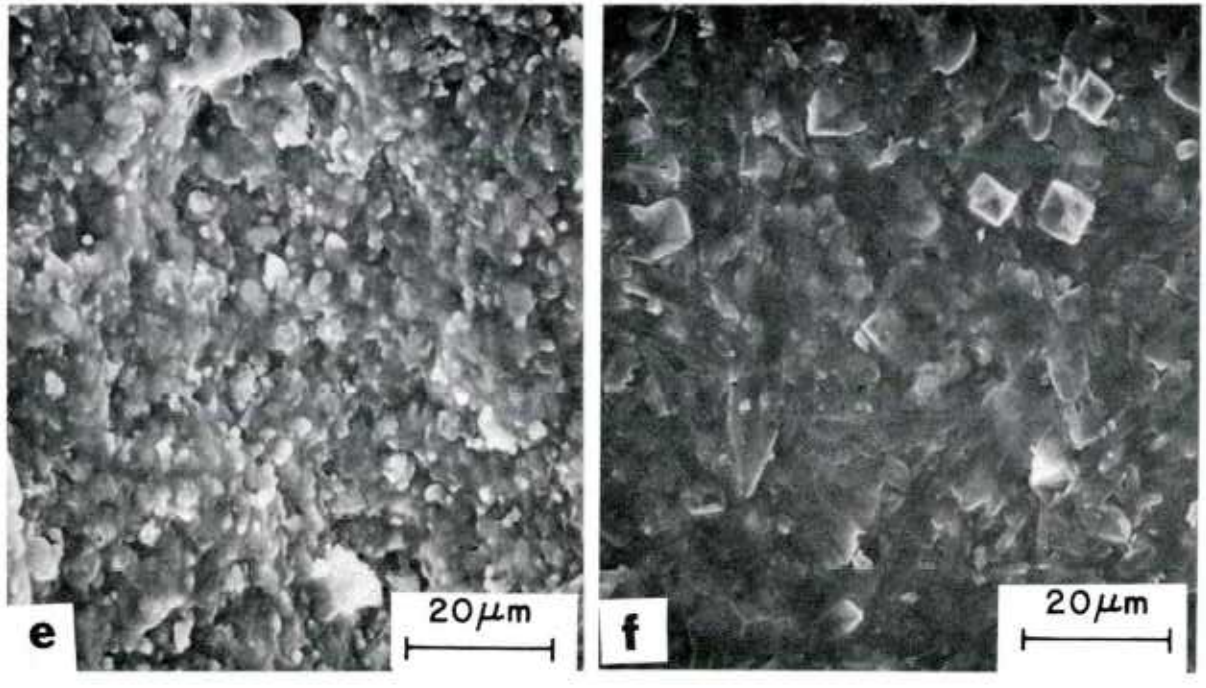

Fig. 5 SEM micrographs taken for the specimen shown in Fig. 5(c), revealing the nature and mode of crack propagation during slow crack growth (SCG) and fast fracture. (e) micrograph taken inside the SCG region revealing intergranualr crack propagation. (f) micrograph taken in the fast fracture region (outside the SCG) showing primarily transgranular fracture and localized intergranular crack propagation.

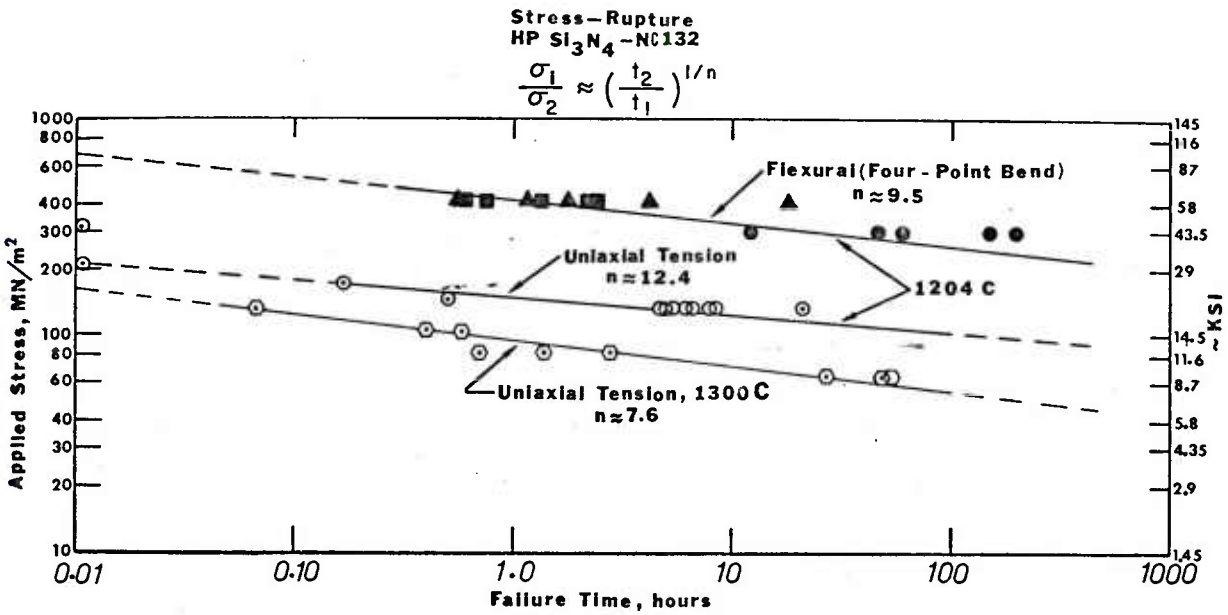

Fig. 6 Flexural and Uniaxial tensile Stress Rupture data and results for NC-132 Si_3N_4.

TABLE 4

MOR (FOUR-POINT BENDING) STRESS RUPTURE DATA AT 1204°C FOR HOT-PRESSED SILICON NITRIDE +3.5% MgO (FHPSN)

Specimen	Applied Stress		Time to Failure, Hrs.
	PSI	~ MN/m^2	
1215 A_1	37,100	256	2.87
A_1	"	"	9.53
A_2	"	"	7.73
A_3	"	"	7.73
A_4	"	"	1.08
A_5			
1216 B_1	37,100	256	9.07
B_1	"	"	63.12
B_2	"	"	18.08
B_3	"	"	83.58
B_4	"	"	95.70
B_5			

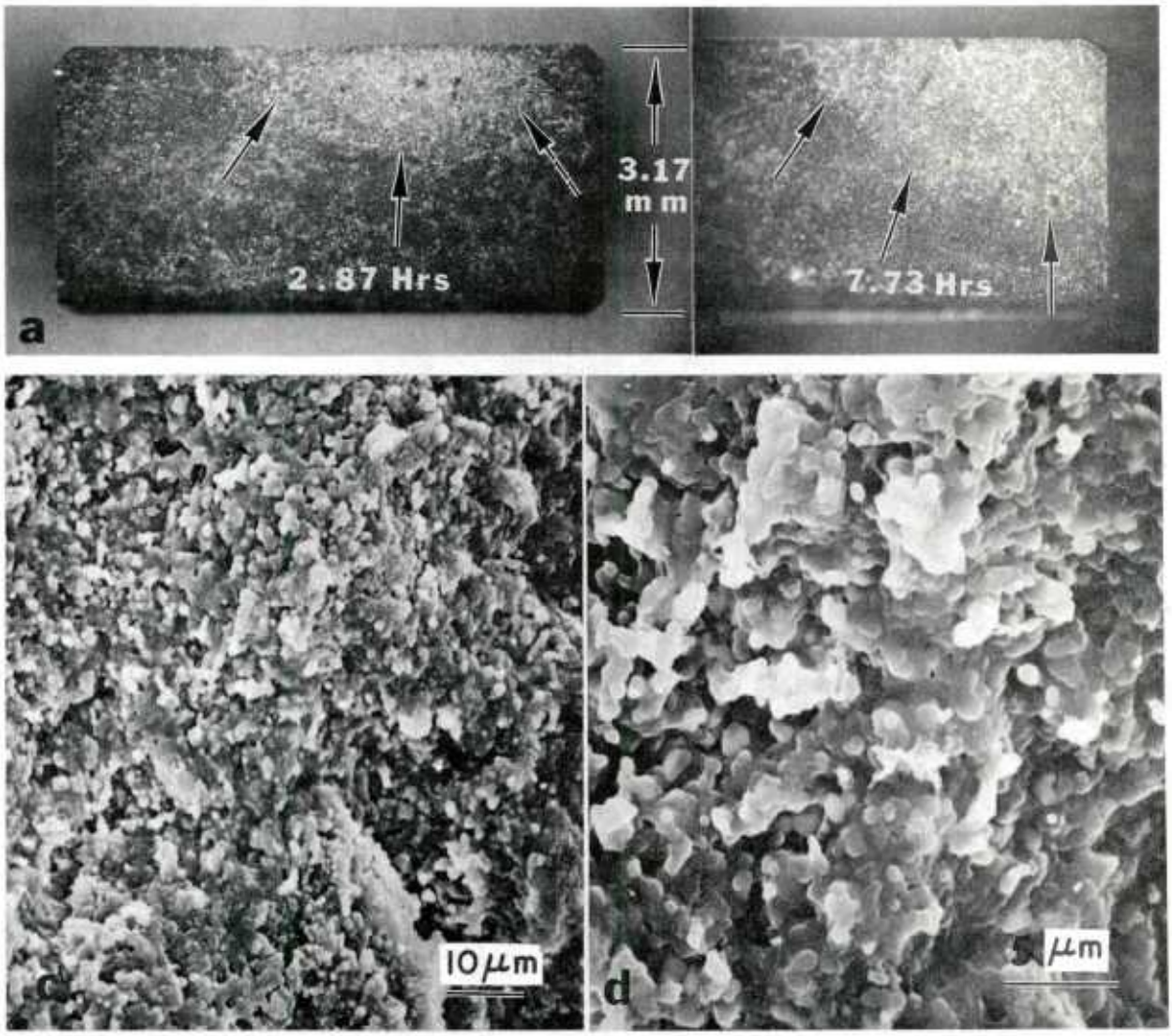

Fig. 7 Typical fracture surface of flexural stress rupture specimens of 3.5% MgO + Si_3N_4 (FHPSN) tested at 1204°C in air at a constant applied stress of ~ 256 MPa. Arrows indicate the extent of slow crack growth region. Micrographs in (a-b) taken with plane polarized light. (c) SEM micrograph taken inside the SCG region of specimen shown in (a). (d) higher magnification SEM view taken inside the SCG region (center of (c)) revealing that the nature of crack propagation in SCG is completely intergranular.

3. WEIBULL ANALYSIS

The Weibull distribution is often used in evaluating fast fracture strength data of brittle ceramic materials and is given by:

$$P_f = 1 - e^{-\int_v \left(\frac{\sigma-\sigma_u}{\sigma_o}\right)^m dv} = 1 - e^{-\int_v \left(\frac{\sigma}{\sigma_o}\right)^m dV} \quad (\text{for } \sigma_u = 0) \qquad (4)$$

In this equation, P_f is the probability of failure for fast fracture of a component subjected to an applied stress, σ. The integral is taken over all volume. σ_u, σ_o and m are three parameters of the distribution defined as follows:

(i) σ_u is the threshold stress below which the failure probability is zero. Usually, it is small in magnitude relative to the mean strength of the material and will be considered as negligible in this study.

(ii) m, the Weibull modulus is a measure of the flaw size distribution in the material. It is an important material parameter which characterizes the scatter of material strength. The higher the value of m the more uniform or consistent is the material.

(iii) σ_o has been termed the Weibull characteristic strength or a normalizing factor. Its dimensions are (stress)(volume)$^{1/m}$.

It is clear from equation (4) that a specimen of unit volume subjected to an applied stress of σ_o has a failure probability of 1 - 1/e or 63.2 percent. σ_o and m can be determined from experimentally obtained flexural strength data. Davies [6] and others [1,7-9] have outlined several methods for determining the Weibull parameters from flexural strength data. In this study, the MLE* (maximum likelihood estimator) method was used to determine the Weibull modulus, m, and

*MLE method has been discussed in detail and a Fortran Computer program listing is available in Ref. 1 for general use. The program calculates the Weibull parameters, e.g., the characteristic (MOR) strength, σ_θ, which refers to that value of fracture strength at which 63.2 percent of the population (specimens) will fail, the Weibull modulus, m, and 90 percent interval estimates for the parameters (σ_θ, m) and the distribution σ_{10} (MOR strength at 10 percent probability of failure), the distribution mean and standard deviation.

a characteristic (MOR) strength, σ_θ, from the flexural strength data. Using these Weibull parameters, the Weibull characteristic strength, σ_0, for unit volume was determined following the work of Davies [6]. If σ_1 and σ_2 are the mean failure stresses of specimens with effective volumes V_{E1} and V_{E2}, then

$$\sigma_1/\sigma_2 = (V_{E2}/V_{E1})^{1/m} \tag{5}$$

In the above Equation (5), if $\sigma_2 = \sigma_\theta$ the characteristic (MOR) strength for which the $P_f = 0.632$, and for $V_{E1} = 1\ cm^3$, then the mean failure stress $\sigma_1 = \sigma_0$, and is given by

$$\sigma_0 = \sigma_\theta\ (V_{E\theta})^{1/m} \tag{6}$$

The effective volume, V_E, for 1/4-point, 4-point bending is given by [6],

$$V_E = V\ (m+2)/4(m+1)^2 \tag{7}$$

where V is the volume of the test area given by

$$V = L_1 \times b \times h \tag{8}$$

where L_1 = outer span length, 1.905 cm

b = width of test specimen, 0.635 cm

h = thickness of test specimen, 0.3175 cm

Using Equations (7-8) and substituting in Equation (6), we get,

$$\sigma_o = \sigma_\theta \left[\frac{L_1\ b\ h\ (m+2)}{4(m+1)^2}\right]^{1/m} \tag{9}$$

In Equation (9), all the parameters are known and the Weibull characteristic strength, σ_0, can be determined. If the strength is controlled by surface flaws rather than volume flaws, then the volume integral in Equation (4) and the effective volumes in Equation (5) are replaced by surface integral and effective surfaces, respectively.

The experimentally obtained flexural strength data and results, Table 1, for NC-132 Si_3N_4 were used in determining the Weibull characteristic strength, σ_0, for unit volume. The statistical strength variation results from 20^o to 1371^oC are shown in Figures 8 to 14, in the form of Weibull diagrams. In these figures, the

data points were plotted using the Table of Median Ranks and the solid line is drawn on the basis of MLE method. On the same figure, another strength curve on the basis of unit volume was drawn and the magnitude of σ_o is shown. The immediate application of these diagrams is apparent. For example, in Figure 8, the characteristic (MOR) strength for NC-132 Si_3N_4 at 20°C and at a machine head speed of 0.5 mm/min is $\sigma_\theta \approx 787$ MPa. The corresponding Weibull characteristic strength for unit volume is $\sigma_o \simeq 410$ MPa, which is what the design engineer could use in a turbine component design. Furthermore, the design engineer could extrapolate the value of σ_o (unit volume) for 1 percent (or lower) probability of failure and use that particular value in design applications for greater reliability. Therefore, σ_o, is a much more realistic measure of strength of the material.

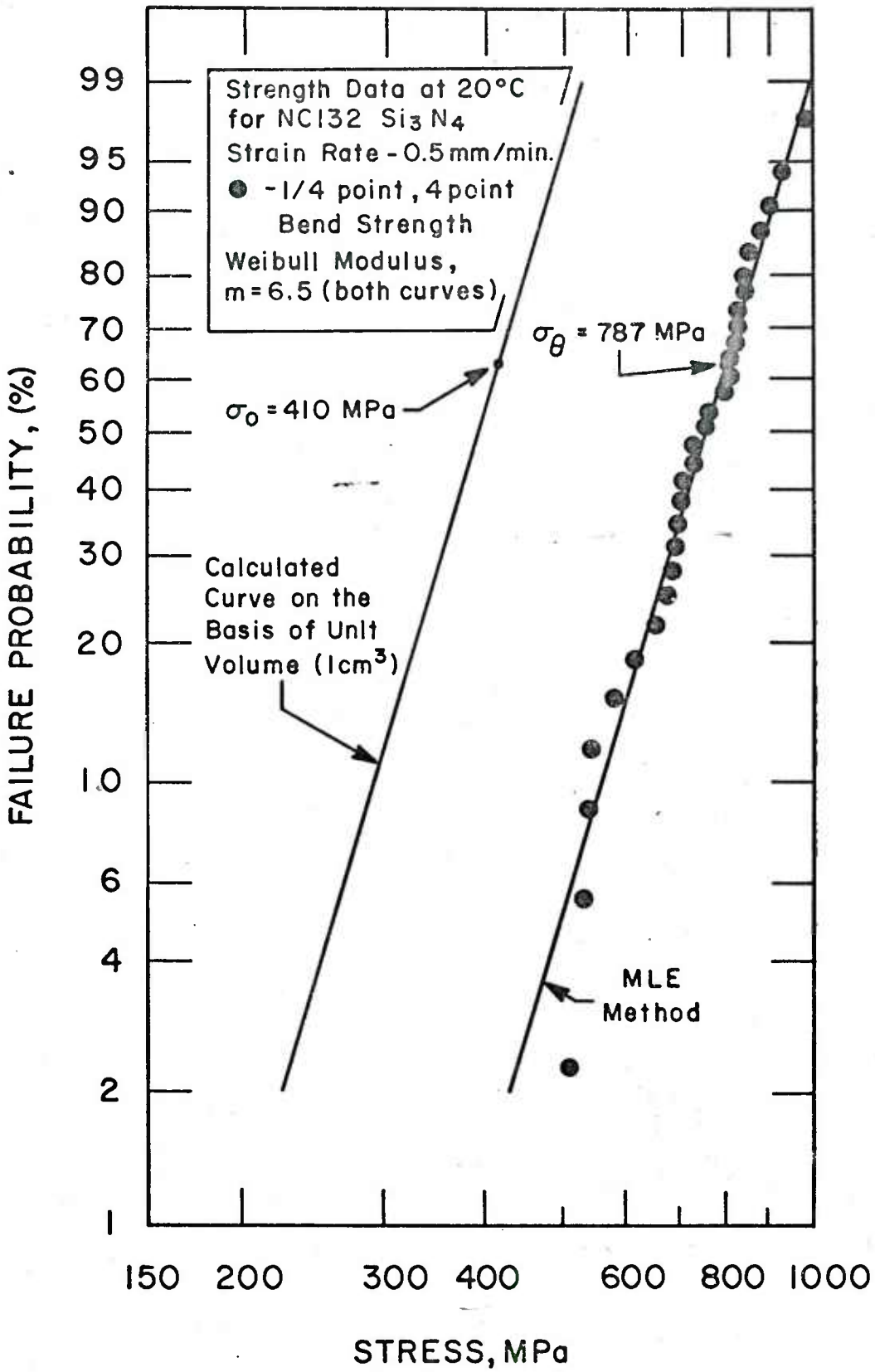

Fig. 8 Statistical variation in fracture strength. Solid line through the data points is drawn using the MLE method.

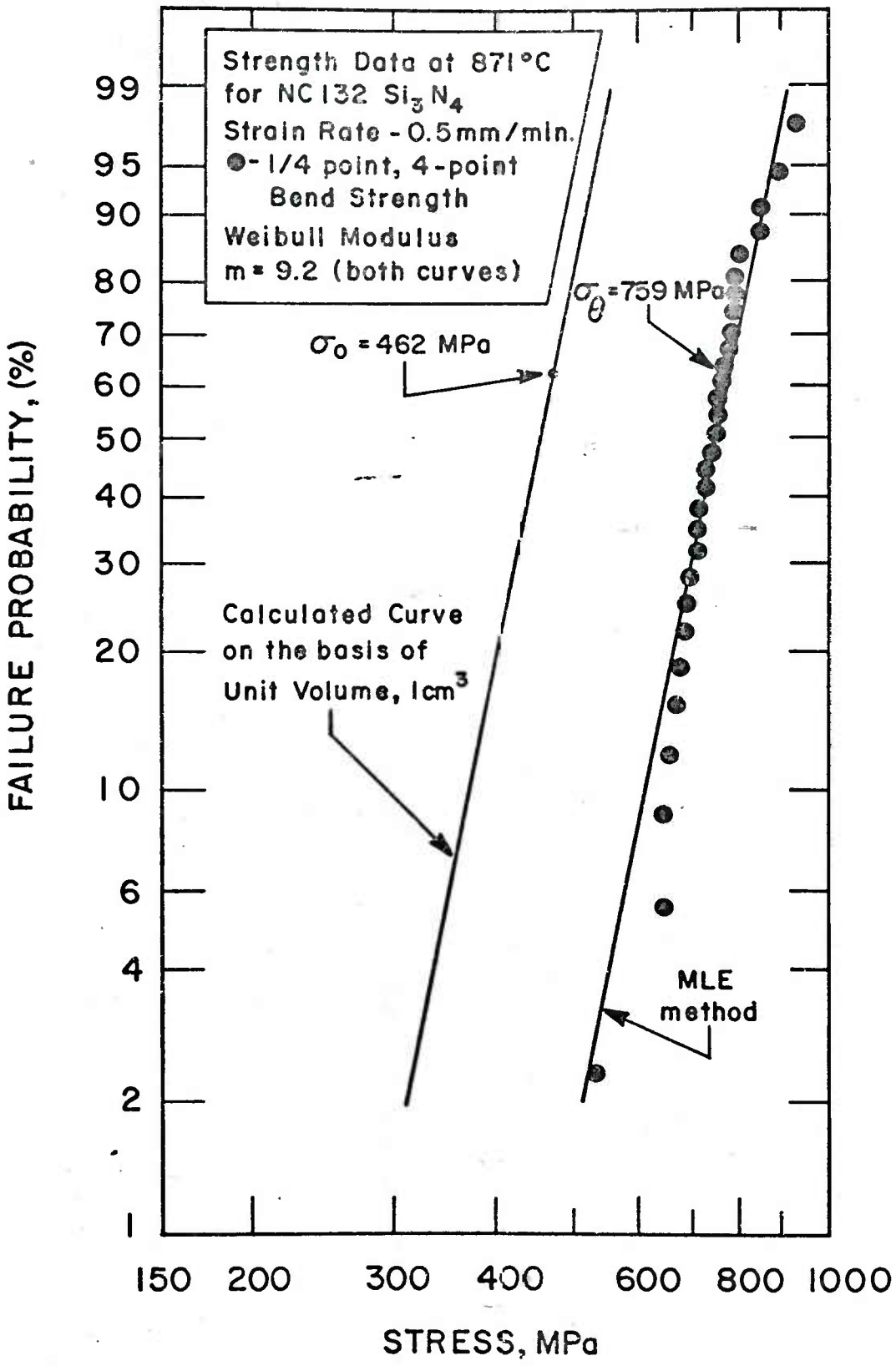

Fig. 9 Statistical variation in fracture strergth. Solid line through the data points is drawn using the MLE method.

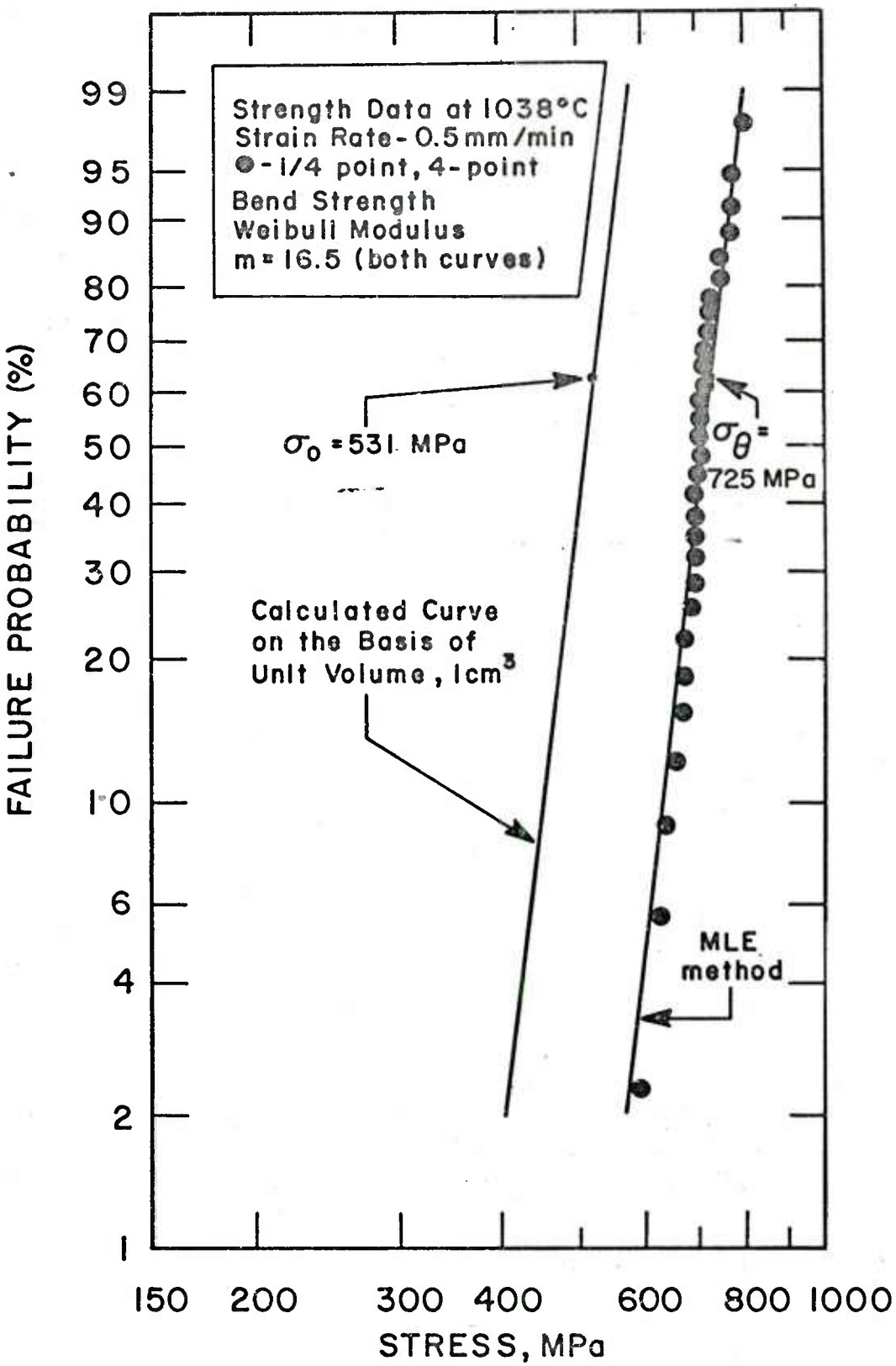

Fig. 10 Statistical variation in fracture strength. Solid line through the data points is drawn using the MLE method.

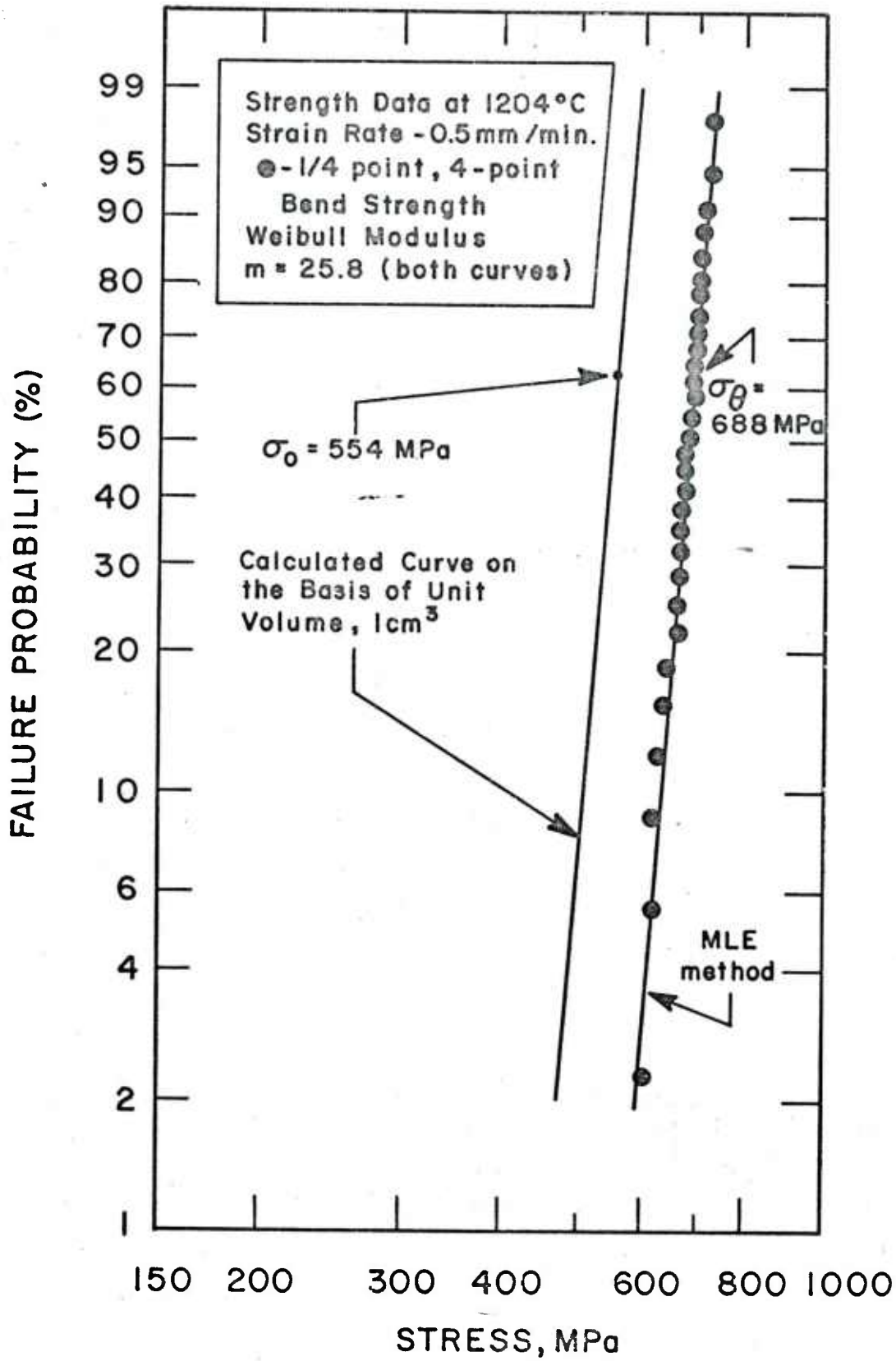

Fig. 11 Statistical variation in fracture strength. Solid line through the data points is drawn using the MLE method.

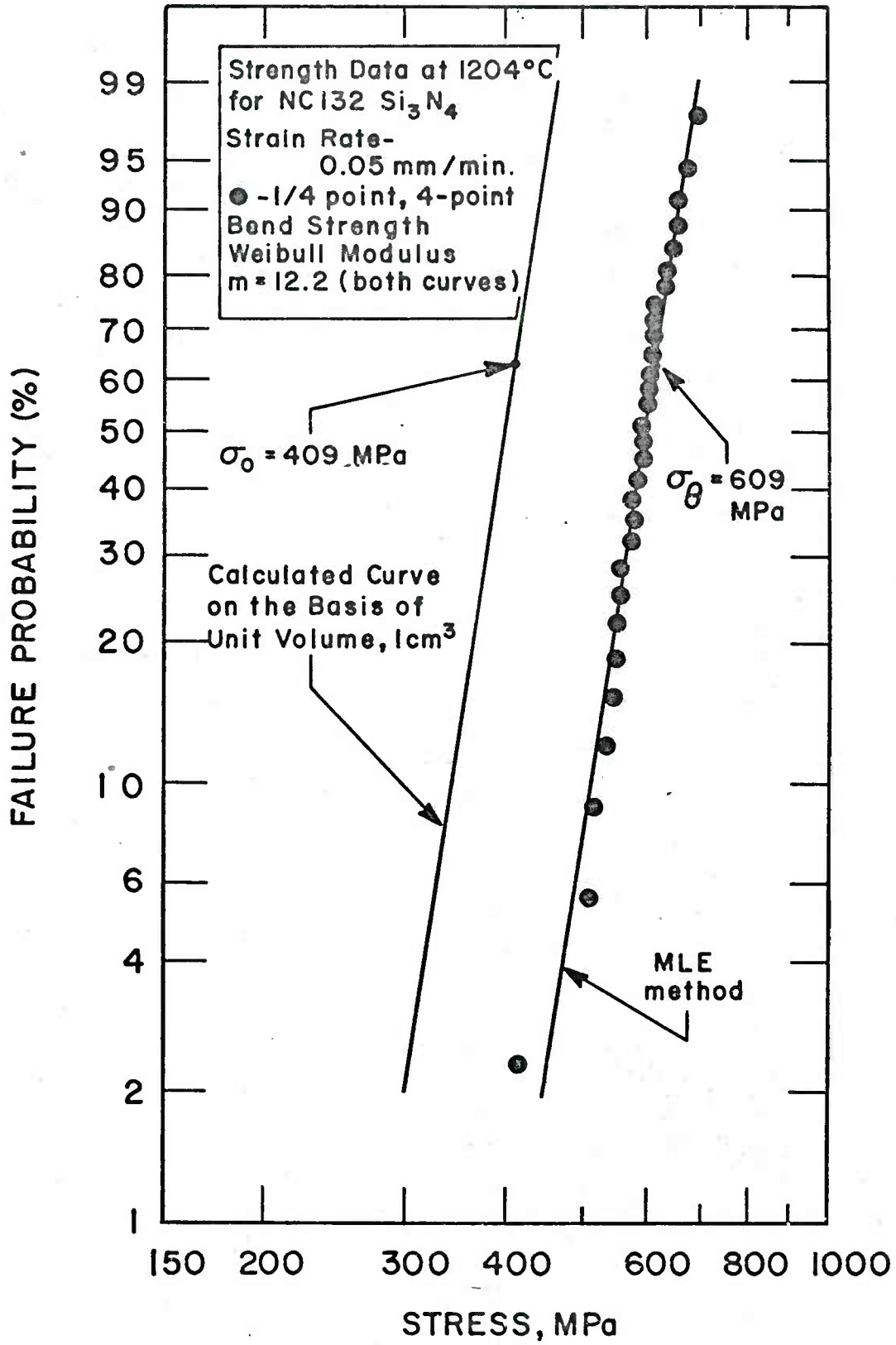

Fig. 12 Statistical variation in fracture strength. Solid line through the data points is drawn using the MLE method.

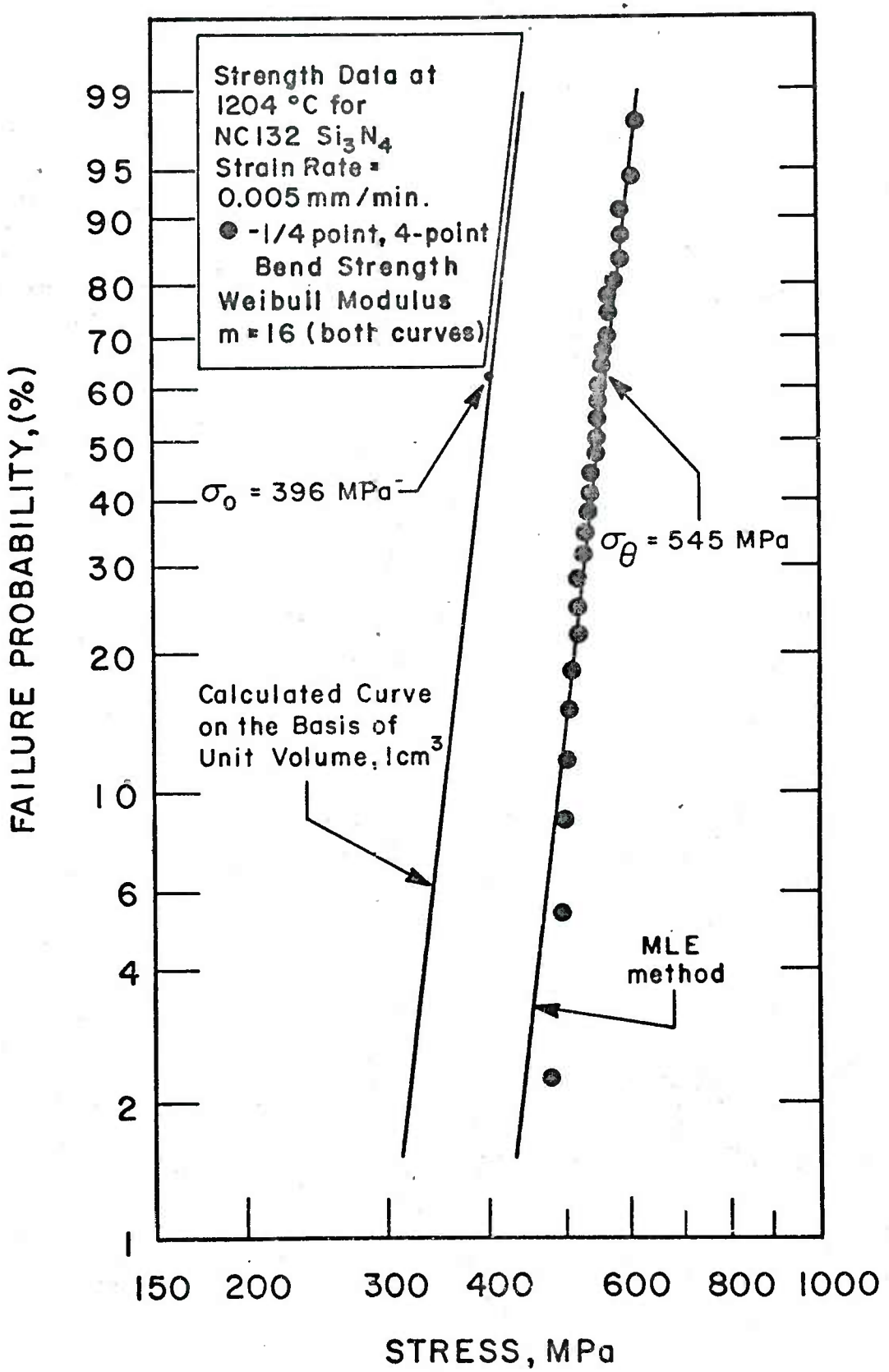

Fig. 13 Statistical variation in fracture strength. Solid line through the data points is drawn using the MLE method.

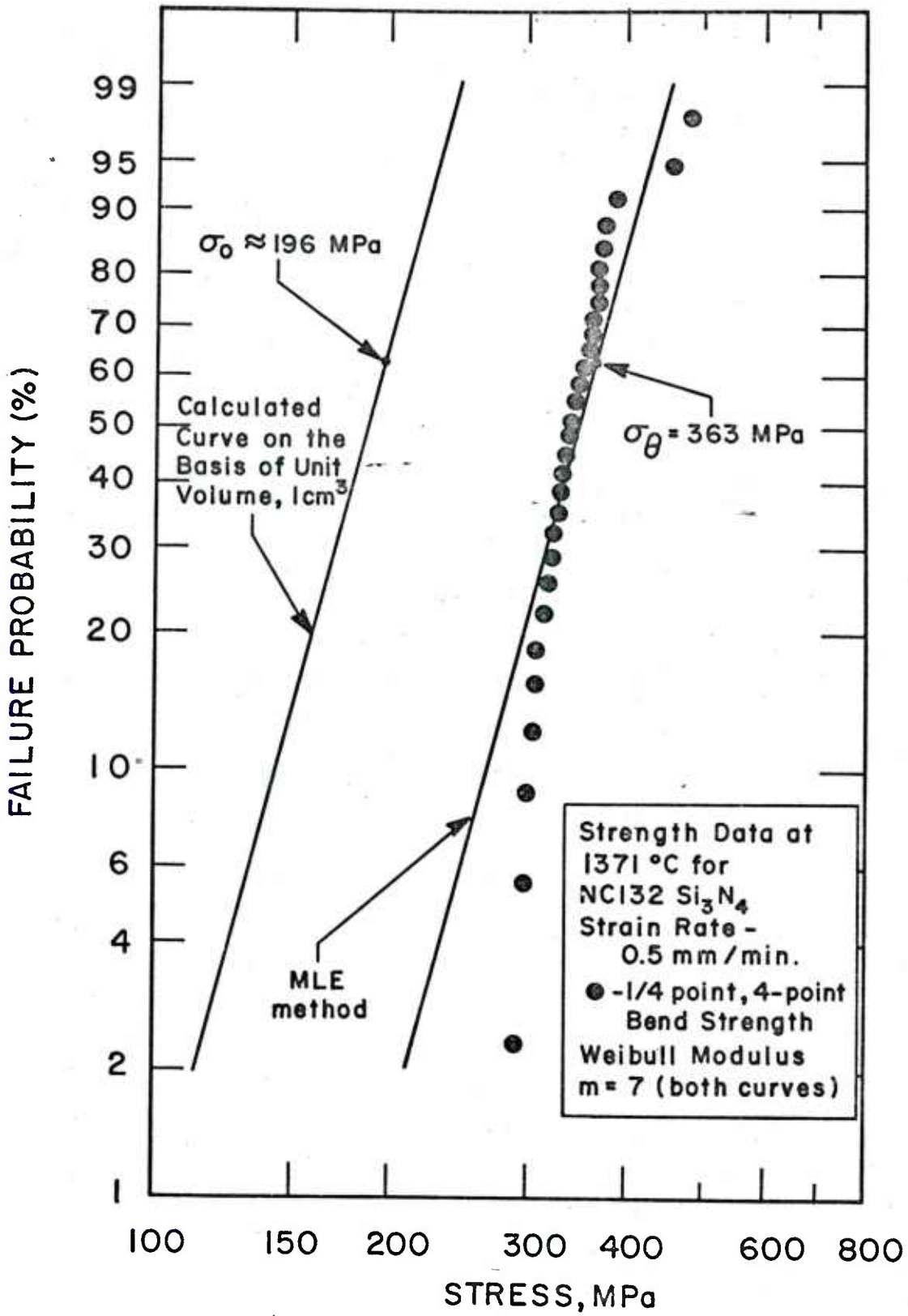

Fig. 14 Statistical variation in fracture strength. Solid line through the data points is drawn using the MLE method.

4. FRACTURE MECHANICS APPROACH

In this section, two methods, namely, the Indentation Induced Flaw (IIF) and the Double Torsion (DT) will be discussed as used in this study for determining the life prediction parameters for NC-132 Si_3N_4 and 3.5% MgO FHPSN. Various other methods for the determination of the critical stress intensity factor, K_{IC}, have been reviewed by Evans [10].

4.1. Indentation Induced Flaw Method and Analysis

Test specimens used in this technique were of similar dimensions as used in flexural strength measurements (Sec. 2.1) except that one surface (the tension face in bending) was carefully hand ground and wet polished to 6 micron diamond paste finish. The specimens were then precracked using the Vickers Diamond Pyramid and Knoop microhardness indenter (Wilson Instrument Division of ACCO, Bridgeport, Conn.) as described later in this section. A self-aligning ceramic fixture (Fig. A_2, Appendix) made from hot-pressed SiC was used for four-point bend tests and specimens both in the as-received and precracked condition were tested in an Instron machine at a constant cross-head speed of 0.005 in. ($\sim$ 0.127 mm) per min. The high temperature bend tests were conducted in air using a rapid temperature furnace (CM, Inc., High Temperature Furnaces, Bloomfield, N.J.) attached to the Instron machine head. In high temperature tests, specimens were held at the test temperature for about 15 mins. in order to achieve equilibrium before testing is started. No preload was applied on test specimens in either the room temperature or high temperature tests.

Indenting the hot-pressed silicon nitride specimens using a Vickers Diamond pyramid or Knoop indenter resulted in the introduction of surface cracks of reproducible geometry and size (depth of crack) controlled by choice of indenter load. The use of the Indentation Induced Flaw (IIF) method for introducing a starting flaw and then testing specimens in flexure for measuring fracture mechanics parameters such as the fracture energy, γ, or the K_{IC}, was first illustrated in single crystals of vanadium carbide [11-13] and later in polycrystalline materials [14,15-17]. The resultant crack geometry, Fig. 15a, and typical examples of a crack produced on the polished surfaces of NC-132 Si_3N_4 test specimens using Diamond pyramid and Knoop indenters are shown in Figs. 15b and 15c, respectively. Great care was taken to make sure that the crack AB, Fig. 15b, or the long diagonal of the Knoop indentation (AB), Fig. 15c, is aligned perpendicular to the direction of the tensile axis. The crack depth, CO, Fig. 15a, was measured directly from the micrographs of fracture faces. Cracks can be produced with indentation loads as low as 500 gm but repropagation of such cracks was not always successful because the inherent flaws in the material were about the same size. At indentation loads up to 4000 gm, the crack fronts were approximately semi-circular. All indentations were made at room temperature.

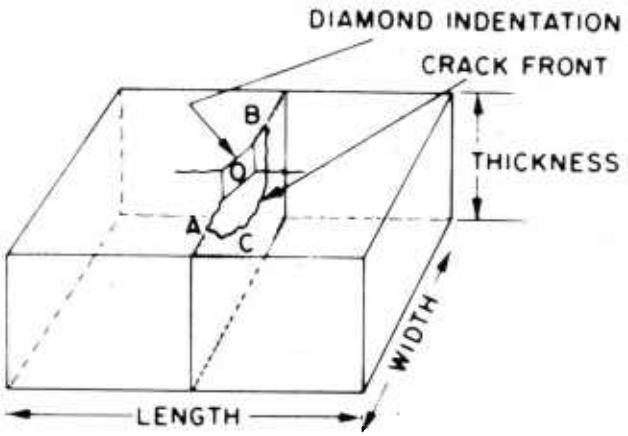

AB – Single Crack Produced by Diamond Indentation

ACB – Crack Front Produced by Indentation

CO – Depth of Crack as Seen on the Fracture Plane

a.

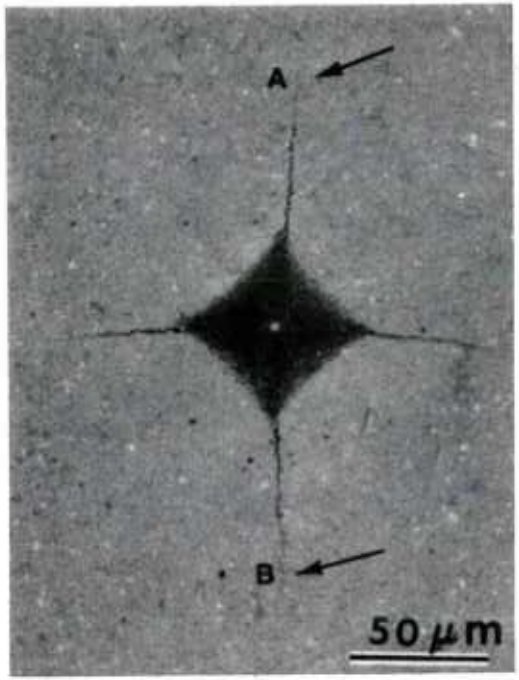

b. 4000 gm

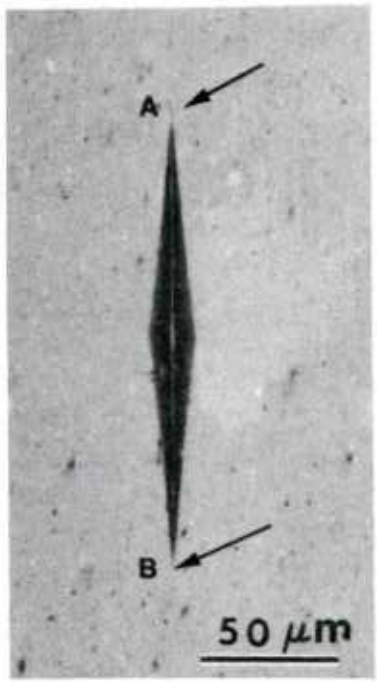

c. 2600 gm

Fig. 15 (a) Schematic representation of crack geometry as produced by microhardness indentation. (b) Typical example of a crack produced on the polished surface of a NC132 Si_3N_4 test specimen using a Diamond pyramid indenter with 4000 gm load. (c) Typical example of a crack produced on the polished surface of a NC132 Si_3N_4 test specimen using a Knoop indenter with 2600 gm load.

Fracture Mechanics of Surface Flaws

The stress indensity, K_I, for a surface flaw in bending [18] is given by:

$$K_I = \sigma M \left[\frac{\pi c}{Q}\right]^{1/2} \tag{10}$$

where σ is the maximum outer fiber tensile stress, c is the flaw depth, and M and Q are numerical factors related to flaw and specimen geometry. M is a function of the ratio of flaw depth to specimen thickness, the ratio of flaw depth to width, and location along the flaw front [19]. For semi-circular flaws [19], M is 1.03. Also,

$$Q = \Phi^2 - 0.212 (\sigma/\sigma_{ys})^2 \approx \Phi^2 \tag{11}$$

where σ_{ys} is the tensile yield stress and $0.212 (\sigma/\sigma_{ys})^2$ is a plastic-zone correction factor and for brittle failure in ceramics, this factor is negligible. Finally, Φ is the elliptic integral given by:

$$\Phi = \int_0^{\pi/2} \left[\sin^2 \theta + (c/b)^2 \cos^2 \theta\right]^{1/2} d\theta \tag{12}$$

where 2b is the total flaw length at the free surface (length of the flaw AB as seen on the polished surface, Fig. 15). This integral is tabulated in some mathematical tables and in Ref. 18.

4.1.1 Crack Size vs Fracture Stress

NC-132 Si_3N_4

A series of specimens was prepared and precracked using Vickers Diamond Pyramid indenter with 500 gm, 1000 gm, 2000 gm and 4000 gm indentation loads. The variation of fracture stresses as a function of indentation load at 20°C for a total of 30 specimens of NC-132 Si_3N_4 are given in Table 5. All specimens tested at 20°C failed at the precrack-site. Typical fracture surface for a specimen precracked with 4 Kg Diamond Pyramid indentation load and tested at 20°C is shown in Fig. 16. The variation of fracture stress σ_F, with crack depth (actually inverse square root of crack depth) for NC-132 Si_3N_4 specimens tested at 20°C is shown in Fig. 17. Although there is scatter in the data, a reasonably good linear relationship is evident which correlates with the Griffith criterion for brittle fracture. Data for a few Kroop indented precracked specimens are also shown, Fig. 17, and behaved in a similar fashion as Diamond Pyramid indented precracked specimens. From a practical point of view, perhaps the most useful application of the data shown in Fig. 17

TABLE 5

FRACTURE STRESS (FOUR-POINT BENDING) AS A FUNCTION OF INDENTATION LOAD AT 20°C FOR HOT PRESSED SILICON NITRIDE NC-132

Specimen No.	Indentation Load, gm	Fracture Stress, MN/m^2	Crack Depth ~μm
	USING DIAMOND PYRAMID INDENTER		
1	500	694	18
2	"	548	28
3	"	586	25
4	"	540	27
5	1000	494	47
6	"	445	52
7	"	421	50
8	"	416	40
9	"	396	43
10	2000	340	68
11	"	303	80
12	"	376	63
13	"	439	52
14	"	353	65
15	"	401	58
16	4000	305	90
17	"	272	106
18	"	367	85
19	"	359	85
20	"	299	85
21	"	286	95
22	"	298	102
23	"	323	92
	USING KNOOP INDENTER		
24	600	512	29
25	"	557	26
26	1100	381	53
27	"	441	48
28	2600	327	81
29	"	296	85
30	4000	267	120

All the above specimens failed at the crack site & crack depths were measured from fracture faces.

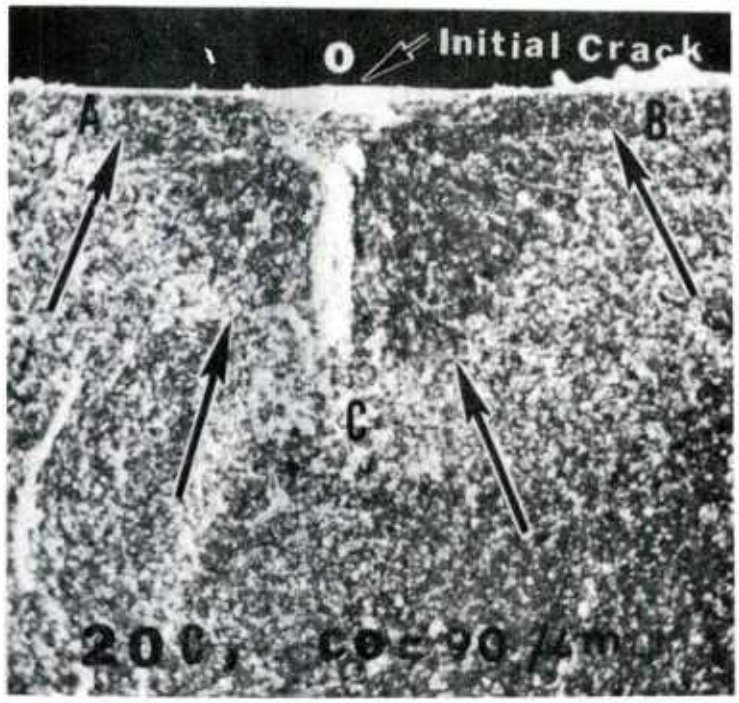

a

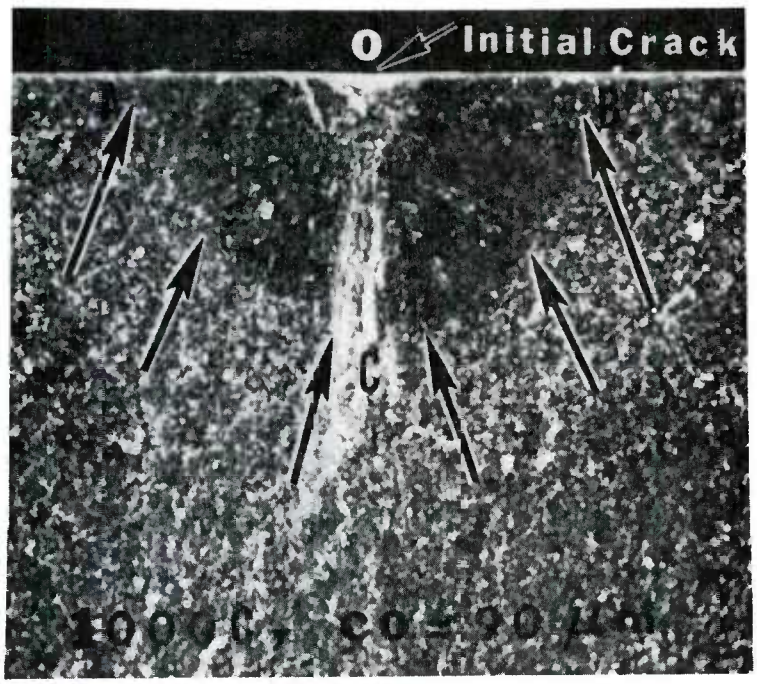

b

Fig. 16 Typical SEM micrographs of fracture surfaces of precracked specimen of NC-132 Si_3N_4 at 20°C and 1000°C. Specimens precracked with 4000 gm indentation load (Diamond pyramid). Arrows indicate the boundary of the precracked region, ACB.

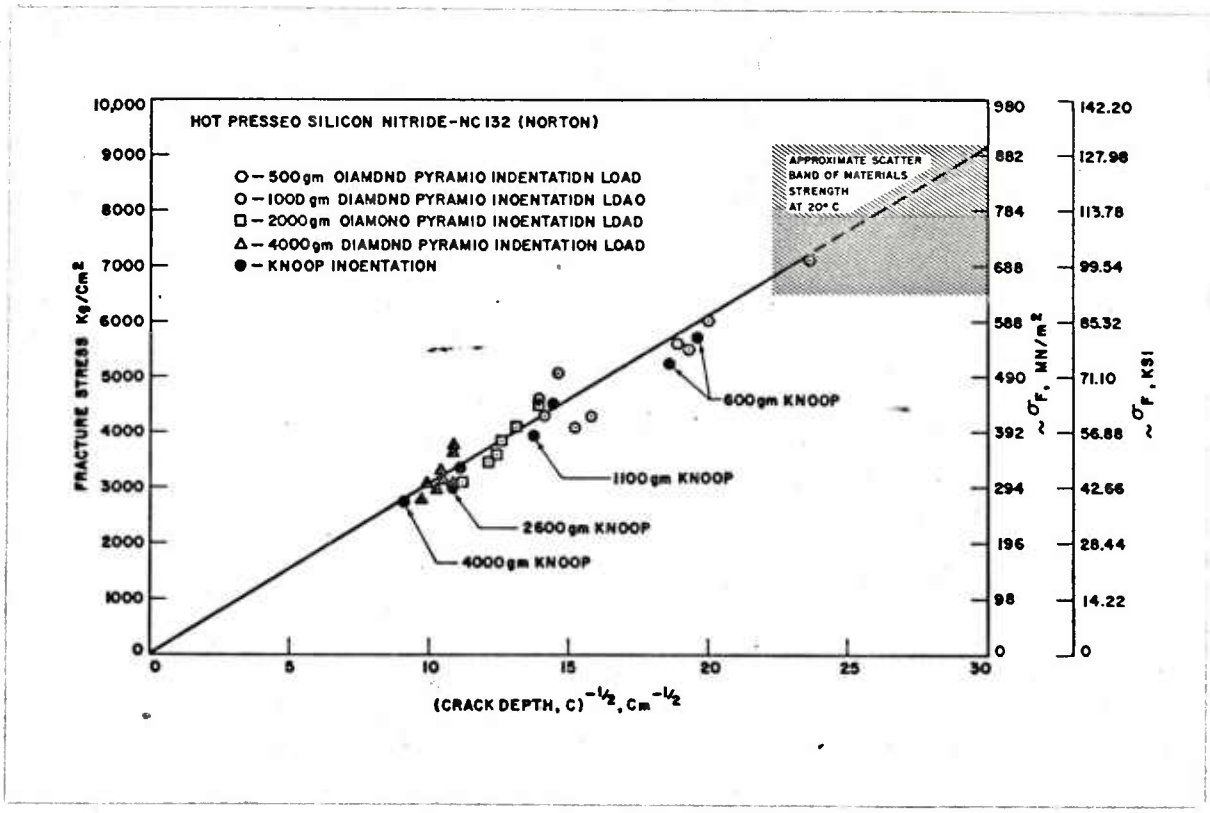

Fig. 17 Variation of fracture stress as a function of inverse square root of crack depth at room temperature for NC-132 Si_3N_4.

is as a means of estimating the inherent flaw* size in hot pressed NC-132 Si_3N_4. Extrapolation of the data in Fig. 17 to the fracture stress of uncracked samples (shown as the approximate scatter band of materials strength) indicates that flaws of the order of 10 to 20 microns in depth are present in the as received (uncracked) Si_3N_4. To date, this is perhaps the best estimate of the inherent flaw size in NC-132 Si_3N_4. Numerous investigations [16, 20-25] relating to mechanical properties and fracture mechanics aspects of a similar type of hot pressed Si_3N_4 are on record but none made an attempt to measure or estimate the inherent flaw size. Lange [26] and Mecholsky, Freiman and Rice [27] have also estimated the flaw size to be around 90 and 53 microns in HS-130 Si_3N_4, from their surface energy and mirror constant measurements, respectively.

3.5% MgO FHPSN Material

Similar fracture studies were carried out in another ceramic material, namely, 3.5% MgO FHPSN (Ford Material). A series of 31 test specimens were precracked with various indentation loads and tested in flexure at 20°C. Complete results showing fracture stresses at 20°C as a function of indentation load are shown in Table 6. All specimens except one (#25 -- precracked with 500 gm Knoop indentation) failed at the precrack site. Although the crack can be seen on the polished surface after making the indentation, the semi-circular or pseudo elliptical type crack front was not visible on the fracture face, Figs. 18a and 18b, respectively. Examination of the polished surfaces and fracture faces in plane polarized light revealed the presence of a "mottled structure" in this material, Figs. 19a and 19b, respectively. From preliminary examination, it appears that this structure is related to extremely fine porosity in the material. It has been suggested by Neil [28] that the presence of this structure in 3.5% MgO hot-pressed Si_3N_4 is primarily due to processing variables such as the pressure, temperature and time for hot pressing and, to a small extent, composition of the material. A similar type of structure has also been observed in yttria added Si_3N_4 (NCX-34, Norton). We believe that the presence of this "mottled structure" obstructed the visibility of the crack front profile, and, as such, our inability to measure the crack depths from fracture faces. Therefore, an estimate of inherent flaw size and stress intensity, K_{IC}, could not be made accurately using the IIF method.

*Inherent flaw size refers to specifically the size of flaws which occur in the virgin (or as processed)material and does not refer to surface flaws caused by machining.

TABLE 6

FRACTURE STRESS (FOUR-POINT BENDING) AS A FUNCTION OF INDENTATION LOAD AT 20°C FOR HOT-PRESSED SILICON NITRIDE + 3.5% MgO (FORD MATERIAL FHPSN)

Specimen No.	Indentation Load	Fracture Stress, MN/m^2
	USING DIAMOND PYRAMID INDENTER	
1	500 gm	477
2	"	542
3	"	462
4	"	586
5	"	472
6	1000 gm	467
7	"	422
8	"	358
9	"	422
10	"	422
11	2000 gm	407
12	"	407
13	"	331
14	"	348
15	"	358
16	4000 gm	348
17	"	407
18	"	268
19	"	290
20	"	273
21	"	343
22	"	348
23	"	343
	USING KNOOP INDENTER	
24	500 gm	592
25	"	686 +
26	1000 gm	472
27	"	506
28	2000 gm	393
29	"	465
30	4000 gm	324
31	"	327

+ Except specimen #25, all other specimens failed at the precrack site.

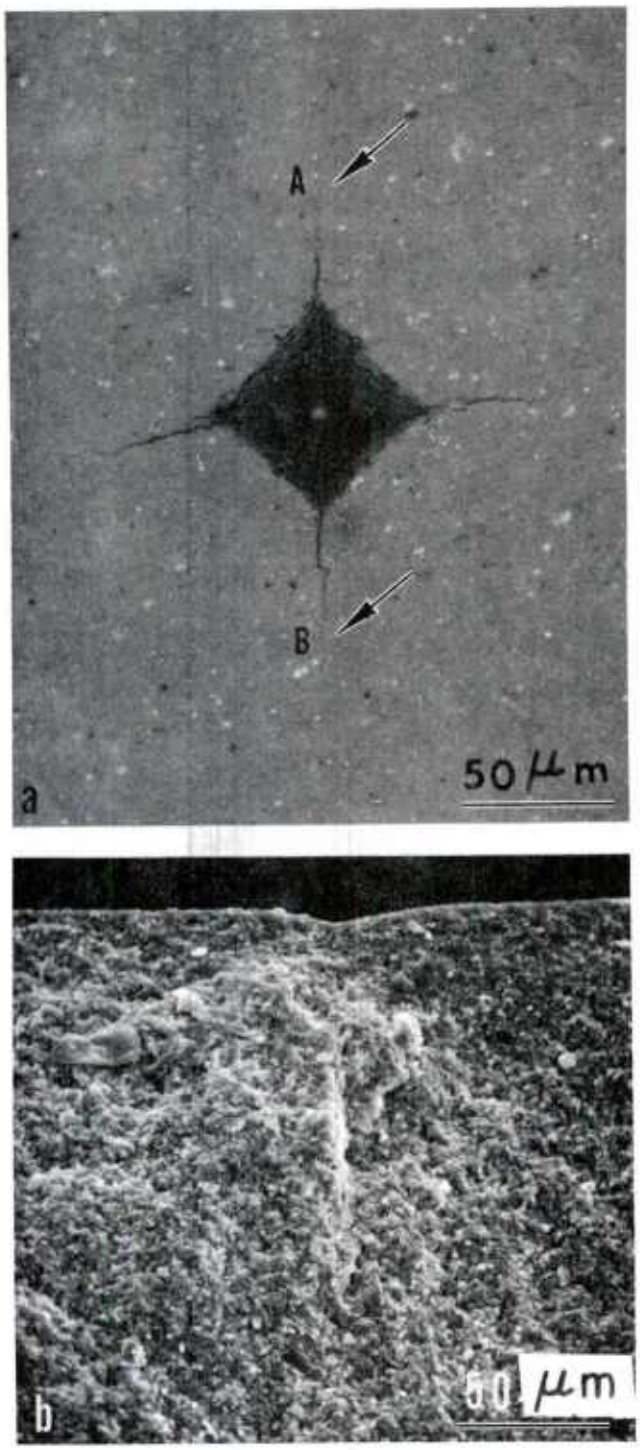

Fig. 18 (a) Typical example of a crack produced on the polished surface of a 3.5% MgO + Si_3N_4 (FHPSN) material using a Diamond pyramid indenter with 4000 gm load at 20°C. (b) SEM micrograph of the fracture face for the precracked specimen (shown in (a)) tested at 20°C. The precracked semi-circular region is not visible.

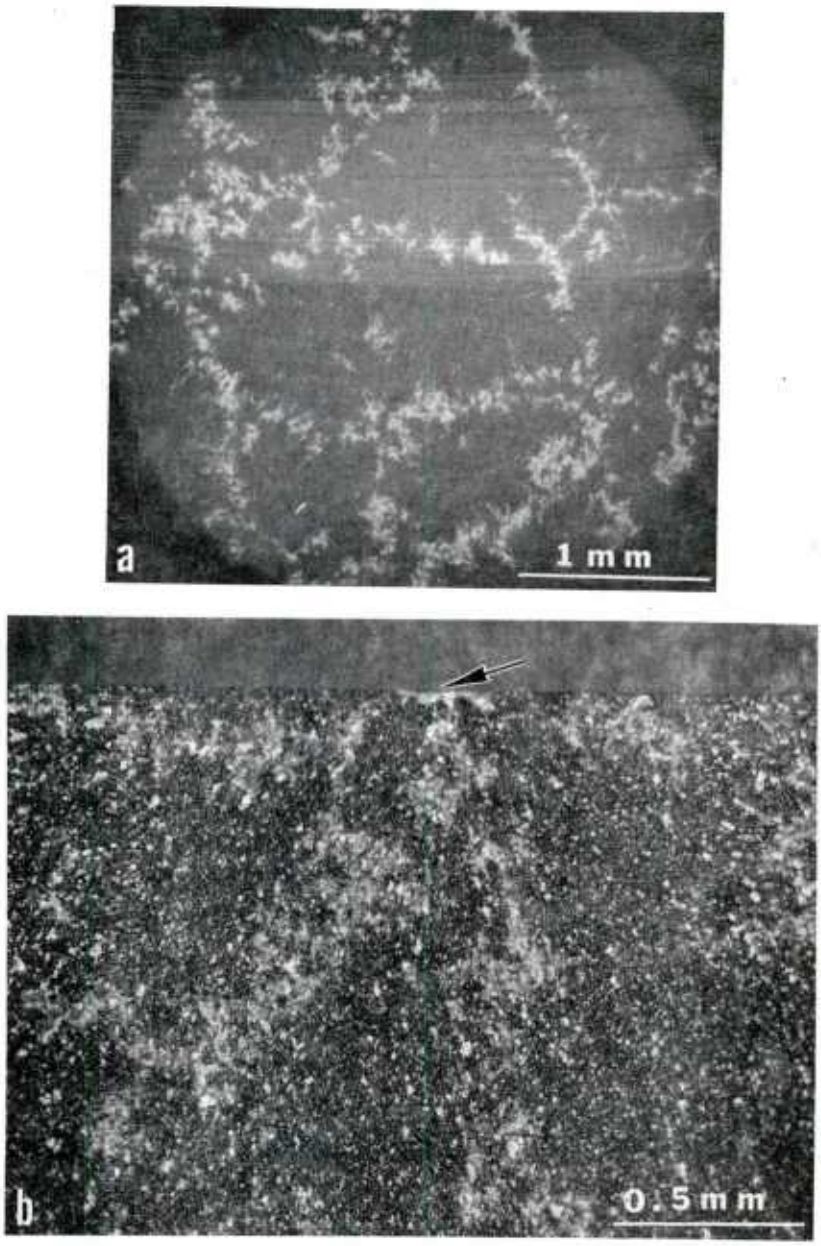

Fig. 19 Appearance of "mottled structure" as seen on the Polished surface and fracture face of a 3.5% MgO + Si_3N_4 (FHPSN) test specimen at 20°C, respectively. (a) Polished (6 μm finish) surface appearance. (b) Fracture face appearance. Test specimen was pre-cracked with Knoop indenter (4000 gm load) and failed at pre-crack site as indicated by arrow. Semi-circular crack front is not visible. Both micrographs taken in plane polarized light.

RBSN-NC 350

The reaction bonded silicon nitride (RBSN)-NC 350 was obtained from the Norton Company in the form of a circular billet. The material had a nominal density of 2.4 gm/cm^3 and typical rectangular MOR bars were machined out of the billet as described earlier (see Sec. 2.1). Since the "as fired" or "nitrided" surface has significant effect on the strength properties, the "as fired" surface layer on one side of each MOR specimen (billet) was removed using a 320 grit diamond wheel. Single cracks of various depths were introduced on this 320 grit finish surface using the Vickers diamond pyramid and Knoop indenter microhardness machine. A total of thirty one (31) MOR type specimens (including eight in the as-machined condition) were tested in flexural mode at 20°C to estimate flaw size and K_{IC}. The variation of fracture stress at 20°C as a function of indentation load is shown in Table 7. Note that a large variation (almost two to one) in flexural strength occurred in the as-received or as-machined samples. The reason for this large variation in strength is due to large variations in porosity in the material which acted as failure initiation sites. From metallographic observations of polished surfaces and fracture faces of test specimens (as shown later), we believe that this NC-350 RBSN billet had a porosity of about 20% by volume. In addition, there is the presence of some unreacted metallic phase, usually silicon, finely dispersed in the matrix which could act as failure initiation sites. Typical porosity on the polished surface of a test specimen is seen in Fig. 20. A Vickers diamond indentation was made to identify the same region when examined in polarized light, Fig. 20b and in SEM, Fig. 20c. Surface crack AB, Fig. 20a, coming out of the indentation can be partly seen. Black spots, Fig. 20a, are all 'pores' and often occur in localized groups. Moreover, these pores appear to be interconnected and could act effectively as a single large flaw in length varying from 10 to 80 microns. Also, there is a uniform distribution of finely (about 0.1 μm) dispersed pores throughout the matrix. In plane polarized light, the black spots, Fig. 20a, appear as white regions, Fig. 20b and the same region when examined in SEM, Fig. 20c, shows a one to one correspondence of black dots to actual pores. The shape of the pores also vary. The porosity as seen in NC-350 RBSN, Fig. 20b, has some resemblance to the 'mottled structure" seen in 3.5% MgO FHPSN, Fig. 19, which is much finer in size.

Typical example of a surface initiated failure in RBSN-NC 350 for the as-received specimen No. 2 (Table 7) is shown in Fig. 21. Sometimes failure occurred at an internal pore in the as-received NC-350 RBSN material and a typical example as observed in specimen No. 6 is shown in Fig. 22. The SEM examination revealed two important facts: The single failure initiation site as seen in Fig. 22a, actually consists of several pores joined together and acting as a one single flaw. Secondly, the NC-350 RBSN has pores all over, Fig. 22b, and the material appears to be like a sponge.

TABLE 7

FRACTURE STRESS DATA FOR RBSN-NC-350 AT 20°C
(FOUR-POINT BEND STRENGTH)

Test No.	Indentation Load	Fracture Stress, MN/m^2	Remarks
	SPECIMENS NO. 1-8 ARE IN THE AS MACHINED (OR AS RECIEVED) CONDITION		
1	none	186	Surface Flaw
2	"	355	" "
3	"	323	-
4	"	179	-
5	"	353	-
6	"	263	Internal Pore Failure
7	"	184	Surface Flaw
8	"	359	Internal Pore Failure
	USING VICKERS DIAMOND PYRAMID INDENTER		
9	500 gm	337	Did not fail at precrack site
10	"	184	" " " " " "
11	1000 gm	217	Failed at precrack site
12	"	230	" " " "
13	"	186	" " " "
14	"	151	" " " "
15	"	118	Did not fail at precrack site
16	2000 gm	144	Failed at precrack site
17	"	140	" " " "
18	"	129	" " " "
19	"	137	" " " "
20	"	156	" " " "
21	4000 gm	93.4	Failed at precrack site
22	"	107.3	" " " "
23	"	108.3	" " " "
24	"	96.4	" " " "
25	"	93.4	" "
	USING KNOOP INDENTER		
26	1000 gm	127	Failed at precrack site
27	"	136	" " " "
28	2000 gm	105	Failed at precrack site
29	"	118	" " " "
30	4000 gm	77	Failed at precrack site
31	"	82	" " " "

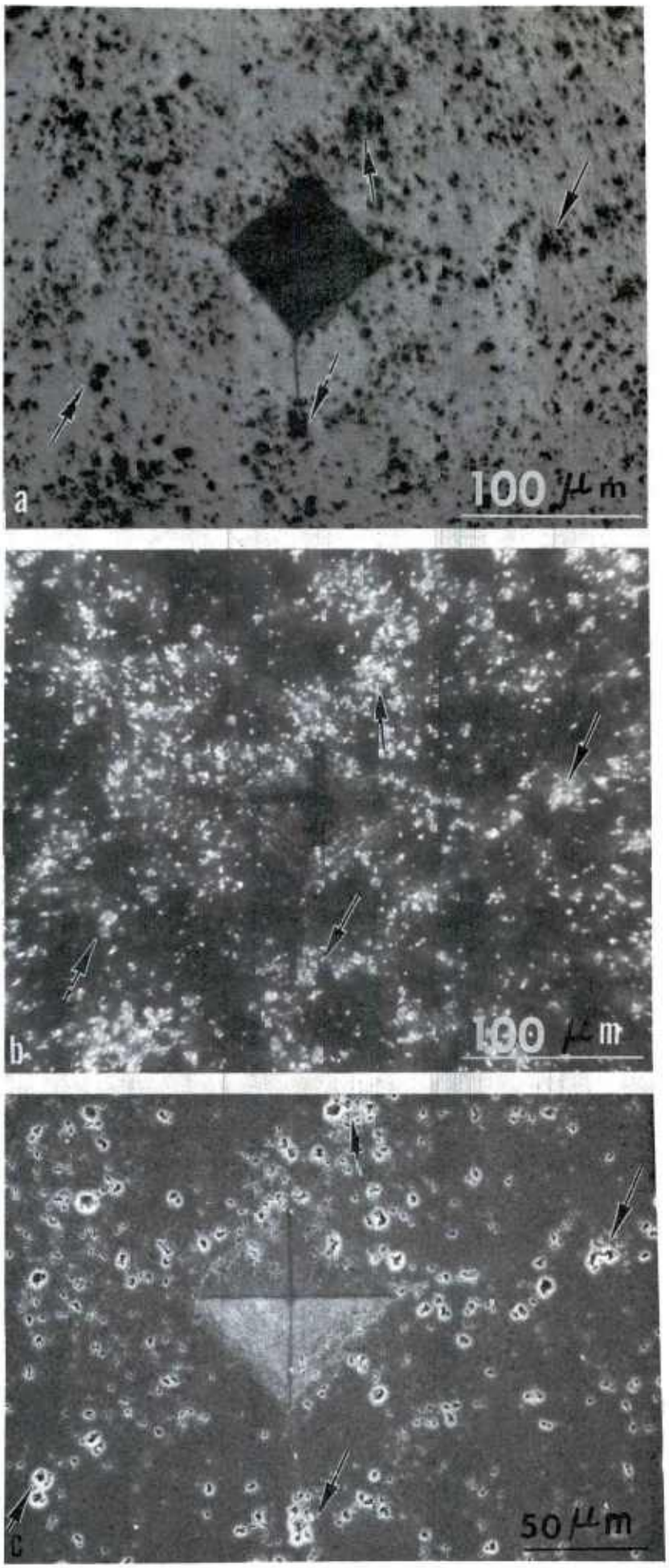

Fig. 20

Typical polished surface of a RBSN-NC-350 specimen showing the large distribution of porosity in the material. The Diamond indentation identifies the same region. Arrows in all three micrographs point to the identical sites. (a) Large distribution of black spots as seen on polished surface in normal white light. (b) Same area (a) seen in plane polarized light. Black spots as seen in (a) appear as 'white dots'. (c) Same area seen in SEM shows that the 'black spots' (a) and 'white spots' (b) are actually 'pores' in the material. Note the shape and size variation in pores.

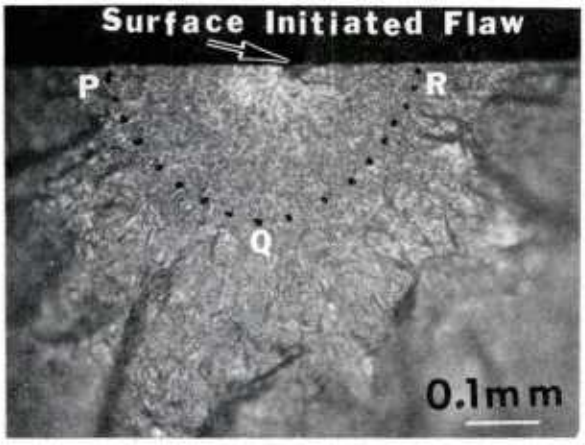

Fig. 21 Fracture surface of a RBSN-NC350 specimen (uncracked) tested at $20^{o}C$ showing surface initiated failure. The semi-circular, PQR, indicates the mirror region.

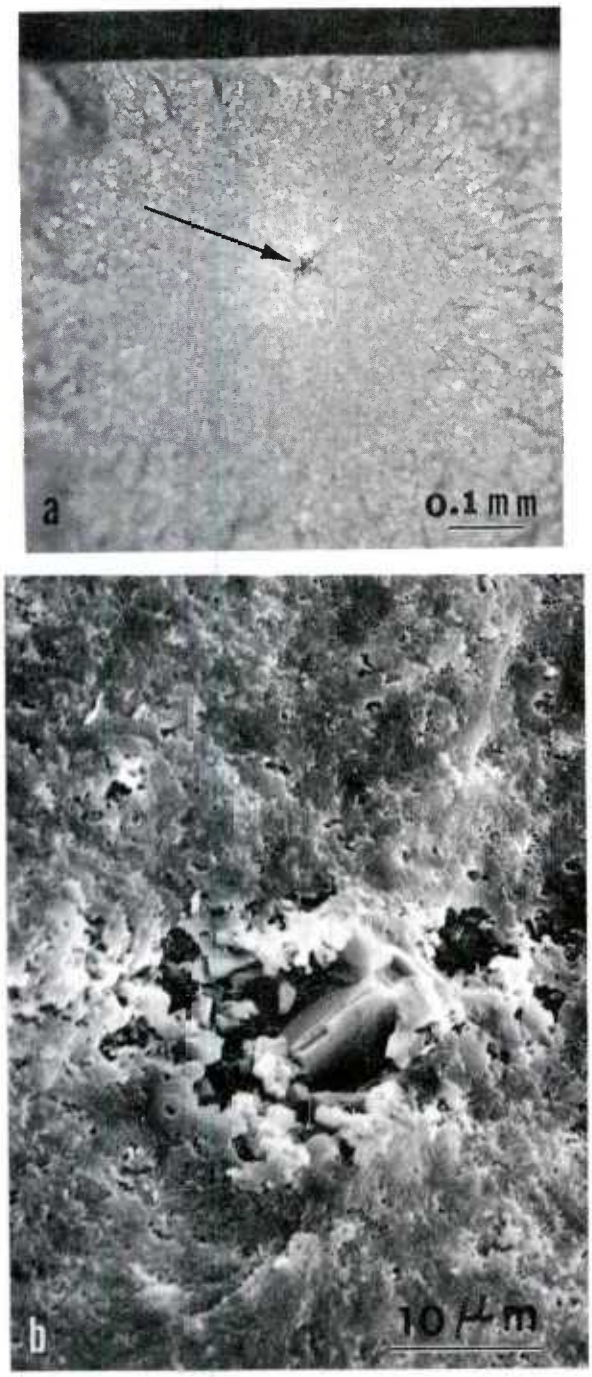

Fig. 22 (a) Fracture surface of a RBSN-NC350 specimen (uncracked) tested at 20°C showing failure initiation occurring at an "Internal Pore" site. (b) Above region seen in SEM shows clearly that the failure initiation site actually consists of several small pores joined internally together.

Typical example of a crack produced on the polished surface of a NC-350 RBSN specimen using the indentation induced flaw (IIF) method with a 4000 gm indentation load is shown in Fig. 23a. The corresponding fracture surface at 20°C for this specimen is shown in Fig. 23b and the precracked region is barely visible. Because of the high degree of porosity in the material, the precracked regions are difficult to distinguish. Note that the scatter in strength decreased considerably with the introduction of a large controlled surface flaw using the IIF technique. From the knowledge of flaw dimension, Fig. 23b, the corresponding magnitude of fracture stress and using Equations (10-12), the critical stress intensity factor, K_{IC}, for catastrophic failure was evaluated. The value of K_{IC} for NC-350 RBSN at 20°C is about 1.38 $MN/m^{3/2}$. This value does not take into account any residual stress [16] effects with indentation and that will be discussed later. An effort was made to estimate K_{IC} from the strength data obtained for as received (Table 7) specimens. Preliminary estimates of K_{IC} range from 1.0 to 1.6 $MN/m^{3/2}$ at 20°C. Comparable magnitudes of K_{IC} for a slightly higher density (2.5 gm/cm^3) NC-350 RBSN material were obtained in earlier studies [29]. A preliminary estimate of inherent flaw size in this material (density 2.4 gm/cm^3) appears to be from 10 to 40 microns depending upon the nature of pore distribution in the matrix. Recently, Moulson [30] has reviewed in great detail the processing and microstructural properties of RBSN.

4.1.2 Flexural Strength vs Temperature (Precracked Specimens)

NC-132 Si_3N_4

The temperature dependence of the fracture stress, σ_F, for uncracked (as received) specimens and for specimens precracked with a Vickers diamond pyramid indenter (4000 gm indentation load produced cracks of about 95 $\pm$ 5 μm deep) and Knoop indenter (2600 gm indentation load produced cracks of about 80 $\pm$ 5 μm deep), and tested at temperatures between 20 and 1400°C in air is shown in Fig. 24.* Data for precracked specimens are given in Table 8. It is clear that σ_F for precracked specimens remains essentially constant and independent of temperature from 20 to 1100°C. The constancy of σ_F suggests that no change in fracture mechanism occurs and indicates little or no blunting of the crack tip by plastic deformation in this temperature region. Typical fracture surfaces of precracked specimens tested at 20 and 1000°C are shown in Fig. 16, Sec. 4.1.1 earlier. Note that the mode of fracture in the precracked region (inside ACB, Fig. 16) and in the repropagated region (outside ACB, Fig. 16) is similar, i.e., a mixed mode of fracture consisting of transgranular and intergranular crack growth. The

*For the as received (uncracked) specimen, bars indicate the max. and min. values. A total of 34 MOR specimens were used (11 at 20°C and 3 at each other temperature and 2 at 1400°C, respectively. The curve is drawn through the lower limits where most of the data points fell. This curve does not represent the data shown in Table 1. All MOR specimens represented in Fig. 24 were from the same billet. Occasionally precracked specimens did not break at $\geq$1300°C and data for those specimens are not shown in Fig. 24.

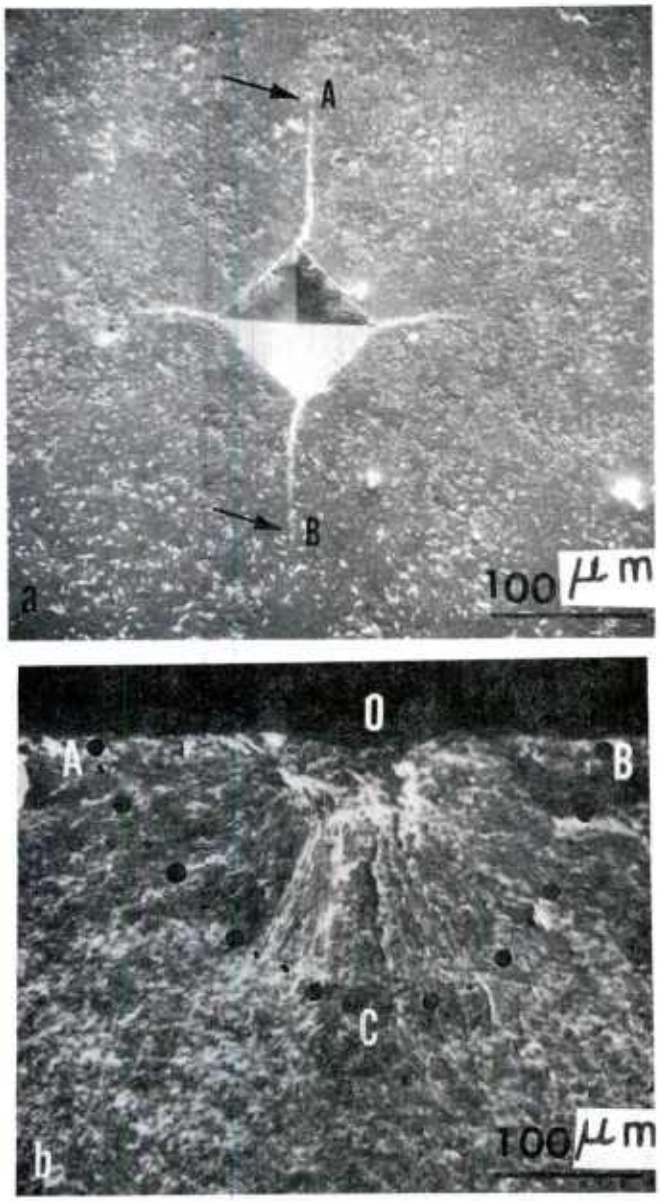

Fig. 23 (a) Typical example of a crack produced on the polished surface of a RBSN-NC350 specimen using a Vickers diamond pyramid indenter with 4000 gm load at 20°C as seen in SEM. (b) SEM micrograph of the fracture face for the precracked specimen shown in (a) and tested in flexural mode at 20°C. The precracked semicircular region, ACB, is not clearly distinguishable and black dots identify an approximate outline of the initial crack front boundary.

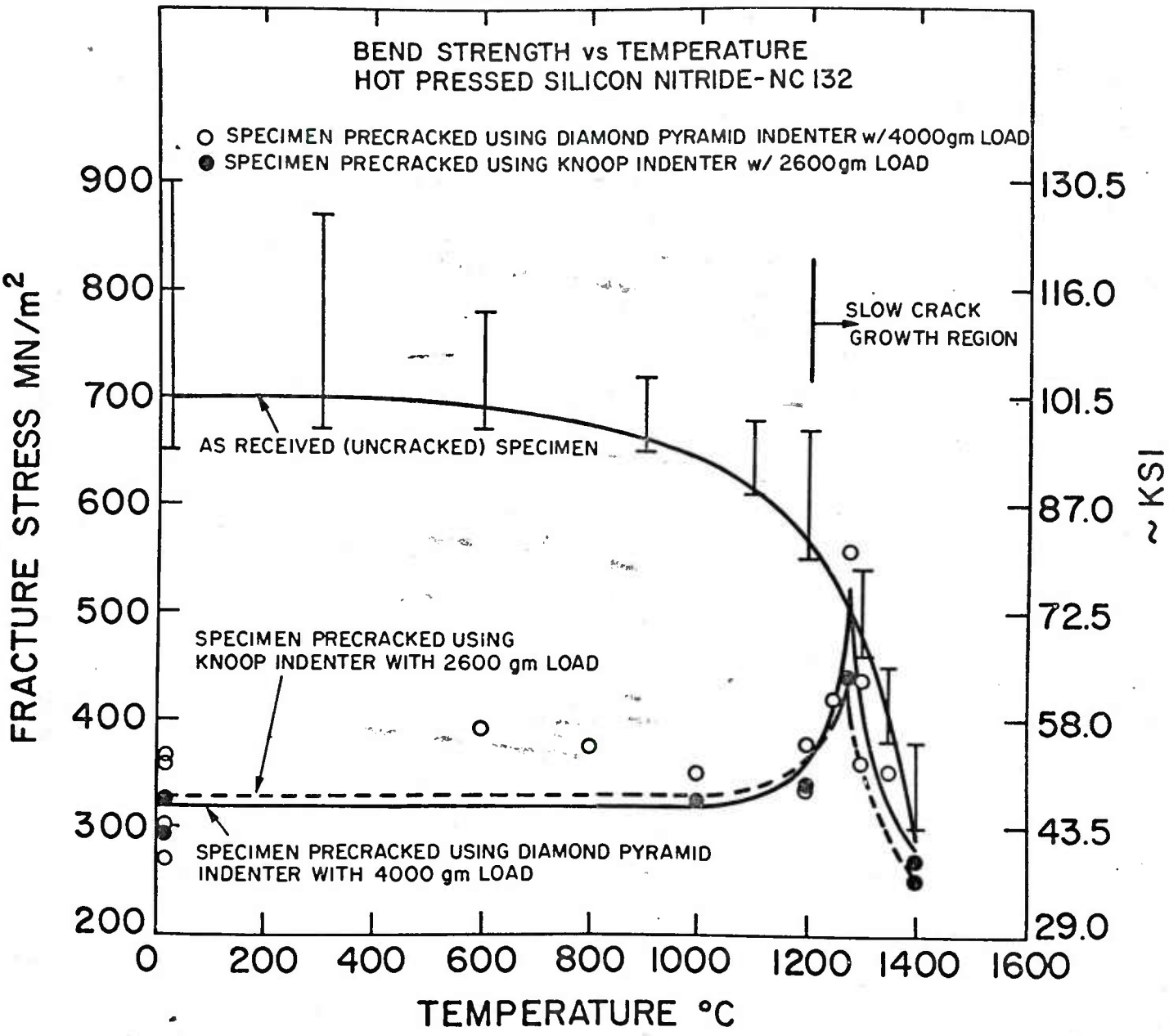

Fig. 24 Temperature dependence of the fracture stress for uncracked and precracked specimens of NC-132 Si_3N_4. Complete data for as received (uncracked) and precracked specimens are given in Table 9 and Table 8, respectively.

TABLE 8

FLEXURAL STRENGTH DATA AT HIGH TEMPERATURES
FOR PRECRACKED SPECIMENS OF NC-132 Si_3N_4

Spec. No.	Precracking Load	Test Temp.	Fracture Stress MN/m^2	Remarks
	USING VICKERS DIAMOND PYRAMID INDENTER			
31	4000 gm	600°C	392	Failed at crack site
32	"	800°C	375	" " " "
33	"	1000°C	350	" " " "
34	"	1200°C	334	" " " "
35	"	"	378	" " " "
36	"	1250°C	420	" " " "
37	"	1275°C	558	Showed Slow Crack Growth
38	"	1300°C	437	" " "
39	"	"	358	" " "
40	"	1350°C	353	" " "
		USING KNOOP INDENTER		
41	2600 gm	1000°C	325	Failed at crack site
42	"	1200°C	337	" " " "
43	"	1275°C	442	Showed Slow Crack Growth
44	"	1400°C	270	" " "
45	"	"	250	" " "

All the above specimens failed at crack site and were tested at a machine head speed of 0.005 in./min.

TABLE 9

FLEXURAL STRENGTH DATA FOR AS-RECEIVED (UNCRACKED) NC-132 Si_3N_4

Specimens as a function of temperature. Data shown in Figure 24. All specimens were tested at a machine head speed of 0.005"/min.

Spec. No.	Test Temp.	Fracture Stress $\sim$ MN/m^2	Remarks
1	20°C	686	Fast Fracture
2	"	649	
3	"	827	
4	"	810	
5	"	676	
6	"	924	
7	"	897	
8	"	882	
9	"	705	
10	"	715	
11	"	730	
12	300°C	710	
13	"	680	" "
14	"	860	
15	600°C	780	
16	"	700	" "
17	"	680	
18	900°C	689	
19	"	710	" "
20	"	660	
21	1100°C	666	
22	"	640	" "
23	"	615	
24	1200°C	674	
25	"	650	" "
26	"	550	
27	1300°C	520	Fracture faces showed slow crack growth
28	"	535	" " " " " "
29	"	460	" " " " " "
30	1350°C	417	" " " " " "
31	"	440	" " " " " "
32	"	380	" " " " " "
33	1400°C	361	Showed extensive slow crack growth
34	"	310	" " " " "

phenomenology of fracture in a similar type of material (HS-130 Si_3N_4) has been discussed in greater detail by Govila, Kinsman, and Beardmore [31]. The sudden and subsequent increase in σ_F at temperatures between 1100 and 1250°C, Fig. 24, is interpreted as indicative of blunting of the microcrack due to the viscous flow. It is believed that the softening of the glassy phases [32,33] at the grain boundary is a more likely mechanism of "crack blunting". Typical fracture surfaces of precracked specimens (containing cracks of about 95 ± 5 μm deep) tested at 1200, 1250 and 1275 and 1350°C are shown in Figs. 25a-d, respectively. The first signs of slow crack growth (SCG) of the initial microcrack were observed on the fracture face in tests made at 1275°C and higher temperatures, Fig. 25c, as indicated by the change in reflectivity. The extent of SCG prior to catastrophic failure increased with increasing temperature (cf. Fig. 25c-d). The SCG region is distinct in its appearance characterized by bright whitish regions. The nature and mode of fracture during SCG is completely intergranular (as discussed in Sections 2 and 5 of this report).

The fracture surface appearances at 1200 and 1250°C, Figs. 25a-b, are similar to that observed at lower temperatures (Figs. 16a-b, Sec. 4.1.1), and does not show the presence of SCG. Above 1250°C, SCG starts and σ_F decreases abruptly, Fig. 24, with a proportional increase in SCG region. The two curves (data for uncracked and precracked specimens), Fig. 24, seem to merge and show a decreasing strength above 1275°C. The temperature at which the two curves merge characterizes the importance of SCG and points out that failure is governed by the extent of SCG and not by initial crack size. It is fair to conclude from the study of precracked specimens that in NC-132 Si_3N_4 the temperature for the onset of SCG is around 1250°C**.

It should be noted that the Knoop indented precracked specimens behaved in a similar fashion as the Vickers diamond pyramid indented specimens, Fig. 24, and a typical fracture surface for a Knoop indented precracked specimen tested at 1275°C is shown in Fig. 26.

3.5% MgO FHPSN Material

Similar types of fracture studies were carried out in this material. A total of 24 MOR type specimens were precracked using a Vickers diamond pyramid indenter with 4000 gm indentation load and tested at temperatures ranging from 400 to 1300°C. Data for precracked specimens are given in Table 10. Even though all these specimens had essentially a constant crack size, yet large scatter in strength was observed, possibly due to the presence of a "mottled structure" as discussed earlier. Furthermore, crack blunting occurred at temperatures ≥ 1200°C and specimens did not break at the precrack site. Again, crack fronts on the fracture faces were not clearly visible and as such crack depths could not be measured. Considerable decrease in flexural strength occurred in tests made at temperatures > 1200°C with the onset of slow crack growth.

** This conclusion is primarily based on the fact that the speed of testing used in data given in Fig. 24 was 0.005 in./min. However, it is likely that the presence of SCG can occur at lower temperatures such as 1200°C if the crosshead speed of testing is one or two orders of magnitude slower or the material contains large amounts of impurities such as Ca, Fe, etc.

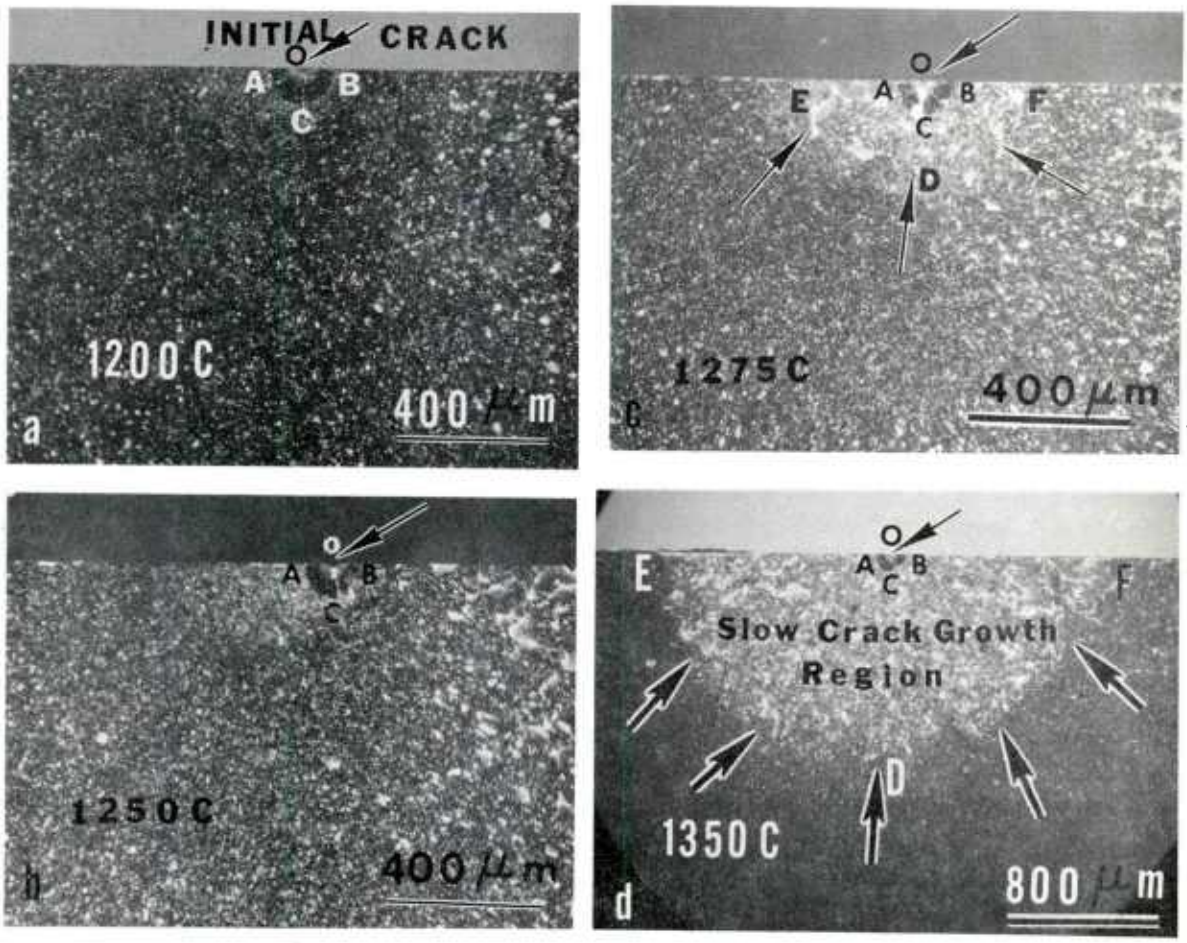

Fig. 25 Typical fracture surfaces of precracked (crack depth $\simeq 95 \pm 5\,\mu m$) NC-132 Si_3N_4 specimens tested in flexure mode at a machine head speed of 0.005 in/min at various temperatures. Pictures taken with plane polarized light. Note the absence of subcritical crack growth (SCG) at 1200° and $1250^{\circ}C$, subsequent appearance of SCG surrounding the initial crack, ACB, at $1275^{\circ}C$ and higher temperatures.

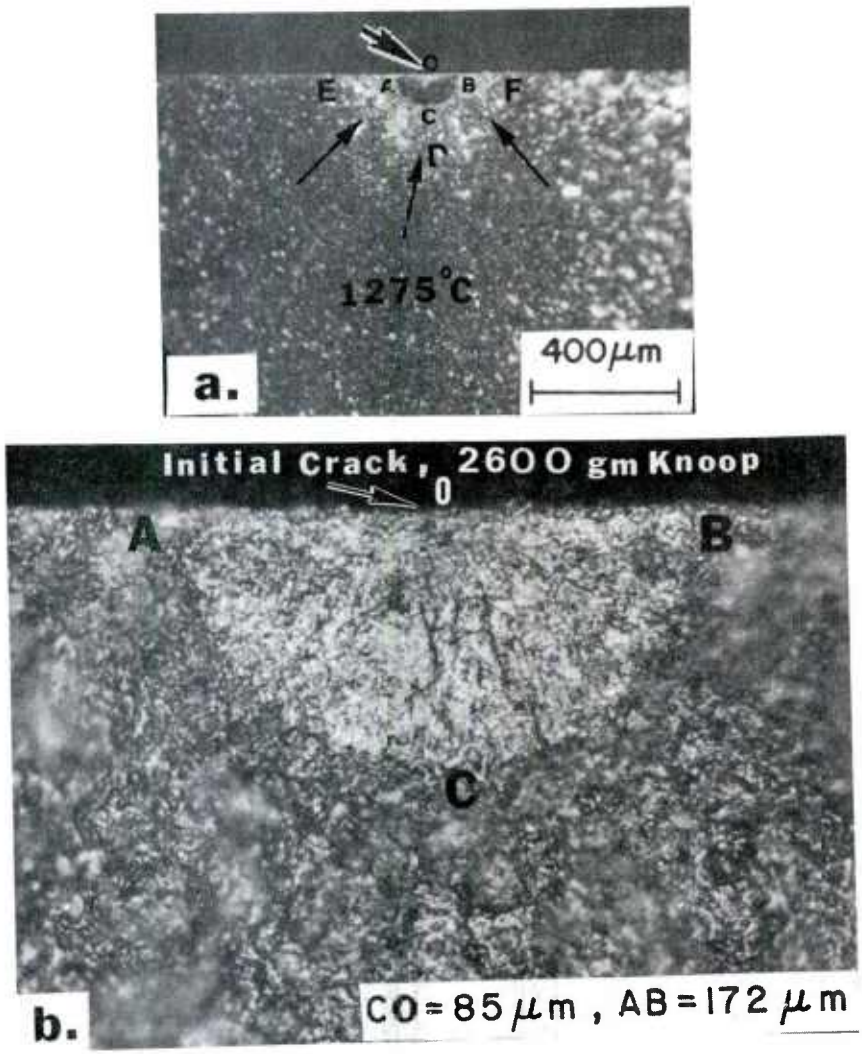

Fig. 26 Typical fracture surface of a NC-132 Si_3N_4 specimen, precracked with 2600 gm indentation load using Knoop indenter and tested in flexure at a machine head speed of 0.005 in./min at 1275°C in air. (a) Micrograph taken in plane polarized light. Note the appearance of SCG surrounding the initial crack, ACB. (b) Higher magnification view of the initial crack, ACB. Picture taken in normal white light.

TABLE 10

FLEXURAL STRENGTH DATA AT HIGH TEMPERATURES
FOR PRECRACKED SPECIMENS OF 3.5% MgO + Si_3N_4 (FHPSN)

Specimen No.	Precracking Load	Test Temp.	Fracture Stress, MN/m^2	Remarks
	USING VICKERS DIAMOND PYRAMID INDENTER			
32	4000 gm	400°C	368	Failed at crack site
33	"	"	412	" " " "
34	"	"	447	" " " "
35	"	600°C	365	" " " "
36	"	"	385	" " " "
37	"	800°C	343	" " " "
38	"	"	368	" " " "
39	"	"	383	" " " "
40	"	900°C	348	" " " "
41	"	"	368	" " " "
42	"	1000°C	368	" " " "
43	"	"	383	" " " "
44	"	"	402	" " " "
45	"	"	407	" " " "
46	"	1050°C	370	" " " "
47	"	1100°C	303	" " " "
48	"	"	371	" " " "
49	"	1150°C	358	" " " "
50	"	"	392	" " " "
51	"	1200°C	314	Did not fail at crack site
52	"	"	341	" " " " " "
53	"	"	366	" " " " " "
54	"	1250°C	268	Did not fail at crack site
55	"	1300°C	248	" " " " " "
56	none	20°C	532	As Received condition
57	"	"	636	" " "

4.1.3 Flexural Strain Rate Measurements (Precracked Specimens, NC-132 Si_3N_4)

Davidge et al. [4] suggested the use of flexural strain rate testing (similar to stress rate testing) in which the ratio of materials fracture strengths (σ_F) at two strain rates ($\dot{\varepsilon}$) for equal probability of failure is given by:

$$\frac{\sigma_{F_1}}{\sigma_{F_2}} = \left(\frac{\dot{\epsilon}_1}{\dot{\epsilon}_2}\right)^{1/n+1} \qquad (13)$$

where σ_{F1} and σ_{F2} are the fracture strengths at strain rates $\dot{\varepsilon}_1$ and $\dot{\varepsilon}_2$, respectively, and 'n' is the crack velocity exponent for SCG. The use of precracked specimens (IIF method) is particularly suitable in revealing the strain rate sensitivity of SCG qualitatively and also insuring equal probability of failure. This was done using specimens containing a constant crack size (about 55 ± 5 μm deep) and tested at varying temperatures and strain rates (or machined head speeds). Values of 'n' determined using Eq. (13) were 11 ± 1 at 1350 and 1400°C and ranged as high as 18-20 at 1300°C. Typical fracture surfaces in tests made at 1300, 1350 and 1400°C are shown in Figs. 27-29, respectively. Increasing the strain rate (or machine head speed) makes the material more brittle and initially raises the fracture stress. In agreement with this view, the extent (or depth) of SCG decreased with increasing the strain rate (see Figs. 27-29). Note that in all cases, Figs. 27-29, fracture was catastrophic.

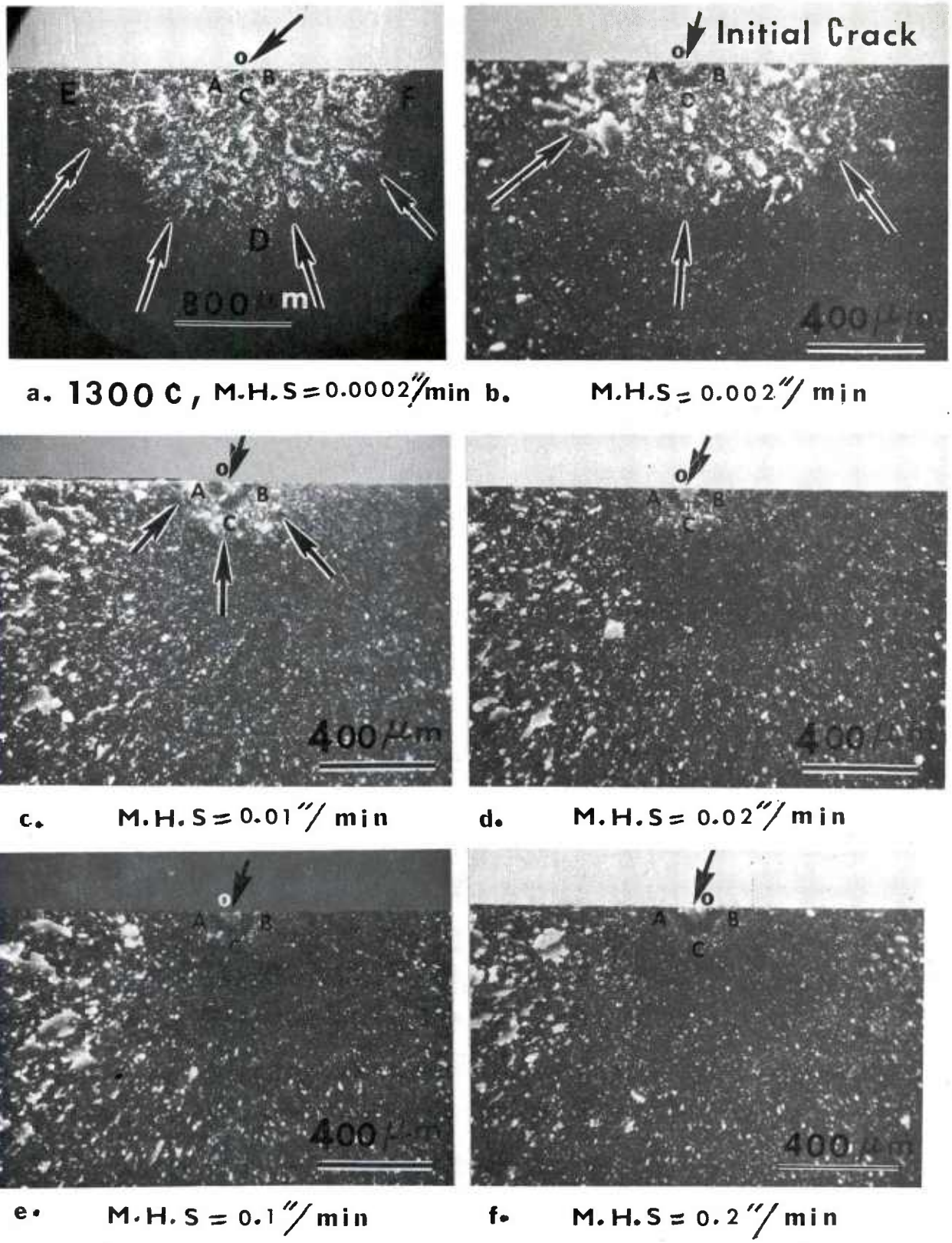

Fig. 27 Successive stages in the slow crack growth of precracked NC-132 Si_3N_4 (crack depth, CO $\simeq$ 95 + 5 μm) specimens tested in flexural mode at 1300°C in air, as a function of machine head speed. All specimens were precracked using a Vickers diamond pyramid indenter with 4000 gm load. Pictures taken in plane polarized light.

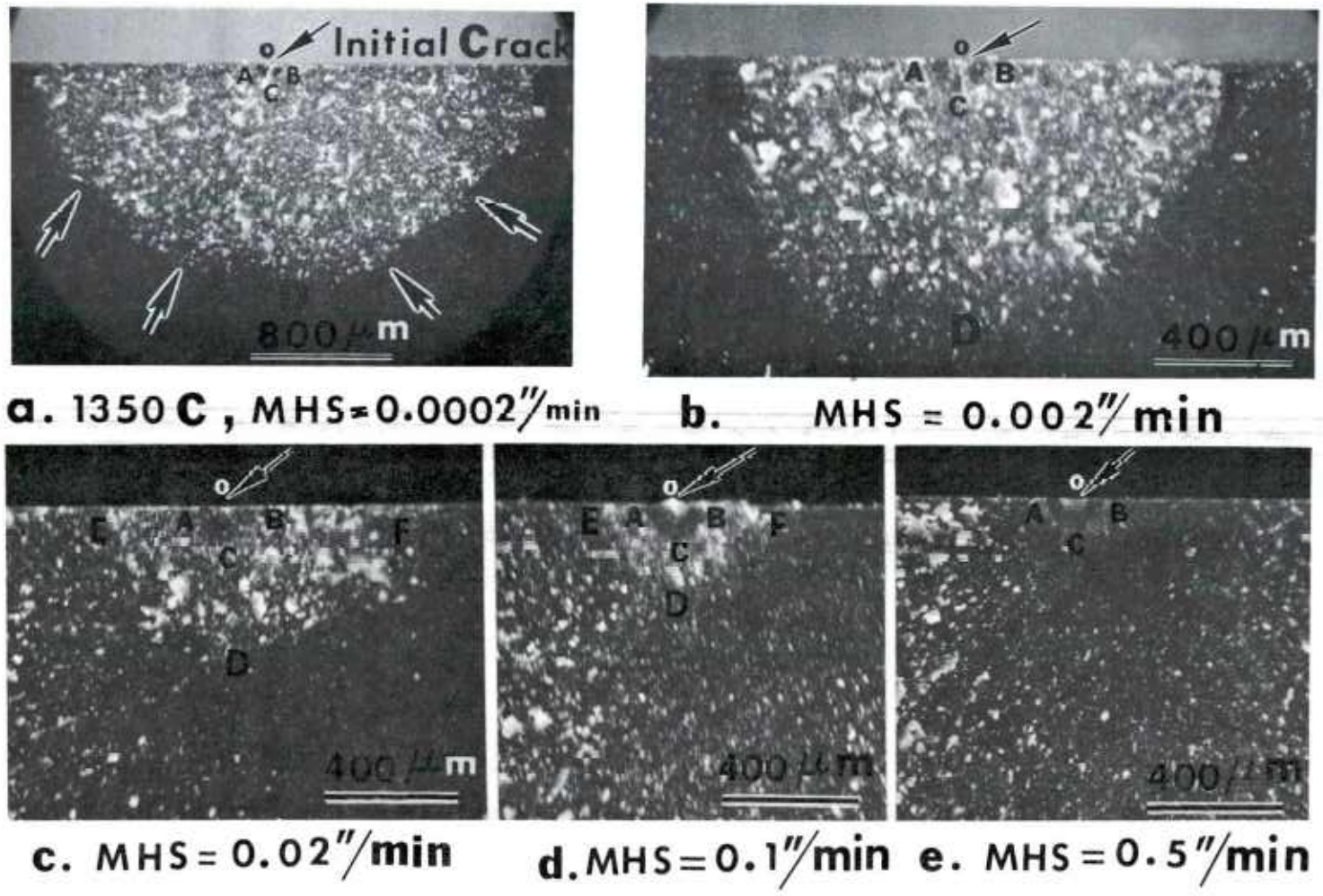

Fig. 28 Successive stages in the slow crack growth of precracked NC-132 Si_3N_4 (crack depth, CO ≃ 95 + 5 μm) specimens tested in flexural mode at 1350°C in air, as a function of machine head speed. All specimens were precracked using a Vickers diamond pyramid indenter with 4000 gm load. Pictures taken in plane polarized light.

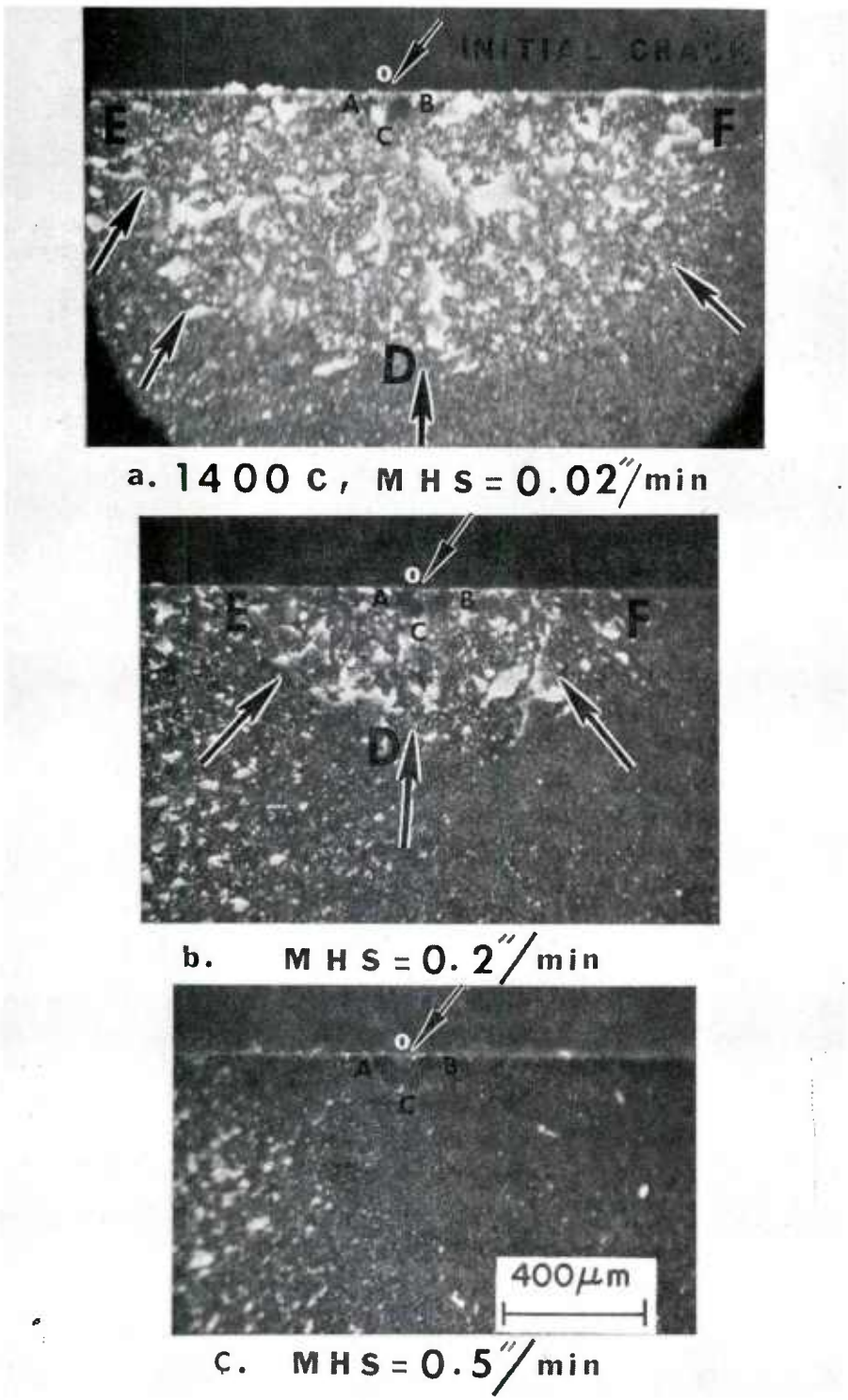

Fig. 29 Successive stages in the slow crack growth of precracked NC-132 Si_3N_4 (crack depth, CO $\simeq$ 95 + 5 μm) specimens tested in flexural mode at 1400°C in air, as a function of machine head speed. All specimens were precracked using a Vickers Diamond pyramid indentor with 4000 gm load. Pictures taken in plane polarized light.

4.1.4 Fracture Toughness Measurements

Room Temperature K_{IC} Evaluation

Typical fracture surfaces of precracked (IIF) specimens tested at 20 and 1000°C are shown in Figs. 16a and 16b (see 4.1.1), respectively. From the knowledge of flaw dimensions, the corresponding magnitudes of fracture stresses, Fig. 17, and using Eqs. (10-12), the critical stress intensity factor, K_{IC}*, for catastrophic failure was evaluated. The value of K_{IC} for NC-132 Si_3N_4 at 20°C is about 3.49 $MN/m^{3/2}$ and is independent of flaw depth due to a constant slope of the curve, Fig. 17. Petrovic, et al. [16] reported a value of $K_{IC} \approx 3.4$ $MN/m^{3/2}$ at 20°C for HS-130 Si_3N_4, using a similar (IIF) technique. It should be pointed out that this value does not take into account the effects of residual stresses [16] associated with IIF and discussed in the next section. It should be noted that the IIF method can be used only if the crack fronts as seen on fracture faces are clearly visible (like Figs. 16, 25-26) otherwise the technique does not allow an easy and accurate determination of K_{IC}. Since crack fronts were not clearly visible on the fracture faces in tests made at $\geq$ 20°C in 3.5% MgO + Si_3N_4 (FHPSN) material, therefore, no K_{IC} or K_I measurements were made.

High Temperature K_I Evaluation

High temperature K_I values were determined using both the DT and IIF methods and the variation of K_I as a function of temperature are shown in Fig. 30. The K_I values for the IIF method, Fig. 30, were calculated using the total depth of flaw, DO, Fig. 25 (initial flaw size, CO + slow crack growth, CD) at the onset of fast fracture and are only approximate in magnitude because plasticity correction factors and shape change in crack front in Eqs. (10-12) have not been taken into account. The variation of K_I as a function of temperature for both methods, Fig. 30, shows a similar form of behavior except values of K_I by DT method at high temperatures are slightly smaller in magnitude relative to IIF method. The reason for this discrepancy is simply due to the fact that faster machine head speeds, 0.2-0.5 in./min., were used in evaluating K_I by DT method while orders of magnitude slower machine head speeds (0.005 in./min.) were used with IIF method. It is clear from Fig. 30, that K_I remains essentially constant from 20 to 1100°C. In this temperature region, K_I is independent of plastic yielding effects and thus represent the critical stress intensity factor K_{IC}.

*A distinction should be made between K_{IC} and K_I. K_{IC} refers to that value of stress intensity when the normal stress at the crack tip reaches a critical value and leads to a catastrophic failure without undergoing any plastic deformation. Under these circumstances, K_{IC} is a material parameter. At high temperatures, when plastic deformation or subcritical crack growth (SCG) occurs prior to final catastrophic failure, stress intensity measured will be referred to as K_I.

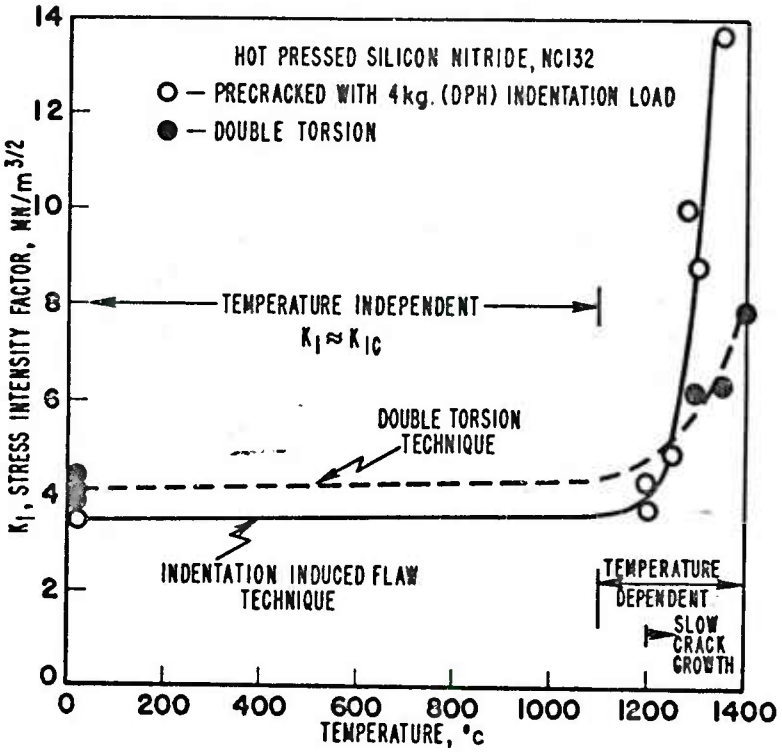

Fig. 30 Variation of stress intensity (nominal fracture toughness), K_I, as a function of temperature for NC-132 Si_3N_4 using Indentation Induced Flaw and Double Torsion techniques.

4.1.5 High Temperature Annealing Effects

As mentioned earlier, Petrovic, et al. [16] reported a value of $K_{IC} \approx 3.4$ MN/m$^{3/2}$ at 20°C for HS-130 Si_3N_4, using the IIF technique--these K_{IC} values were lower than values obtained using the double torsion [21] (4.7 MN/m$^{3/2}$) and double cantilever beam [26] (5.1 MN/m$^{3/2}$) methods in the same material. Furthermore, when precracked specimens were annealed at high temperatures (1000-1400°C) in air for 6 hrs. and subsequently tested in flexure at 20°C, they showed an increase in σ_F (with a corresponding increase in K_{IC}) comparable to those found by other workers [21,26]. In their study, fracture occurred at the flaw site in all annealed specimens. Therefore, Petrovic, et al. [16] suggested the presence of "residual stresses" (tensile at the crack front) in precracked IIF specimens and possible elimination by annealing at high temperatures (1200-1400°C). Similar suggestions have been made earlier by Ingelstrom and Nordberg [15] in their studies of cemented WC. Although it is equally probable that annealing removes the 'residual stresses' associated with microhardness indentation, we believe that it causes 'crack blunting' of precracked specimens, thereby increasing σ_F or K_{IC}. Metallographic evidence to support the "crack blunting" phenomenon due to annealing at high temperatures (1000-1400°C) will be presented in this study.

Test specimens of NC-132 Si_3N_4 were precracked with an approximate constant crack size (95 $\pm$ 5 μm), annealed in air at temperatures between 600-1400°C for 4 hrs. and subsequently tested in flexure at 20°C. The room temperature fracture stress, σ_F, variation as a function of annealing temperature is shown in Fig. 31, and complete data are given in Table 11. It is true that a significant increase in σ_F at 20°C occurred in specimens annealed at 1000 and 1200°C, Fig. 31, relative to room temperature strength of unannealed specimens. But in this study this increase in strength was noted only for those specimens which did not fail at the precrack site. The simple reason for this behavior was "crack blunting", possibly due to softening of the glassy phases in the Si_3N_4 matrix at these high temperatures (1000-1200°C). In addition, oxidation would also assist in blunting a sharp crack. The magnitude of σ_F would depend on the degree of crack blunting. Typical appearance of a crack on polished surface of a specimen after annealing for 4 hrs. at 1000°C is shown in Figs. 32a and 32b, for Vickers diamond pyramid and Knoop indentations, respectively. The crack is no longer visible on the surface (cf. Fig. 15b, and Fig. 32a) due to oxidation. Typical fracture surface for an annealed specimen at 1000°C (No. 6 in Table 11) which failed at the crack is shown in Fig. 33. Note the precracked region ACB is not clearly distinguishable (cf. Fig. 16b with Fig. 33) and the semi-circular crack front is diffused with the matrix possibly due to small disruptions of the grain boundary along the crack front. Similar behavior to a greater degree was observed in case of annealing at 1200°C. The phenomenon of "crack blunting" has been discussed in detail by Govila, Beardmore and Kinsman [34] for a number of ceramic materials (Si_3N_4, SiC, Sialons and LAS glass ceramic) which behaved basically in a similar fashion. Typical fracture appearance on the surface for a specimen which did not fail at the precrack site is shown in Fig. 34. In short, metallographic (qualitative) and quantitative (magnitude of σ_F) evidence has been presented to support the viewpoint that the increase in σ_F or K_{IC} after annealing is primarily due to 'crack blunting' and not necessarily due to removal of the tensile residual stress associated with microhardness indentation.

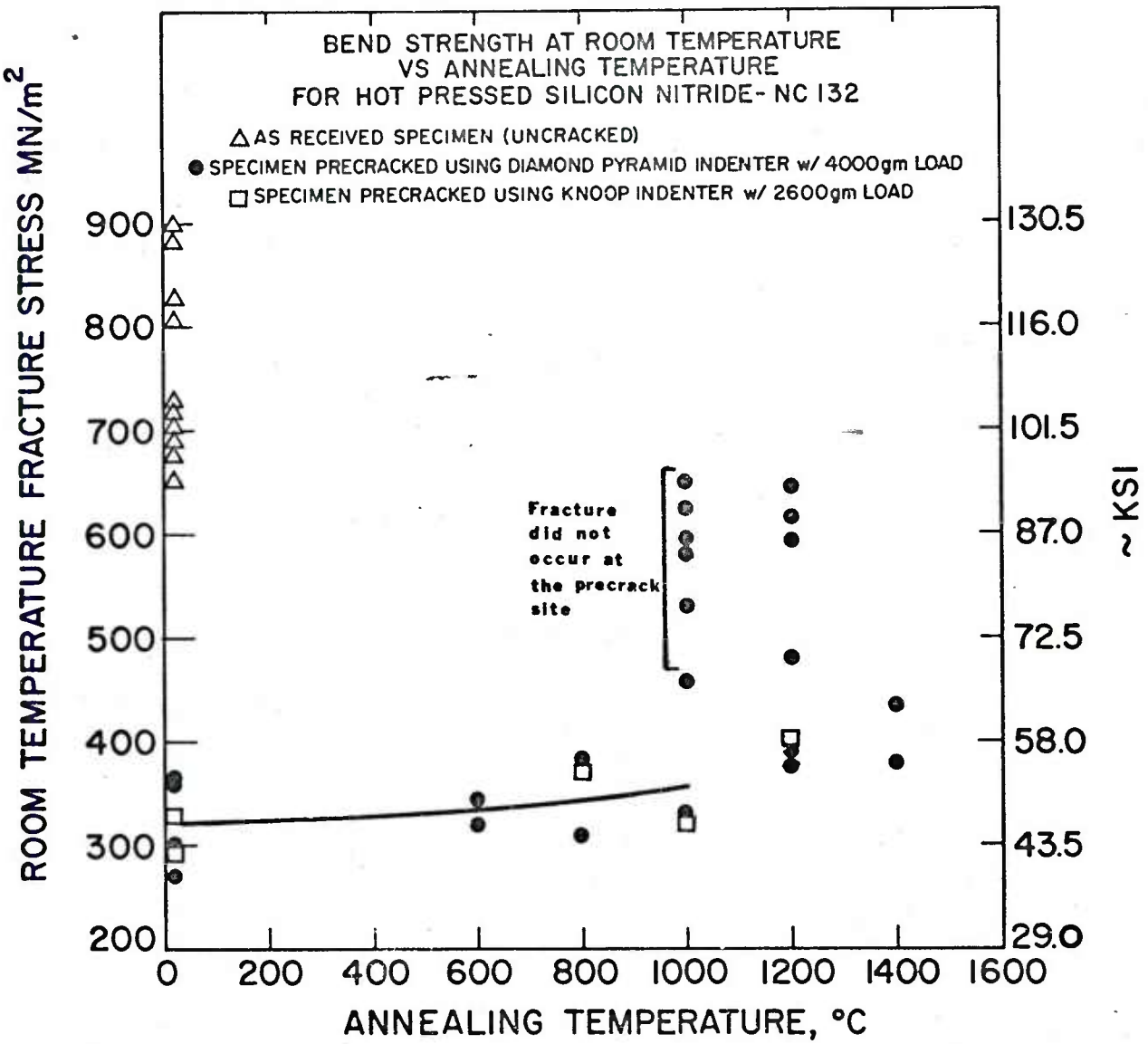

Fig. 31 Flexural strength (four-point bend) at room temperature for precracked specimens of NC-132 Si_3N_4 as a function of annealing temperature. Test specimens were annealed at temperatures (600 to 1400°C) for 4 hrs. in air. Data for as received specimens at 20°C are also included.

TABLE 11

FLEXURAL (4-POINT) STRENGTH VS. ANNEALING TEMPERATURE DATA FOR NC-132 Si_3N_4

Spec. No.	Precracking Load	Annealing Temp.	Fracture Stress at 20°C, MN/m^2	Remarks
		USING VICKERS DIAMOND PYRAMID INDENTER		
1	4000 gm	600°C	318	Failed at precrack site
2	"	"	343	" " " "
3	"	800°C	308	" " " "
4	"	"	383	" " " "
5	"	1000°C	329	" " " "
6	"	"	457	" " " "
7	"	"	580	Did not fail at precrack site
8	"	"	649	" " " " " "
9	"	"	531	" " " " " "
10	"	"	583	" " " " " "
11	"	"	595	" " " " " "
12	"	"	625	" " " " " "
13	"	1200°C	375	Failed at crack
14	"	"	392	" " "
15	"	"	481	Did not fail at precrack site
16	"	"	595	" " " " " "
17	"	"	615	" " " " " "
18	"	"	645	" " " " " "
19	"	1400°C	377	Failed at precrack site
20	"	"	434	" " " "
		USING KNOOP INDENTER		
21	2600 gm	800°C	372	Failed at precrack site
22	"	1000°C	322	" " " "
23	"	1200°C	398	" " " "

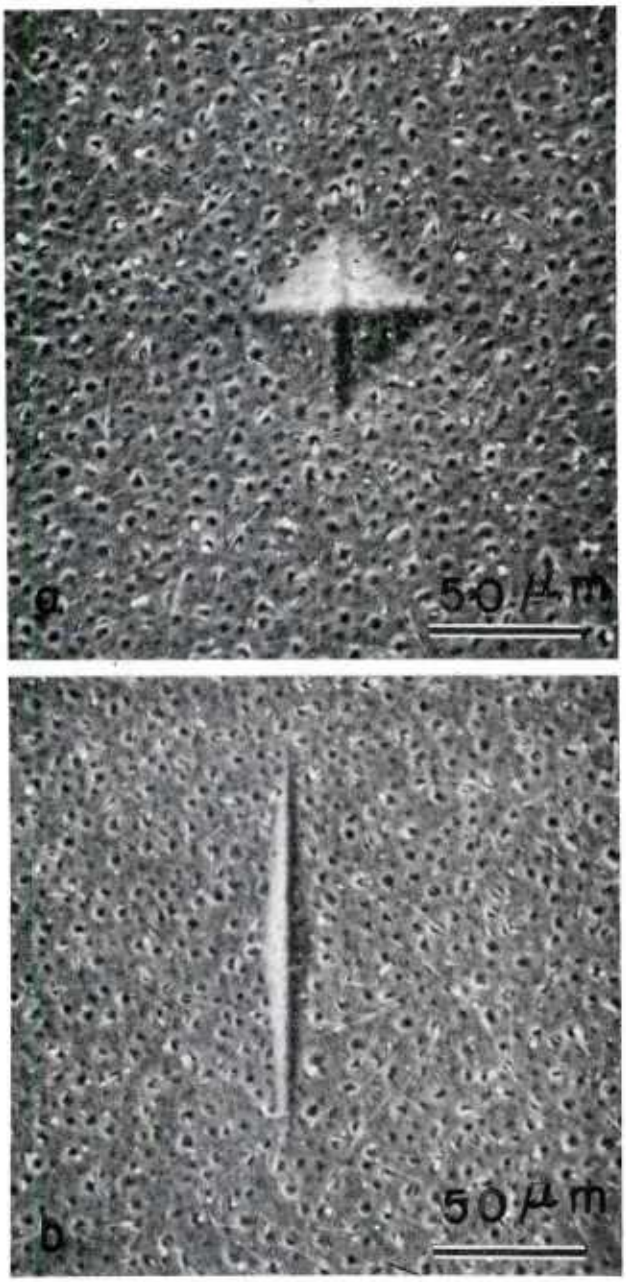

Fig. 32 Typical surface appearance after annealing at 1000°C for 4 hrs. in air for precracked specimens of NC-132 Si_3N_4 as seen in SEM. (a) A Vickers diamond pyramid indentation with 4000 gm load. (b) A Knoop indentation with 2600 gm load.

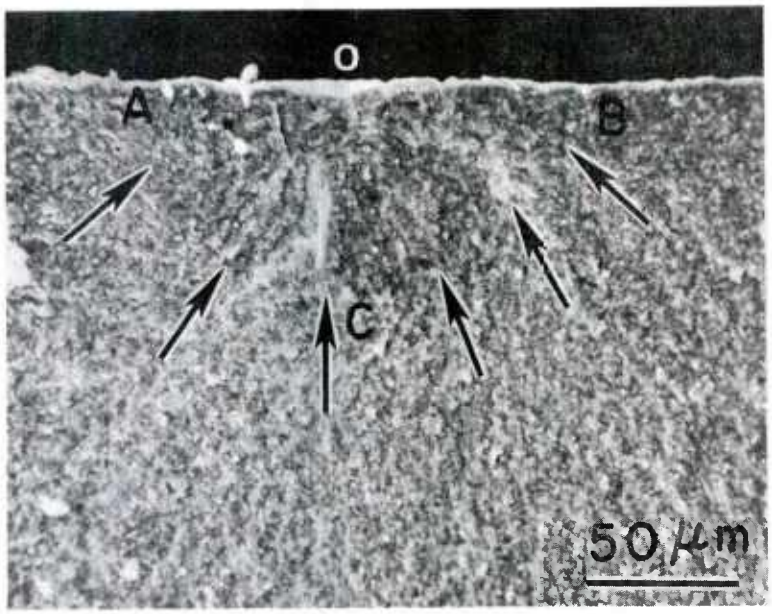

Fig. 33 Fracture surface as seen in SEM for precracked NC-132 Si_3N_4 (Vickers diamond indentation with 4000 gm load) specimen annealed in air at 1000°C for 4 hrs. and subsequently tested in flexure at 20°C. Note, the initial precracked region is not clearly distinguishable and the crack front boundary, ACB, is diffused with the matrix.

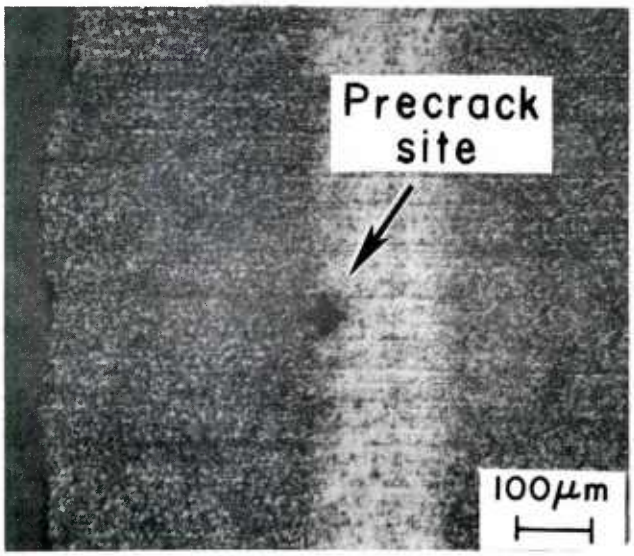

Fig. 34 Typical surface appearance for precracked (Vickers diamond pyramid indentation with 4000 gm load) NC-132 Si_3N_4 specimen annealed in air at 1000°C for 4 hrs. and subsequently tested in flexure at 20°C. Note the specimen did not fail at the precrack site, but failed away (to the left).

4.2 Double Torsion Method and Analysis

The double torsion (DT) specimens used were approximately 3 in. ($\sim$ 75 mm) long, 1 in. ($\sim$ 25 mm) wide and 0.050 in. ($\sim$ 1.25 mm) thick. A schematic of the DT specimen and loading configuration is shown in Fig. 35. A prerequisite of the DT test is the presence of a precrack in the test specimen with a crack length of approximately one-half the width of the specimen [35]. For crack velocity and corresponding stress intensity measurements, it is the precrack which is to be repropagated at test temperature. Normally a very fine notch or slit is made in the center of a DT specimen in order to facilitate the initiation of a precrack when loaded in the DT fixture. The notch or slit is usually accompanied by a narrow groove along the central length of the specimen to guide crack propagation. The groove depth was varied from 0.005 in. ($\sim$ 0.127 mm) to 0.010 in. ($\sim$ 0.254 mm). The DT testing fixture used, Fig. 35, was similar in design to that used by Evans and Wiederhorn [21] and made from hot-pressed SiC. Complete details regarding the use of this technique have been reviewed by others [21,22,35-39].

Stress Intensity, K_I, Evaluation

The stress intensity factor, K_I, for a DT specimen [37] of an elastic material under plane stress conditions is given by:

$$K_I = P W_m \left[\frac{3(1+\nu)}{W d^3 d_n} \right]^{1/2} \qquad (14)$$

where P is the applied load, ν is Poisson's ratio, W_m, W, d and d_n are specimen dimensions shown in Fig. 35. Note that K_I depends only on the applied load P, specimen dimensions and Poisson's ratio, and is independent of crack length. It is this feature that makes the DT test very popular for making SCG studies.

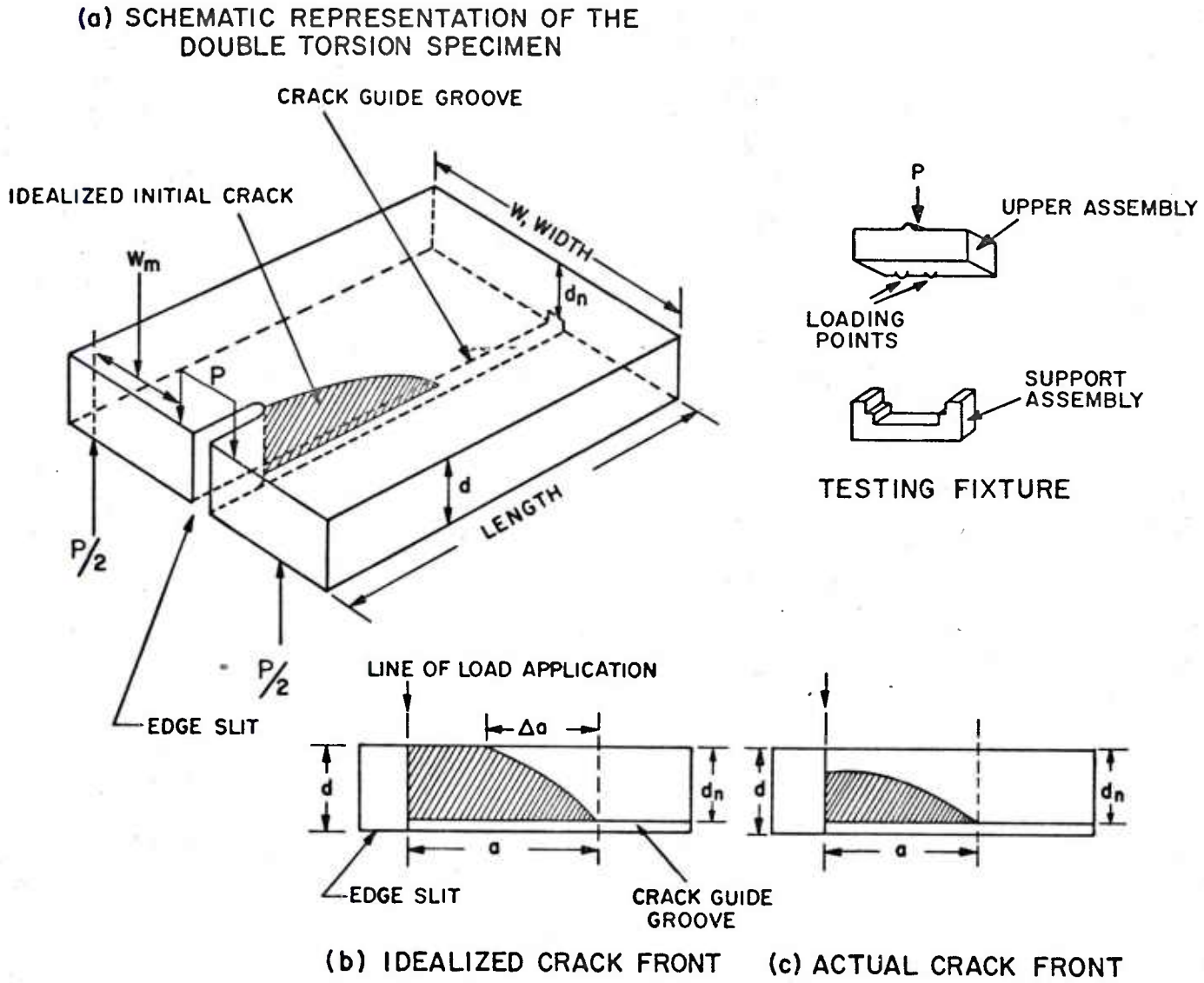

Fig. 35 Schematic display of double torsion specimen and testing fixture.

Crack Velocity, V, Evaluation

The stress intensity-crack velocity data were obtained by the load-relaxation method as applicable to the DT technique. In this, a sharp crack is initiated, the DT specimen is reloaded in the testing fixture in the Instron testing machine at a fast speed, the machine crosshead is stopped, and the load-relaxation recorded on the chart recorder. Following the work of Evans [36] and others [21, 37-39], the crack velocity, V = da/dt at a particular load P is computed from the rate of load relaxation (at constant displacement dy/dt = 0, y is the displacement of loading points or the elastic specimen deflection) is given by:

$$V = -\frac{da}{dt} = -\phi \frac{P_{i,f}}{P^2}\left(a_{i,f} + \frac{C}{B}\right)\left(\frac{dP}{dt}\right)_y \qquad (15)$$

where $P_{i,f}$ is the initial (or final) load, P is the instantaneous load, $a_{i,f}$ is the initial (or final) crack length, and B and C are constants relating to the slope and intercept of a compliance analysis calibration curve of the DT specimen and ϕ is a geometrical factor relating to crack front profile [36], Fig. 35. Assuming that the initial crack is large and contributions due to various constants (as indicated in Eq. 15) are small, the crack velocity expression can be further simplified and given as follows:

$$V = -\frac{P_{i,f}\, a_{i,f}}{P^2}\left(\frac{dP}{dt}\right)_y \qquad (16)$$

In general, the following method was used for measuring K_I and V from the DT specimen:

(a) After placing the DT specimen in the test fixture, it is loaded in the Instron machine at a slow crosshead speed of 0.001 in. ($\sim$ 0.0254 mm) per min. at room temperature (or higher temperature) in air. The Instron machine is kept running until a sudden load drop occurs indicating the nucleation or pop-in of a precrack and immediately the crack is arrested by stopping the machine crosshead speed. The specimen is unloaded at a fast crosshead speed in order to examine the precrack on the surface. The corresponding loads for crack pop-in and arrest are designated P_0 and P_A, respectively. When the initial crack is nucleated at a higher temperature such as 1300 or 1400°C, the load-deflection curve does not show a sudden load drop but simply rounds off at the maximum load and a rapid decrease in load occurs indicating the nucleation of a crack. The precracking method is shown schematically in Fig. 36(a).

(b) For K_{IC} determination the precracked specimen is reloaded in the Instron machine at a fast crosshead speed of 0.10 in. ($\sim$ 2.54 mm) or 0.5 in. ($\sim$ 12.7 mm) per min. at the desired test temperature and the fracture load, P_C, for catastrophic crack propagation is measured. This load is usually slightly smaller than the load P_0. Schematic representation is shown in Fig. 36(d).

(c) For crack velocity measurements, the DT specimen containing the initial crack is reloaded at a fast crosshead speed of 0.1 in. ($\sim$ 2.54 mm) per min. to some load P such that $P_A < P < P_0$, at the desired test temperature and the crosshead stopped to get the load-relaxation curve, Fig. 36(b). Using Eq. (16) and the load relaxation curve, the crack velocity V can be calculated. It should be noted that usually the total load drop during load-relaxation is very small (3 to 10 lbs.) and a major part of load-drop and the associated crack growth occurs during the very initial part of the relaxation curve and this limits the number of data points for which the slope $(dP/dt)_y$ (see Eq. (16) can be measured accurately.

The DT test appears simple but in our work a number of experimental difficulties were encountered as summarized briefly below:

(1) The initiation of the precrack at 20°C often does not occur inside the leading groove, but occurs tangential to it. Upon repropagation, the initial crack (precrack) runs out to the side instead of following the straight path and such tests were considered unsuccessful. This behavior was observed in both grooved and ungrooved specimens and typical examples are shown in Figs. 37 (a-d) while Fig. 37(e) shows crack propagating centrally all

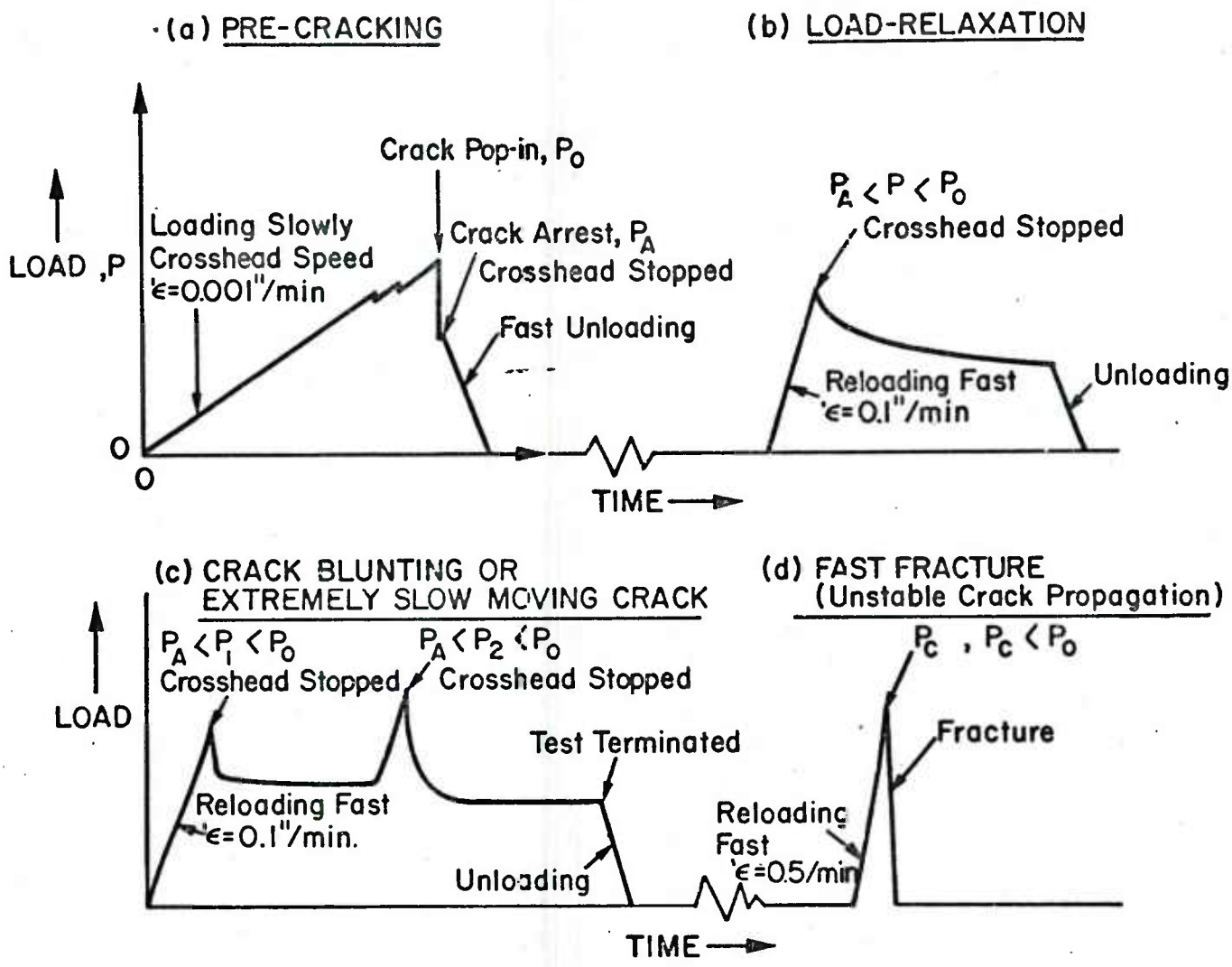

Fig. 36 Schematic representation of the several steps involved in testing a double torsion specimen.

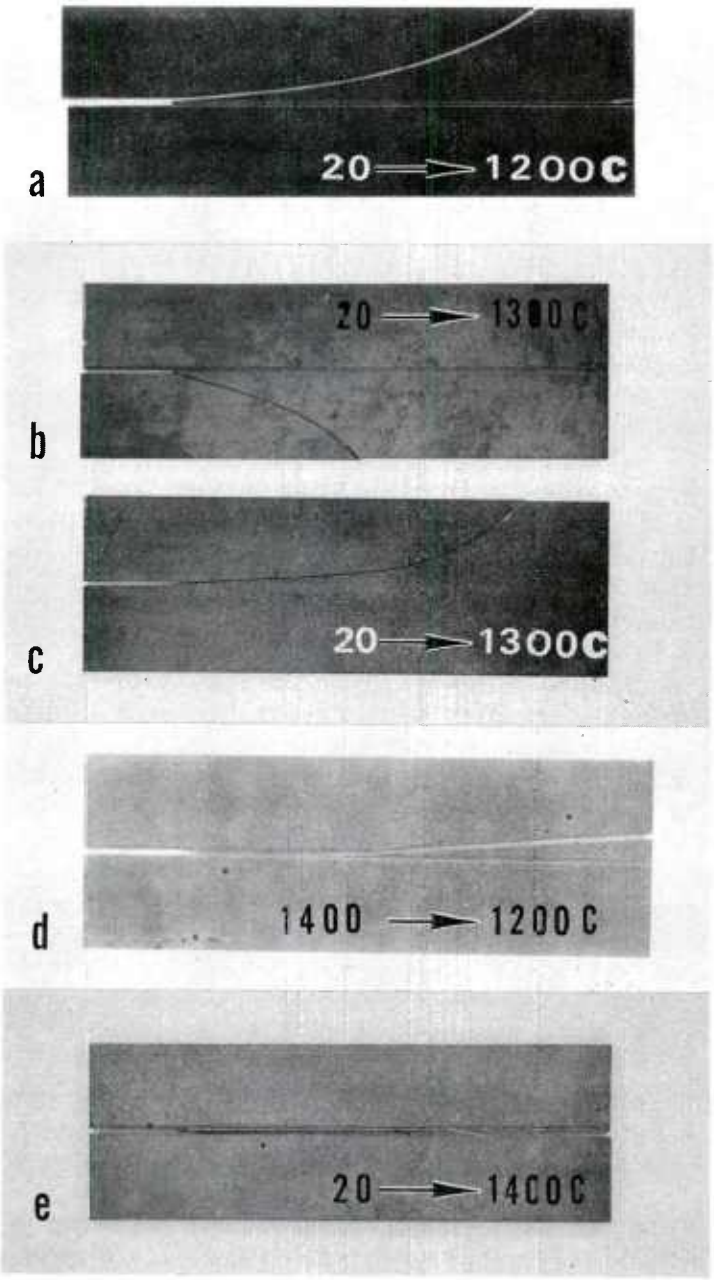

Fig. 37 Crack initiation and repropagation behavior in double torsion specimens of NC-132 Si_3N_4. (a) Crack initiated at 20°C, repropagated at 1200°C. Upon repropagation, the initial crack did not follow the lead groove and curved out. (b-c) In both cases, the initial crack was produced at 20°C, repropagated at 1300°C and curved out. (d) Initial crack was produced at 1400°C and repropagated at 1200°C. For some distance, the initial crack propagated inside the lead groove and later curved out. All DT specimens which displayed the behavior as shown in (a-d) were considered as unsuccessful tests. (e) Initial crack was produced at 20°C and repropagated at 1400°C. Crack propagated centrally all through the length of the specimen and a successful load-relaxation curve was obtained. Such tests were considered good.

through the length of the specimen. In measuring K_{IC}, only those tests were considered successful in which the crack propagated centrally all through the length of the specimen as displayed by Fig. 37(e).

(2) The initial crack which is nucleated or produced during pop-in, Fig. 36(a) is often discontinuous and broken along its length Fig. 38(a) and uncracked material is bridged along its length, Fig. 38(b). During repropagation of such cracks for fast fracture to measure K_{IC}, it is possible that small amounts of elastic energy are first consumed in breaking apart this joined material and thereby raising the value of critical load, P_c (Fig. 36(d)),to failure

(3) Often during the load-relaxation curve, the moving crack gets blunted at the tip either due to plastic deformation or crack branching, Fig. 36(c), which then leads to an unsuccessful load relaxation curve. Typical fracture surface of a DT specimen which behaved in a similar fashion as displayed schematically in Fig. 36(c), is shown in Fig. 39. Note the tip of the initial room temperature crack is blunted (position B) due to cleavage steps produced by machining of the groove. The behavior shown in Fig. 36(c) could also occur without crack blunting if the crack velocities are extremely low. In this study crack velocity measurements are made only from those tests which displayed a continuously decreasing load-relaxation curve like the one schematically shown in Fig. 36(b), crack propagating centrally for a significant length (at least twice or more the initial crack length), and finally upon fast fracture the crack propagated centrally all through the length.

4.2.1 Stress Intensity Measurements

A total of 52 DT specimens of NC-132 Si_3N_4 were tested at various temperatures between 20-1400°C and complete data are given in Table 12. Typical fracture surfaces* of DT specimens tested at 20°C are shown in Figs. 40(a-c). Values of K_{IC} for fast fracture were determined using Eq. (14) as given in Table 12 and varied from 3.9 to 4.4 $MN/m^{3/2}$, resulting in an average value of about 4.1 $MN/m^{3/2}$. Evans and Wiederhorn [21]

*Note that the fracture surface at 20°C seen in Fig. 40(a), shows three crack fronts, the first two crack fronts--B_1B and C_1C are due to small load drops which occur sometimes during initial loading, Fig. 36(a), and the crack front D_1D represents the large load drop corresponding to crack pop-in at which time the crack is arrested. Similar behavior occurred in Fig.40(b), which showed six crack fronts, while Fig.40(c), showed a single crack front corresponding to crack pop-in.

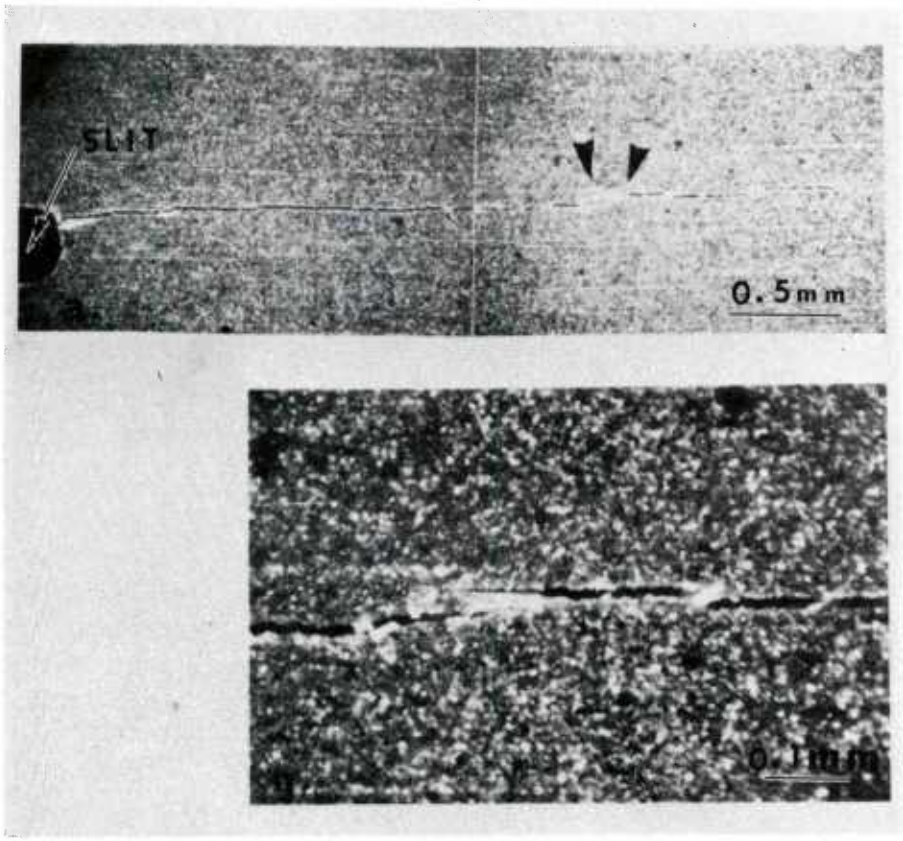

Fig. 38 (a) Tension side of a double torsion specimen in which the crack was initiated at 1350°C, showing discontinuous nature of initial crack. (b) Enlarged view of area marked with arrows in (a); crack is broken, and uncracked material is bridged along its length.

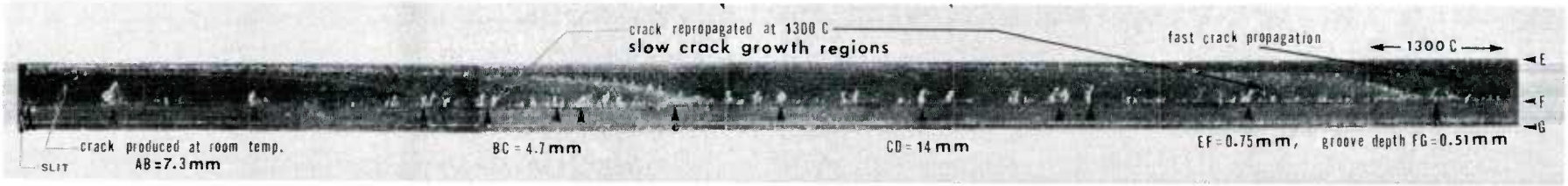

(72)

Fig. 39 Fracture surface of a double torsion specimen in which the initial crack was produced at 20°C. Upon repropagation the crack at 1300°C, the test specimen produced a load-relaxation curve similar to that shown schematically in Fig. 36 (c). Upon fast crack propagation at 1300°C, the crack curved out. Note the damage (cleavage steps or fine cracks) which occurred all along the groove length (as pointed out by small vertical arrows) due to machining.

TABLE 12

DOUBLE TORSION DATA FOR HOT-PRESSED SILICON NITRIDE, NC-132

Specimen No. & Condition	Crack Initiation Temp.	Crack Repropagation Temp.	Stress Intensity, $MN/m^{3/2}$		Remarks
			K_{IC}	K_I	
1-2 No Groove	20°C	20°C	-	-	Failed during loading
3 No Groove	20°C	20°C	3.9	-	Crack propagated centrally
4 No Groove	20°C	20°C	4.4	-	Crack propagated centrally
5 No Groove	20°C	20°C	4.15	-	Crack propagated centrally
6 Grooved (0.127 mm)	20°C	20°C	4.06	-	Crack propagated centrally
7-9 Grooved (0.127 mm)	20°C	20°C	-	-	Crack curved out
10-12 No Groove	20°C	20°C	-	-	Crack curved out
13-23 Grooved (0.127 mm)	20°C	1200°C	-	-	Crack curved out
24-29 Grooved (0.127 mm)	20°C	1300°C	-	-	Crack curved out
30-31 Grooved (0.20 mm)	20°C	1300°C	-	-	Crack blunted & curved out
32-33 Grooved (0.30 mm)	20°C	1300°C	-	-	Crack blunted & curved out
34 Grooved (0.51 mm)	20°C	1300°C	-	-	Crack blunted & curved out
35 Grooved (0.64 mm)	20°C	1300°C	-	-	Crack blunted & curved out
36-38 Grooved (0.127 mm)	20°C	1350°C	-	-	Crack blunted & curved out
39 Grooved (0.127 mm)	20°C	1400°C	-	7.87	Crack propagated centrally
40 Grooved (0.127 mm)	1200°C	1200°C	-	-	Crack curved out
41 Grooved (0.127 mm)	1300°C	20°C	-	5.46	Fast fracture centrally
42 Grooved (0.127 mm)	1300°C	20°C	-	-	Crack curved out
43 Grooved (0.127 mm)	1300°C	1200°C	-	-	Crack curved out
44-46 Grooved (0.127 mm)	1300°C	1300°C	-	-	Crack curved out
47 No Groove	1350°C	20°C	-	6.63	Fast fracture centrally
48 Grooved (0.31 mm)	1350°C	1350°C	-	6.40	Crack propagated centrally
49 Grooved (0.127 mm)	1400°C	1200°C	-	-	Crack curved out
50 Grooved (0.127 mm)	1400°C	1300°C	-	6.34	Fast fracture centrally
51 Grooved (0.127 mm)	1400°C	1300°C	-	6.6	Crack propagated centrally
52 Grooved (0.127 mm)	1400°C	1300°C	-	6.34	Crack propagated centrally

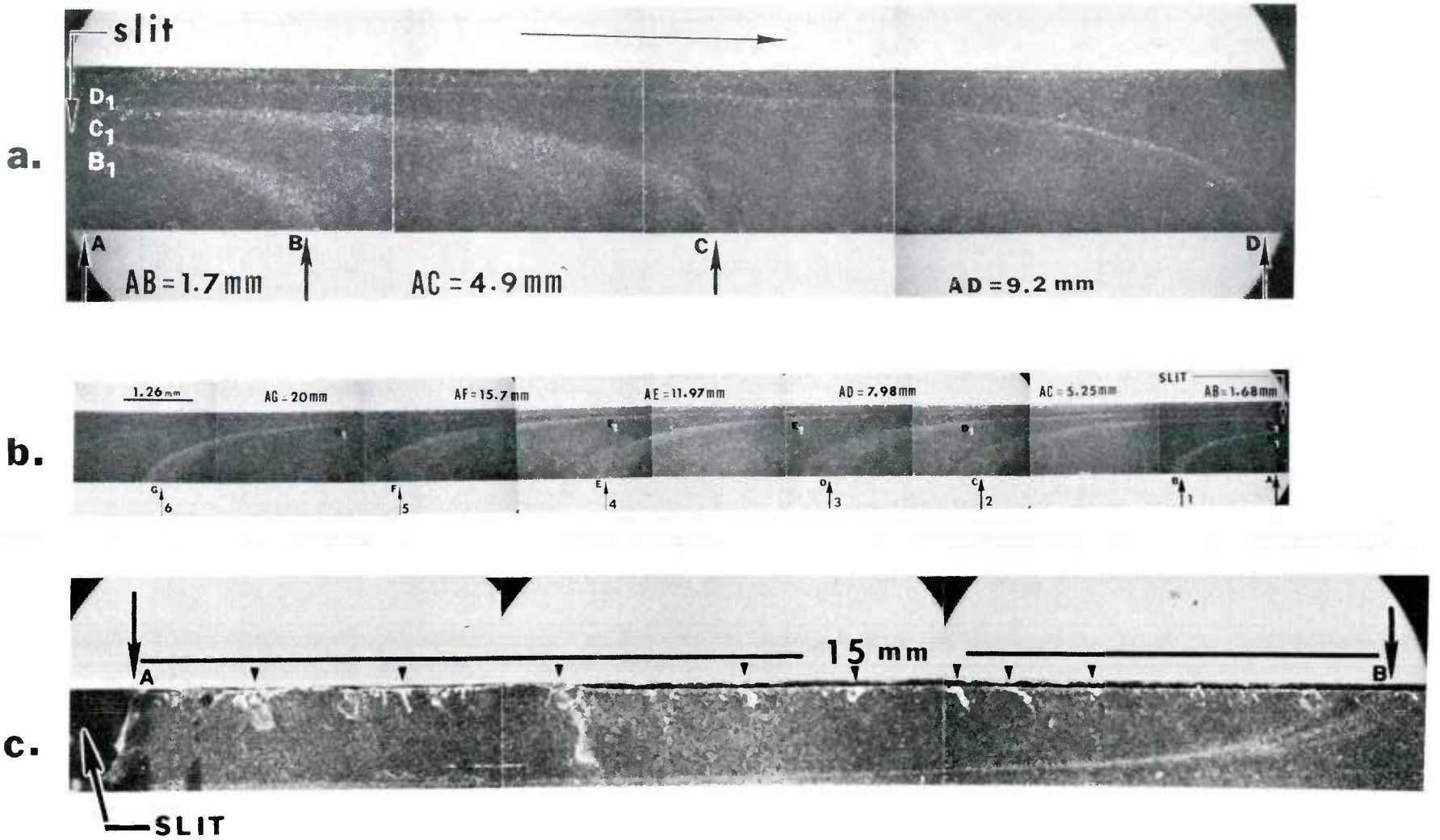

Fig. 40 Fracture surfaces of double torsion NC-132 Si_3N_4 specimens in which the initial crack was produced at 20°C and subsequently repropagated rapidly at 20°C for unstable crack propagation (catastrophic failure) determine K_{IC}. Crack propagated centrally all through the length of the specimen. Horizontal arrows show the direction of crack propagation. (a) shows three crack fronts; the first two crack fronts B_1B and C_1C were due to small load drops which occured during initial loading of the specimen. (b) shows six crack fronts; the first five crack fronts were due to small load drops which occurred during initial loading before crack pop-in at which time the large load drop occurred to crack front AG. (c) Grooved specimen showing a single crack front, AB. Note the damage which occurred along the groove length due to machining.

using this technique in HS-130 Si_3N_4, found K_{IC} at 20°C to vary from 4.2 to 5.3 $MN/m^{3/2}$ with an average value of 4.7 $MN/m^{3/2}$, while Lange [26] reported a value of 5.1 $MN/m^{3/2}$ using the double cantilever beam method. Considering the fact that the two hot-pressed silicon nitrides NC-132 and HS-130 differ slightly in chemical composition and strength, the difference in K_{IC} values determined using the common DT technique is within reasonable limits.

High temperature K_I values were also determined using the DT method, data shown in Table 12, and the variation of K_I as a function of temperature is shown in Fig. 30 (Sect. 4.1.4). Typical fracture surfaces of DT specimens at high temperatures (1350-1400°C) are shown in Figs.41a and 41b, respectively. The DT method is simple in its determination of stress intensity factor, K_I (providing a single crack is attained) as a function of temperature.

It is important to note that the initial cracks in the indentation induced flaw (IIF) technique are very small, ranging from 30 to 100 μm deep or long while in the DT technique, initial cracks are very large ranging from 8 to 15 mm long and the two methods could be considered as 'micro' and 'macro', respectively. Nevertheless, the K_{IC} and K_I values obtained from the two methods are comparable.

3.5% MgO FHPSN

Similar stress intensity measurements were also made in another ceramic material, 3.5% MgO FHPSN, using double torsion technique and complete data for a total of 16 specimens are given in Table 13. On fracture faces, the initial crack fronts are difficult to distinguish due to the presence of the "mottled structure' as discussed in Sec. 4.1.1. K_{IC} values determined at 20°C varied from 5.33 to 5.98 $MN/m^{3/2}$ with an average of 5.72 $MN/m^{3/2}$. Crack velocity measurements could not be made in this material due to the fact that initial or final crack lengths could not be measured accurately on the fracture faces.

4.2.2 Crack Velocity (V) Stress Intensity (K) Relationship

A functional relationship between crack velocity (V) and the corresponding stress intensity K_I for subcritical crack growth (SCG) has been approximately described by the following relationship:

$$V = A K_I^n$$

where A and n are constants for a given temperature and environment. Using the DT method and Eqs.(14) and (16), and the procedure outlined in Section 4.2, the V-K relationship and its variation with temperature is shown in Fig. 42. The curves represent the region of slowly varying velocity and similar behavior has been observed in HS-130 Si_3N_4 [21] at the same temperatures. It should be noted that the

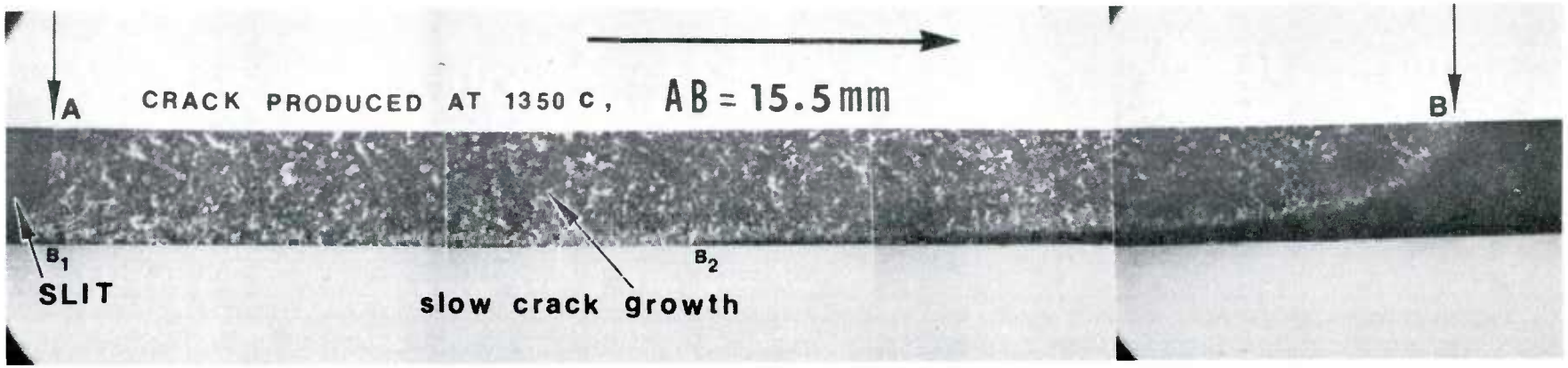

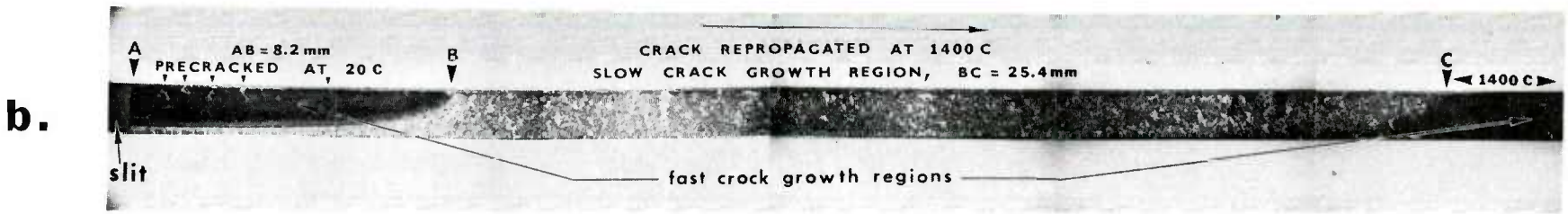

Fig. 41 (a) Fracture surface of a double torsion NC-132 Si_3N_4 specimen in which the initial crack AB was produced at 1350°C and subsequently repropagated rapidly at 20°C for unstable crack propagation (catastrophic failure) to determine K_I. Crack propagated centrally all through the length of the specimen.

(b) Fracture surface of a double torsion NC-132 Si_3N_4 specimen in which the initial crack AB was produced at 20°C and subsequently repropagated at 1400°C. A successful load-relaxation curve was obtained at 1400°C on this specimen and finally the specimen was subjected to fast fracture at 1400°C to measure K_I. Crack propagated centrally all through the specimen length.

TABLE 13

DOUBLE TORSION DATA FOR FORD MATERIAL - FHPSN (3.5% MgO + HPSN)

Specimen No.	Specimen Condition	Crack Initiation Temp.	Crack Repropagation Temp.	Stress Intensity, $MN/m^{3/2}$		Remarks
				K_{IC}	K_I	
1	Grooved (0.20 mm deep)	20°C	20°C	-	-	Crack curved out
2	" " "	"	"	-	-	" " "
3	" " "	"	"	-	-	" " "
4	No Groove	"	"	-	-	" " "
5	" "	"	"	-	-	" " "
6	" "	"	"	-	-	" " "
7	Grooved (0.20 mm deep)	"	"	5.85	-	Crack propagated centrally
8	" " "	"	"	5.98	-	" " "
9	" " "	"	"	5.33	-	" " "
10	" " "	"	"	5.73	-	" " "
11	Grooved (0.20 mm deep)	20°C	1300°C	-	6.71	Crack propagated centrally
12	" " "	"	1371°C	-	-	Failed during repropagation
13	" " "	"	"	-	-	Crack propagated centrally
14	No Groove	1200°C	1200°C	-	-	Crack curved out
15	No Groove	1300°C	20°C	-	7.14	Crack propagated centrally
16	No Groove	1371°C	20°C	-	7.38	Crack blunting

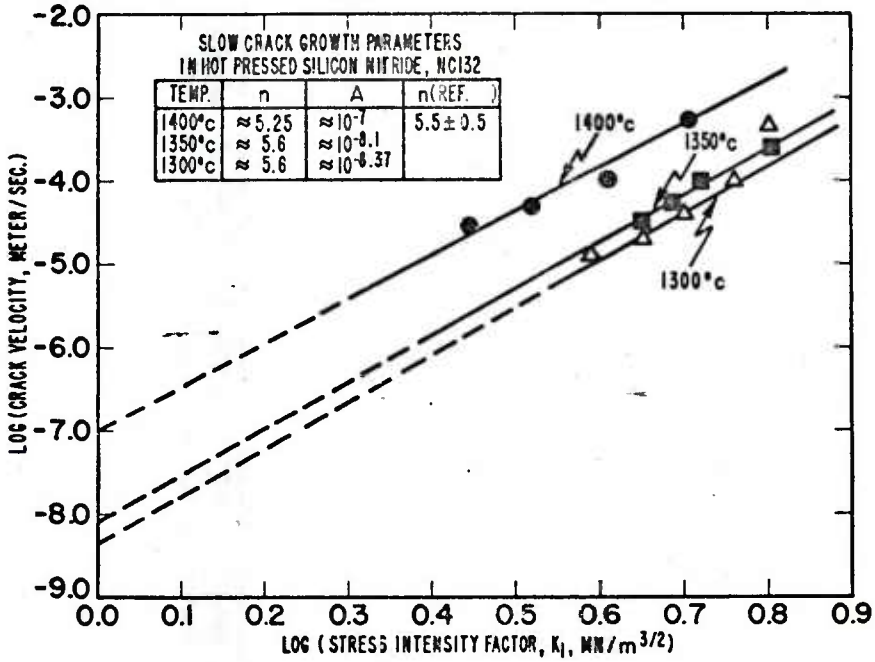

Fig. 42 Subcritical crack growth rate data for NC-132 Si_3N_4 as a function of temperature using the double torsion technique. The value of n = 5.5 ± 0.5 at 1400°C is for HS-130 Si_3N_4 (Ref. 22).

curves at 1300, 1350, and 1400°C are essentially parallel and characterized by a constant slope. The individual values of n and A for SCG at these high temperatures are listed in Fig. 42. The constant slope of the curves indicate that once large amounts of slow-crack growth occur, n does not vary significantly for a given environment and is independent of temperature for the SCG temperature regime (1300-1400°C or higher). The approximate value of n at 1400°C is about 5.25. This value of "n" is in good agreement with work reported by others [21,22] in HS-130 Si_3N_4 at the same temperature using similar technique.

Recently, Mendiratta and Petrovic [25] used the IIF method using multiple cracks and propagated them in vacuum under a constant stress for different times at temperatures from 1100 to 1300°C, and measured average velocities which were about two orders of magnitude higher than the DT method [21,22] reported in the same material (HS-130 Si_3N_4). Some stress rupture studies in HS-130 Si_3N_4 have also been reported by us [31] and it is clear from the micrographs that the path taken by SCG region is pseudo elliptical in shape and therefore, velocities measured from surface extensions of crack could be significantly different than those from depth of crack. Furthermore, even if the crack growth or crack front is semi-circular in nature, it is believed that using the IIF method would result in average crack velocities for SCG for two reasons. First, the load-deflection curves for precracked specimens showed linear elastic behavior to the point of fracture (especially for the machine head speeds of 0.005 in./min. and higher) even though large amounts of SCG or extension of the initial crack occurred. From such tests, only the total time to failure can be measured from the Instron recorder chart and would result in much lower than actual velocities. Secondly, the load-deflection curve does not indicate the exact instant at which the crack moves and, therefore, the time to travel a given length of crack cannot be measured accurately.

4.3 Subcritical Crack Growth Exponent, n

The subcritical crack growth exponent, n, can be determined in a number of ways as outlined below:

a. The Double Torsion Method

b. Flexural Stress Rate Method

c. Flexural Strain Rate Method

d. Flexural Stress Rupture Method

e. Uniaxial Tensile Stress Rupture Method

All of these methods have been discussed in detail in this report and the values for crack growth parameter 'n' as obtained for NC-132 Si_3N_4 are summarized in Table 14.

TABLE 14

EXPERIMENTALLY DETERMINED SLOW CRACK GROWTH PARAMETERS FOR NC-132 Si_3N_4

Method	Temp. °C	n	A
Double Torsion	1400	5.25	10^{-7}
	1350	5.6	$10^{-8.1}$
	1300	5.6	$10^{-8.37}$
Flexural Stress Rate	1371	17.2	-
	1204	19.1	-
Flexural Strain Rate	1400	10-12	-
	1350	10-12	-
	1300	18-20	-
Flexural Stress Rupture	1204	9.5	-
Tensile Stress Rupture	1300	7.6	-
	1204	12.4	-

5. UNIAXIAL TENSILE STRESS RUPTURE TESTING AND ANALYSIS

Uniaxial tensile stress rupture testing is one method by which the actual verification of the analytically obtained life prediction times using the various fracture mechanics parameters as described above can be made and this was the main objective for carrying out the tests. Furthermore, because of uniformity of stress distribution in the cross-section of a uniaxial tensile specimen, this method is much more sensitive in revealing the time dependent deformation behavior compared to flexural stress rupture testing. This is especially true in the low temperature range (< 1200°C) where short term flexural stress rupture and stress rate testing methods are incapable of detecting the presence of subcritical crack growth (SCG). Evidence for this will be shown in this study. Considerable time and effort were spent in carrying out the uniaxial tensile stress rupture testing of NC-132 Si_3N_4 specimens.

The tensile stress specimen consisted of a simple rectangular geometry with a narrow cross-section in gage length and large radii at the shoulders necessitated by the sensitivity of ceramic materials to stress concentrations. The specimen geometry and dimensions are shown schematically in Fig. 43. The fracture face of the lower half of each broken specimen was examined metallographically and the edges of the fracture face were identified in a fashion shown in the cross-section A-A, Fig. 43. This procedure would also help in identifying whether the fracture initiation sites were random or preferential. A standard creep testing Satec machine with a modified load train assembly was used for tensile stress-rupture testing. The specimen is retained in two slotted SiC holders by large SiC pins. The SiC holders are retained in water cooled metal adaptors which in turn are attached to the standard Satec machine head which includes crossed (90°) knife edges. The assembly procedure includes hanging the load train parts from the Satec head as influenced by gravity. At this point the lower Satec crossarm is lowered to snub the train in this position. The load train assembly is shown schematically in Fig. 44. Each test specimen contained a total of eight strain gages (two on each face in the gage-length area) for axial alignment and for each test, tailored efforts were made to keep the bending stresses below 3% at full load. Initial alignment of the specimen is done at 20°C with full load. A typical test specimen with strain gages attached in the gage section is shown in Fig. 45. A high temperature furnace capable of reaching 1400°C is mounted on the side area of the Satec machine and encloses the full area between the water cooled metal adaptors, Fig. 46. Complete details regarding the load train instrumentation and continuous monitoring of applied stress, test temperature and time are given in the Appendix.

From the flexural stress rupture and stress rate studies (see Sec. 2) of NC-132 Si_3N_4, it was obvious that the onset of SCG occurs around 1200°C and significant SCG occurs at 1300°C or higher temperatures and SCG did not occur at temperatures of 1000°C. Therefore, three temperatures, namely 1000, 1200 and 1300°C were chosen to conduct the tensile stress rupture studies in order to investigate the presence of SCG as a function of constant applied stresses.

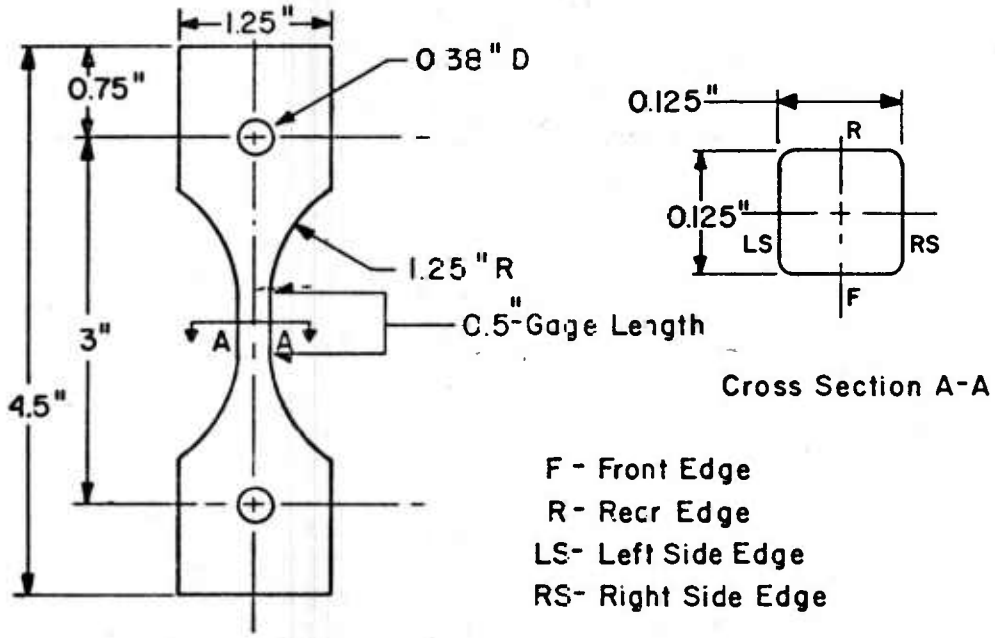

Fig. 43 Tensile Stress Rupture Test Specimen Dimensions.

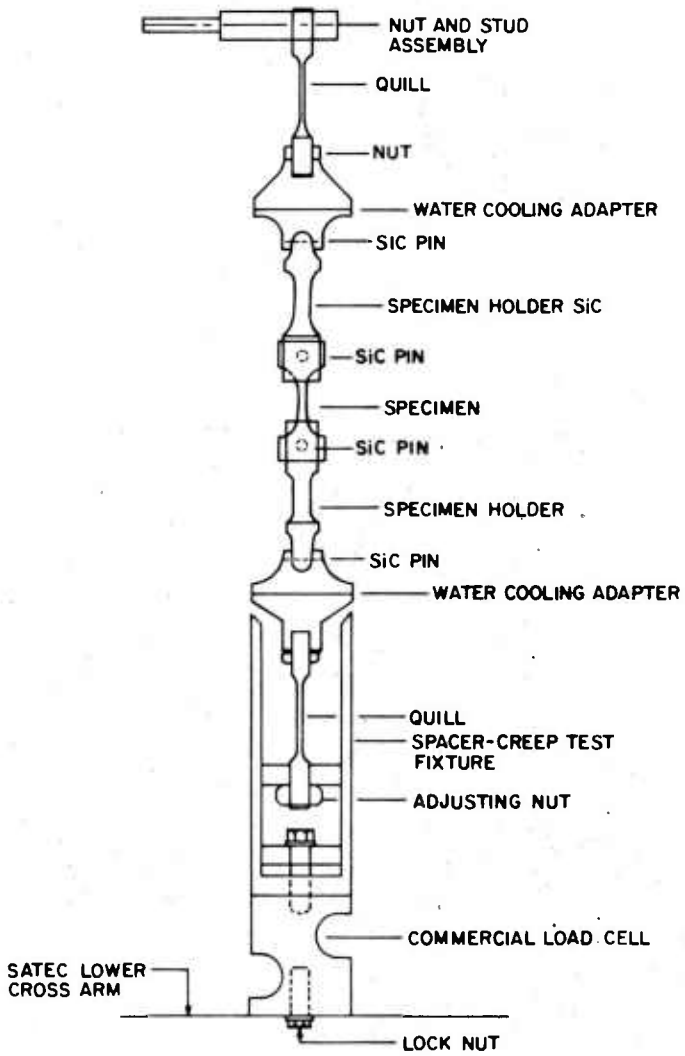

Fig. 44 Schematic representation of the load train assembly used for tensile stress rupture testing at high temperatures.

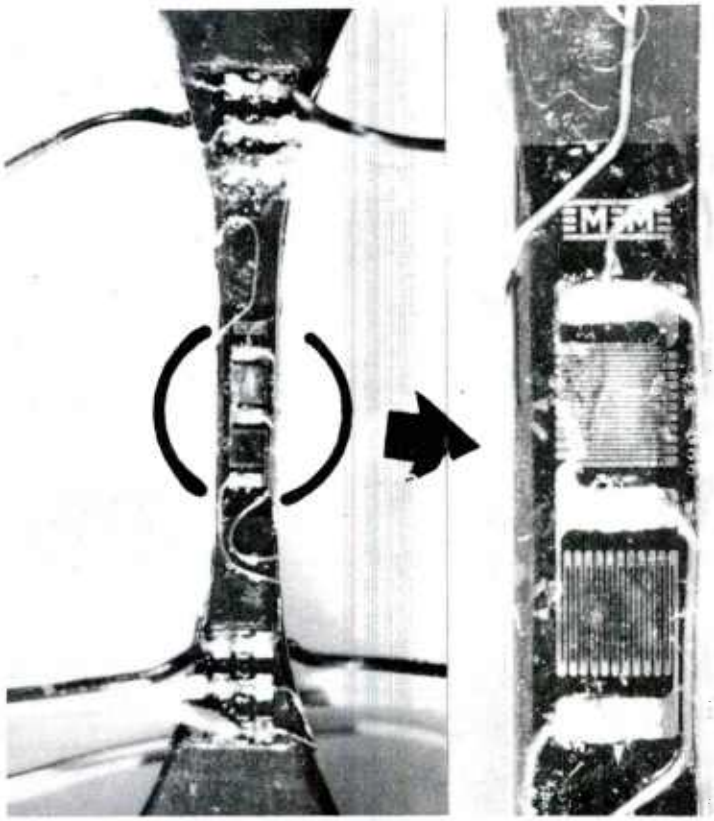

Fig. 45 Typical tensile stress rupture test specimen of NC-132 Si_3N_4 with strain gages attached to the gage length.

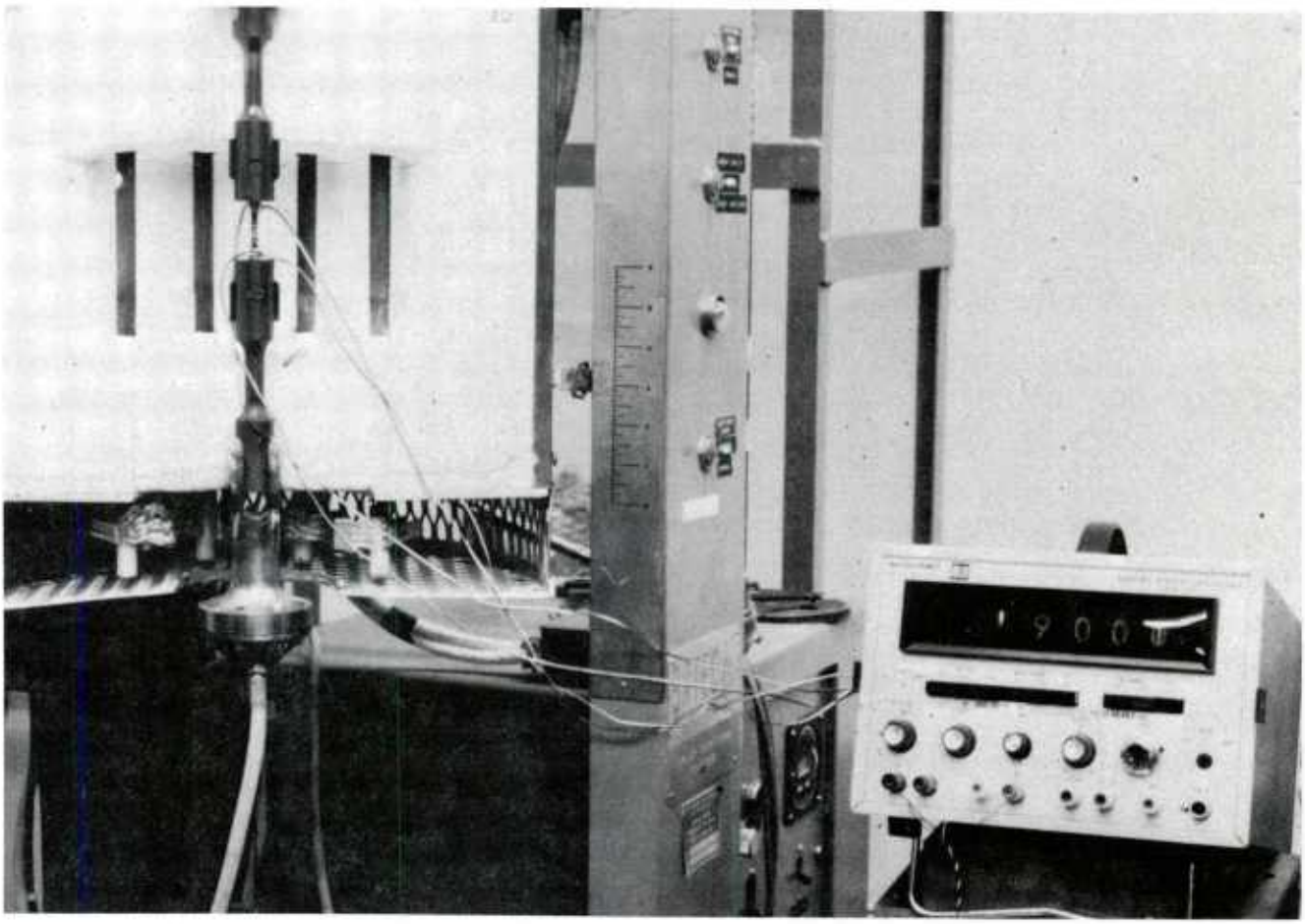

Fig. 46 A partial view of the test set-up showing the furnace, strain-gaged specimen, strain indicator and lower part of the load train assembly.

5.1 Tensile Stress Rupture Results at 1204°C

A total of sixteen (16) tersile stress rupture specimens were tested at 1204°C at various applied stress levels and the results are given in Table 15. Majority of the test specimens failed in the center of the gage length (see #2, Fig. 47) but some failed at the lower or upper end of gage length (see #3 and #5, Fig. 47). It should be noted that among the twelve (12) specimens tested at 1204°C at a constant stress of 19,200 psi, all except one (#4) sustained the applied stress in a fairly uniform fashion and the time-to-failure varied from 4 to 8 hrs. giving an average of 6.4 hrs. All of these specimens showed the localized failure origin sites and the associated SCG regions. Typical fracture surfaces for specimens (#1, #3, #8 and #9) are shown in Fig. 48. Arrows indicate the possible failure sites and the associated SCG regions. In these micrographs it is questionable whether the failure started inside or on the surface. They appear to indicate internal failure origins. Figure 49 shows both halves of the fractured specimen #2 and clearly the failure started internally. Arrows point out the region of SCG. Specimens #5 and #7 (Figs. 50 and 51, respectively) both showed the failure origin sites as internal, and the associated regions of SCG. These localized regions were examined in SEM and a typical micrograph taken inside the region of SCG, Fig. 51a, is shown in Fig. 51b. The nature of crack propagation during SCG is clearly intergranular and will be discussed in greater detail in other examples.

Upon increasing the applied stress by a small magnitude such as 2000 psi, the time-to-failure decreased drastically as indicated by specimen #13. Typical fracture surfaces for these specimens are shown in Fig. 52. Possible failure sites are indicated by arrows.

The tensile stress rupture data can also be used in a similar fashion as the flexural stress rupture data (Sec. 2) and the results are shown in Fig. 6. An approximate value of $n \approx 12.4$ at 1204°C is obtained from the slope of the curve and is comparable to the value obtained by the flexural stress rupture method.

Table 15

Tensile Stress-Rupture Data at 1204 C for HP Si_3N_4-NC132

Specimen No.	Applied Stress		Time to Failure
	psi	MN/m^2	
1	19,200	132.5	4.7 Hrs.
2	"		8.4 "
3	"		6.1 "
4	'		21.0 '
5	'		5.3 '
6	'		6.1 '
7	'		8.5 '
8	'		5.1 '
9	'		7.7 '
10	'		6.5 '
11	'		4.9 '
12	'		7.4 '
13	21,200	146.3	30 min
14	25,000	172.5	10 min
15	30,400	210	Fast Failure
16	45,760	316	"

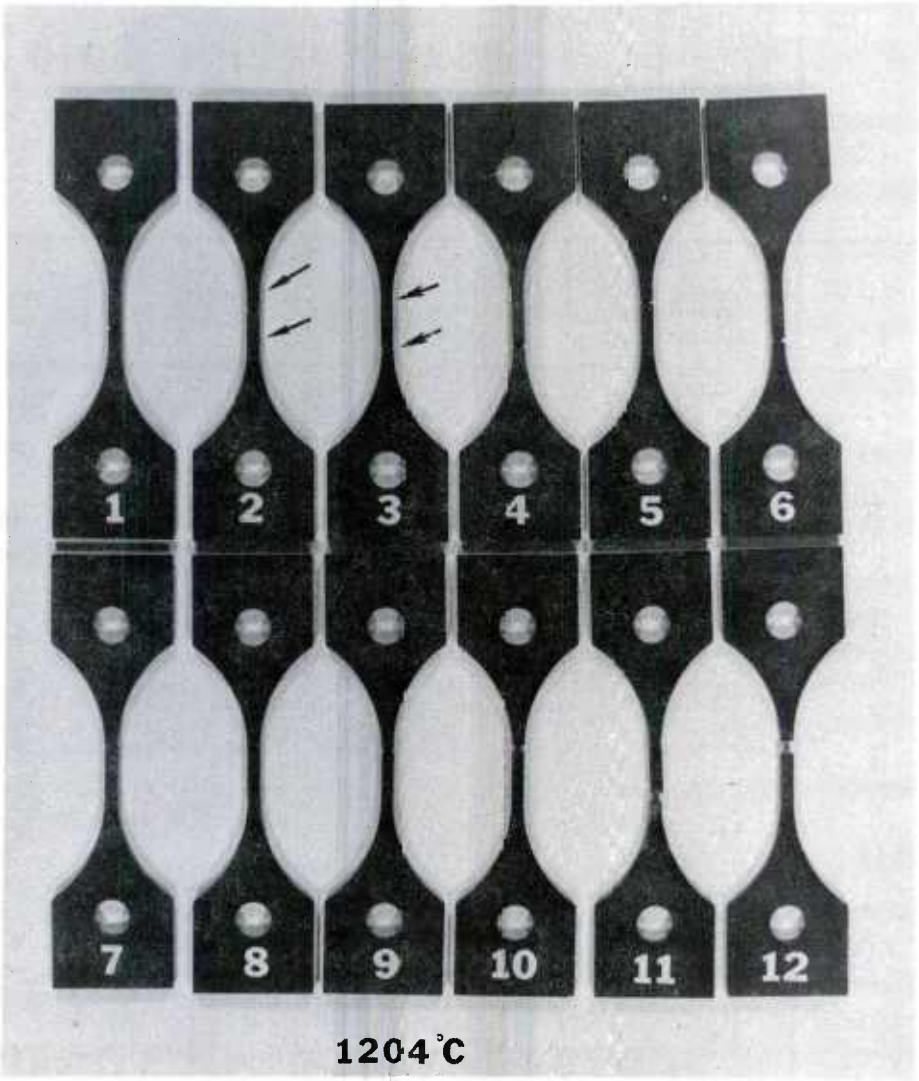

Fig. 47 Typical appearance of the broken specimens of NC-132 Si_3N_4 tested at 1204°C in air in uniaxial tensile stress rupture mode. Arrows indicate the central gage length area. Some specimens failed in the center of the gage length (#2) while others failed at the lower or upper end of gage length (see #3 and #5).

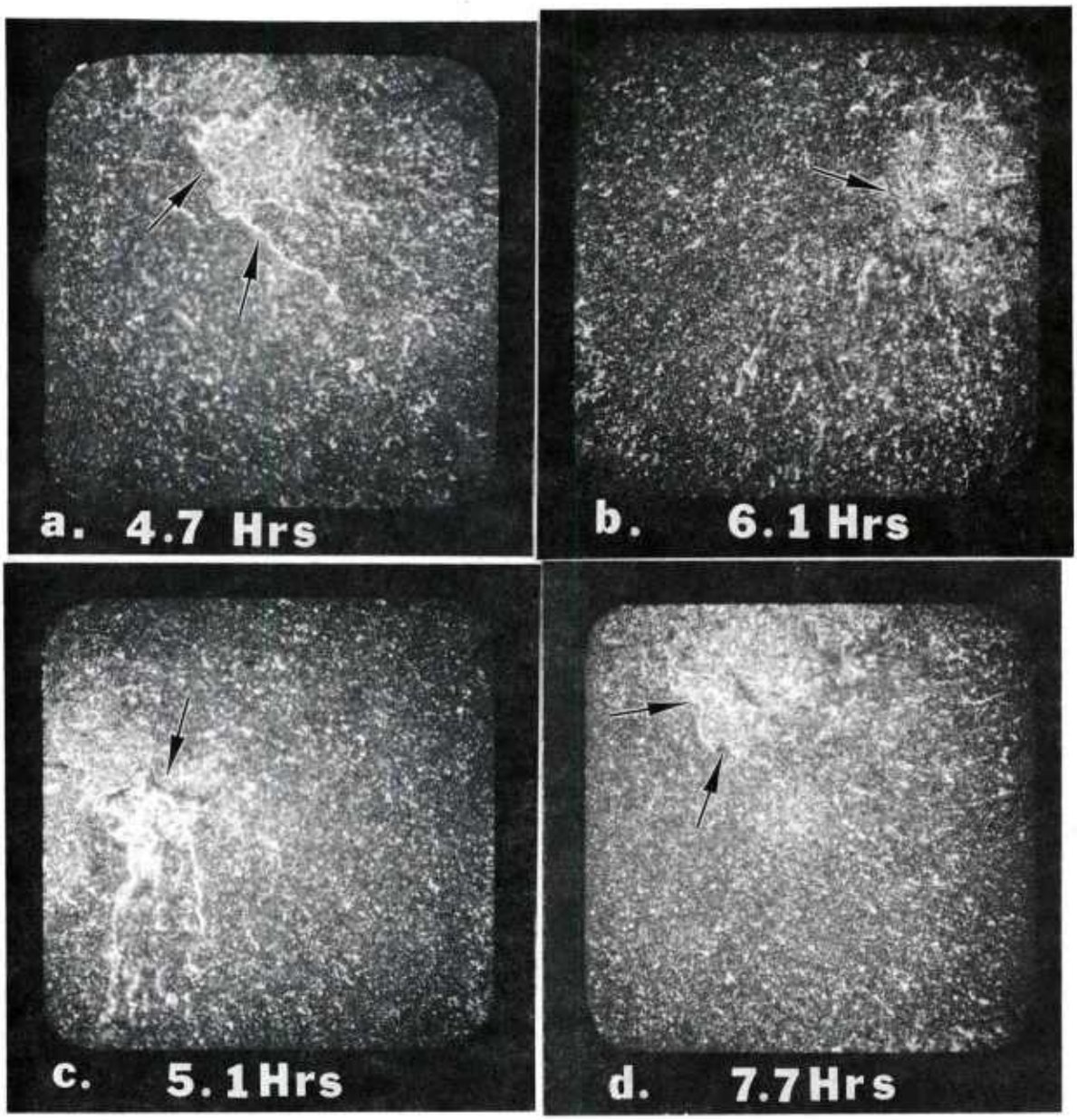

Fig. 48 Typical fracture surfaces for tensile stress rupture specimens of NC-132 Si_3N_4 tested at an applied stress of 19,200 psi and 1204°C. Arrows indicate the possible regions of crack initiation and the associated slow crack growth regions. Micrographs taken in plane polarized light and show full cross-section of test specimen.

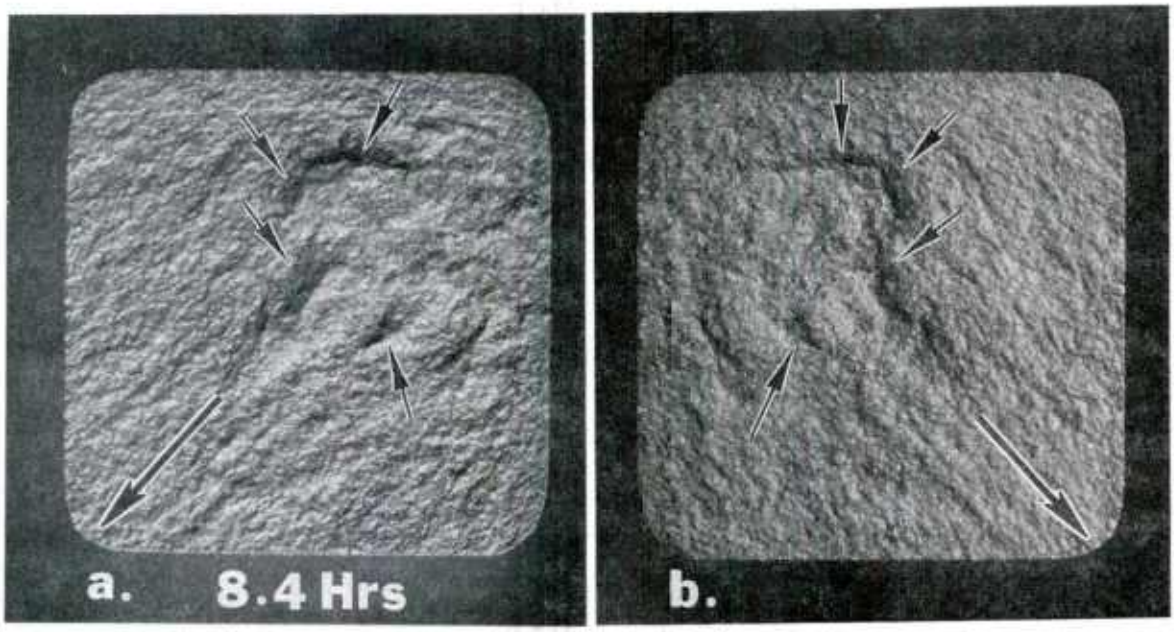

Fig. 49 Fracture surface appearance as seen in matching broken halves of tensile stress rupture specimen of NC-132 Si_3N_4 tested at a stress of 19,200 psi and 1204°C. Arrows identify the region of subcritical crack growth. Micrographs taken in normal white light.

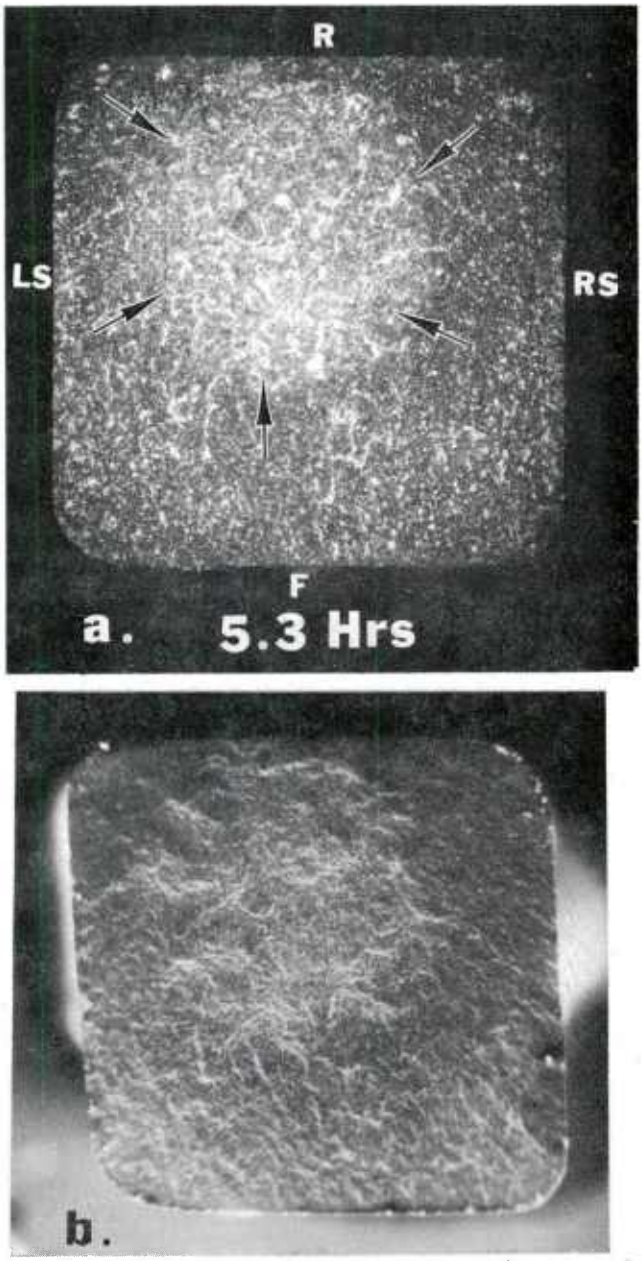

Fig. 50 Fracture surface appearance for tensile stress rupture specimen of NC-132 Si_3N_4 tested at applied stress of 19,200 psi and 1204°C in air.

(a) Plane polarized light micrograph shows the failure origin site as internal and the associated slow crack growth region indicated by arrows. Specimen #5.

(b) Same area as seen in SEM shows the slow crack growth region clearly.

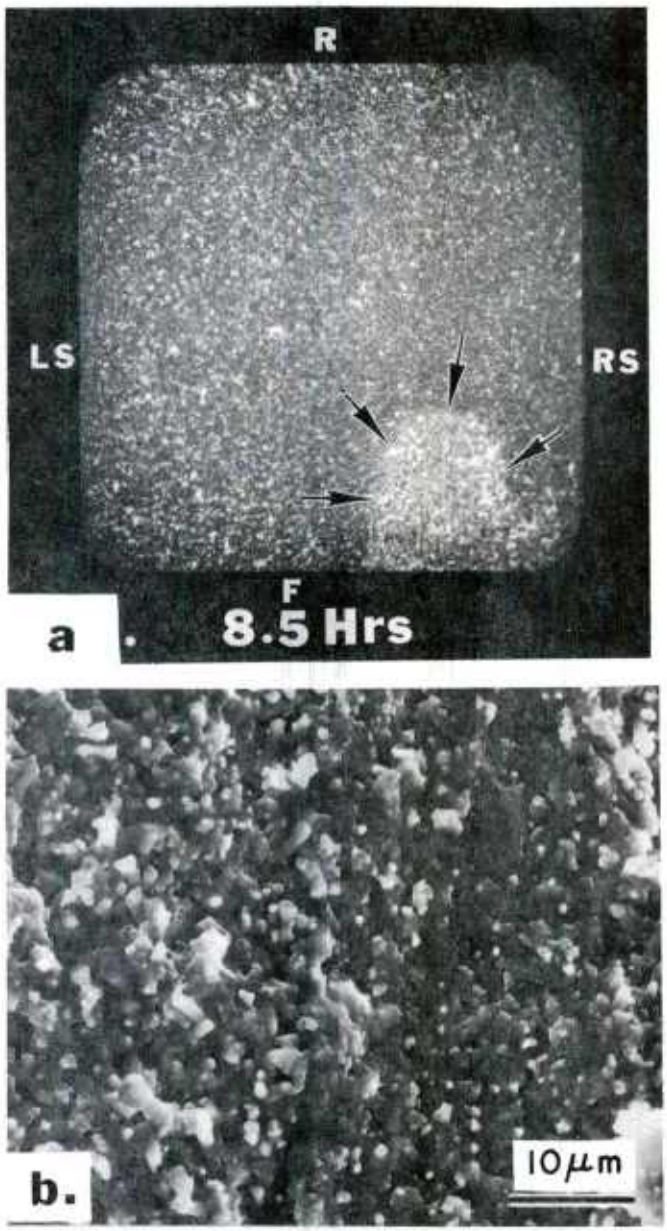

Fig. 51 Fracture surface appearance for tensile stress rupture specimen of NC-132 Si_3N_4 tested at an applied stress of 19,200 psi and 1204°C in air.

(a) Another example of internal failure origin site as seen in plane polarized light. Arrows indicate the region of slow crack growth. Specimen #7.

(b) SEM micrograph taken inside the slow crack growth region shown in (a). Micrograph clearly shows that the mode of crack propagation during slow crack growth is completely intergranular.

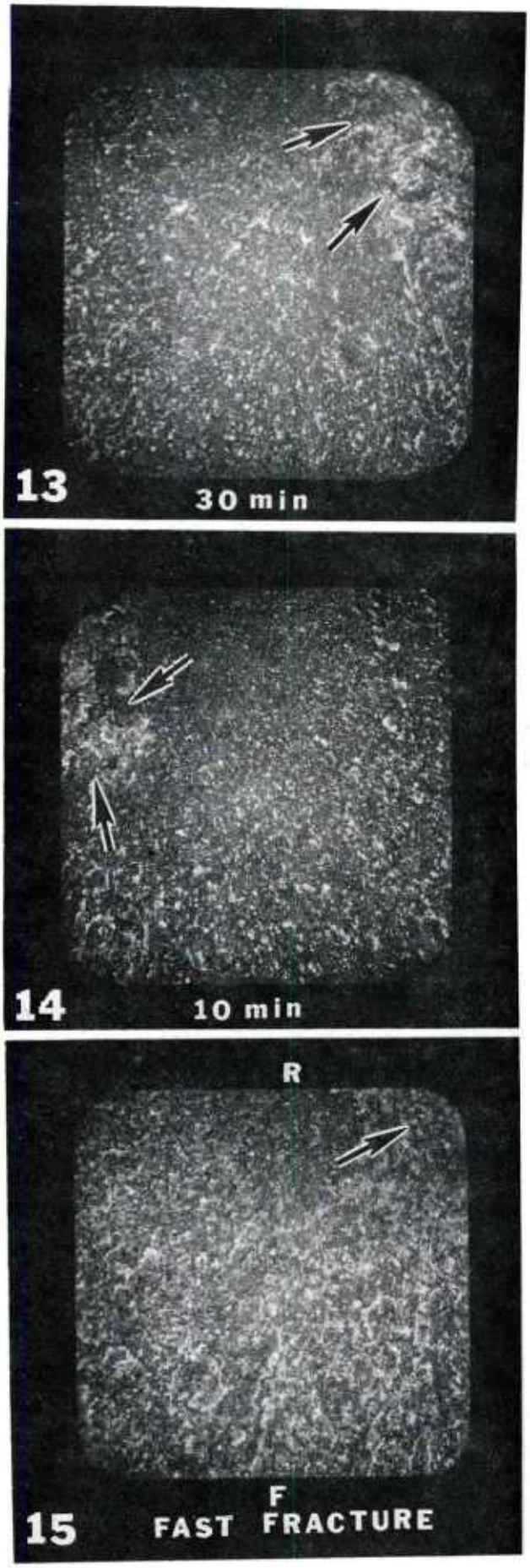

Fig. 52 Typical fast fracture surface appearances as seen in tensile stress rupture specimens of NC-132 Si_3N_4 tested at 1204°C in air. Failure initiation regions marked by arrows.

(a) Test specimen #13, subjected to an applied stress of 21,200 psi and failed after 30 min.

(b) Test specimen #14, subjected to an applied stress of 25,000 psi and failed after 10 min.

(c) Test specimen #15, subjected to an applied stress of 30,000 psi and failed in less than 1 (one) min.

5.2 Tensile Stress Rupture Results at 1300°C

A total of eleven (11) tensile stress rupture specimens of NC-132 Si_3N_4 were tested at 1300°C in air at various applied stress levels and the results are given in Table 16. Majority of the test specimens failed in the center of the gage length (see #17) but some failed at the lower or upper end of the gage length (see #24 and #25) as typically shown in Fig. 53. Typical fracture surfaces showing possible fracture initiation regions and the associated SCG regions are shown in Fig. 54. Arrows indicate the boundary of the SCG region. In this temperature series, the extent of SCG occurs very rapidly. This is shown by the fact that the time-to-failure decreased by two orders of magnitude at an applied stress of 19,200 psi with a corresponding increase in test temperature of 100°C from 1200°C to 1300°C. This shows the importance of SCG at temperatures above 1200°C. Furthermore, the results obtained at 1300°C also support the viewpoint that design stresses (tensile) for any component made of NC-132 Si_3N_4 should not exceed 10,000 psi at 1300°C and limited life (about 30 hrs.) of the component is expected. In short, use of this material should be avoided in applications where high temperatures such as 1300°C will cause time dependent failure.

The tensile stress rupture data was used in a similar fashion as the flexural stress rupture data and the results are shown in Fig. 6. An approximate value of $n \approx 7.6$ at 1300°C was obtained. Note that the value of n is considerably smaller at the higher temperature of 1300°C relative to the value at 1200°C. We believe that the parameter 'n' is a measure of SCG and should show small variation in the temperature range of 1300-1400°C.

Table 16

Tensile Stress Rupture Data, 1300 C, NC 132

Specimen No.	Applied Stress		Time to Failure
	psi	MN/m^2	
17	9600	~66	11 min
18	"	"	27 Hrs.
19	"	"	49 "
20	"	"	51 "
21	12,000	~83	42 min
22	"	"	83 "
23	"	"	165 "
24*	"	"	16 Hrs.
25	15,000	~104	24 min
26	"	"	35 "
27	19,200	~132.5	4 min

* stepped rupture series

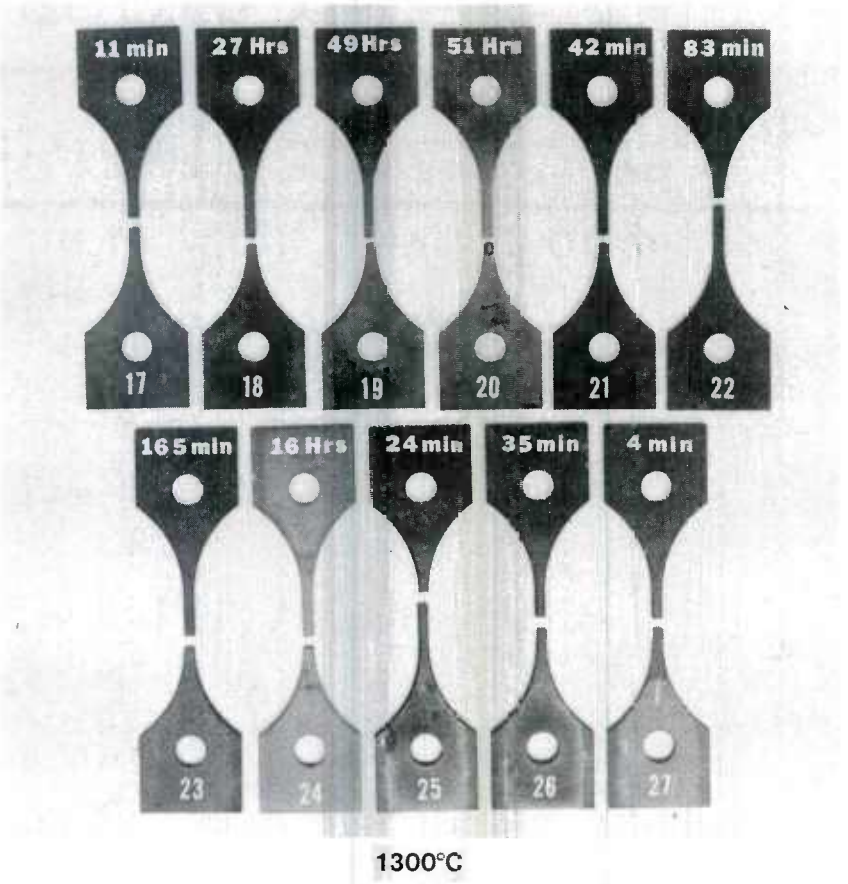

Fig. 53 Typical appearance of the broken specimens of NC-132 Si_3N_4 tested at 1300°C in air in uniaxial tensile stress rupture mode. Some specimens failed at the lower or upper end of gage length (see #24 and #25) while others broke in the center (see #17).

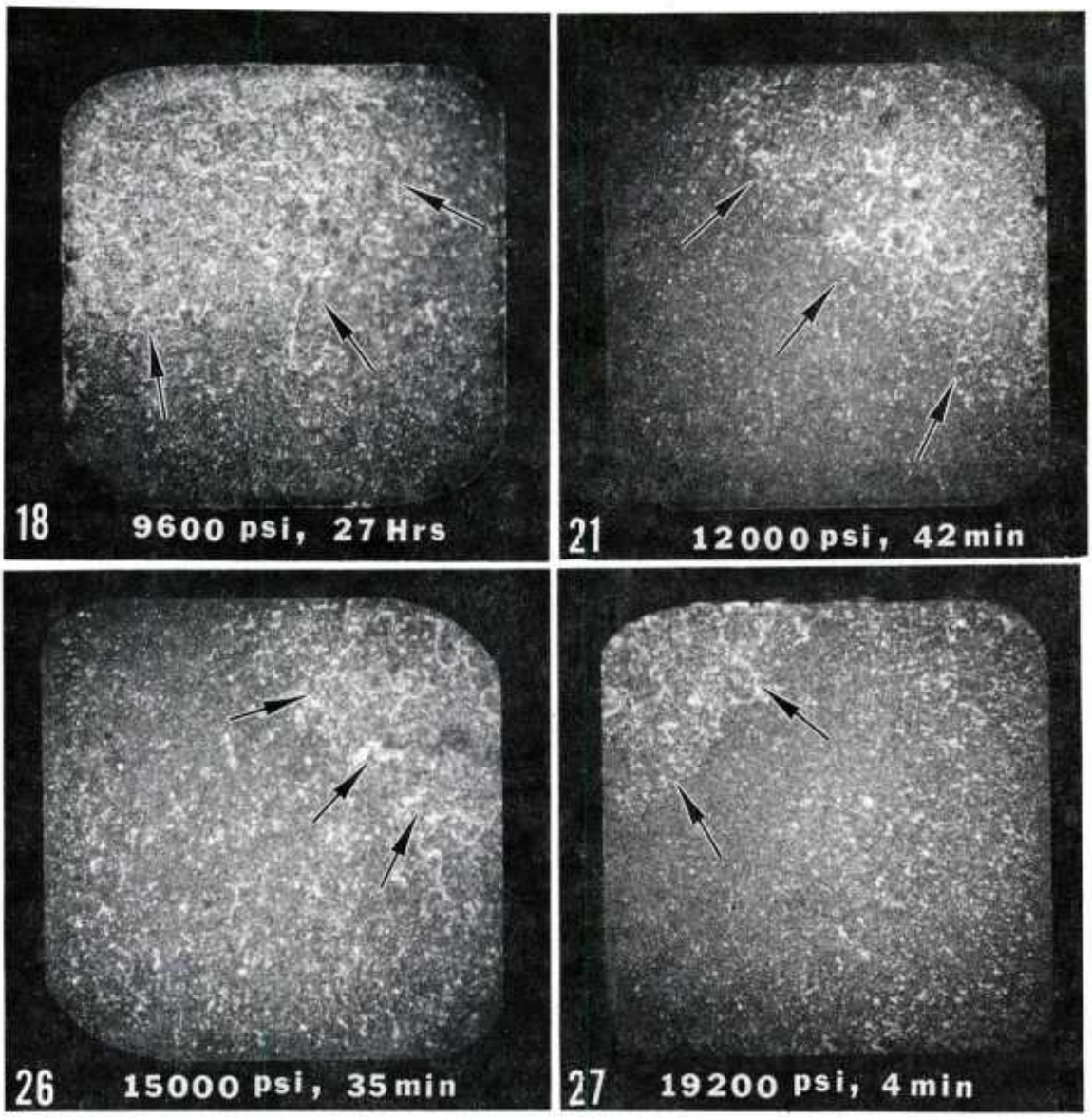

Fig. 54 Typical fracture surfaces for tensile stress rupture specimens of NC-132 Si_3N_4 tested at 1300°C in air. Arrows indicate the extent of subcritical crack growth regions. Micrographs taken in plane polarized light.

5.3 Tensile Stress Rupture Results at 1000°C

A total of fourteen (14) tensile stress rupture specimens of NC-132 Si_3N_4 were tested at 1000°C at applied stresses varying from 30,000 psi to 50,000 psi. Complete results are given in Table 17. The first specimen tested in this temperature series (#28) was subjected to 30,000 psi and the specimen survived 984 hrs. at 1000°C with no signs of early failure. Actually we did not expect the test to last this long and in order to test additional specimens, it was decided to test the specimen in a stepped rupture series fashion as shown in Fig. 55. The specimen failed in 20 mins. after being subjected to an applied stress of 40,000 psi and did not show any sign of localized SCG region, Fig. 55, as had been observed in tests made at 1200 and 1300°C. Oxidation pits along the edges are visible (Fig. 55b) and possibly led to failure at increased stress. Typical fracture surfaces for specimens tested at applied stresses of 35,000 psi, 40,000 psi, 41,000 psi and 45,000 psi (#29, #33, #35, and #38) at 1000°C are shown in Figs. 56 (a,b,c,d), respectively. The localized fracture initiation sites are indicated by black arrows, Fig. 56 and in Figs. 56(a) and 56(b), the regions of SCG are also clearly visible. The localized regions of fracture initiation as seen in Figs. 56(a),(c) and (d) are too close to the edge of the specimen and it is possible that failure could have originated from some surface flaw due to machining damage. Figure 56(b) shows clearly the origin of failure site as internal. The other half of this specimen (#33) was also examined and the fracture face as seen in plane polarized light and SEM are shown in Figs. 57(a) and 57(b), respectively. The SEM micrograph, Fig. 57(b) shows distinctly the SCG region, surrounded by a fast fracture region of smooth appearance. Note the smooth appearance of the fracture surface along the upper edge of the specimen suggesting that the failure site was completely internal and free from any surface machining flaws causing failure. The nature of crack propagation inside and outside the localized region of failure initiation (SCG) is shown in Figs. 57(c) and 57(d), respectively. Primarily the fracture mode is transgranular with small evidence of intergranular crack growth, Fig. 57(c). Typical fracture surface for specimen #41 which was subjected to an applied stress of 50,000 psi at 1000°C and failed after 243 hrs. is shown in Fig. 58. The overall view of the fracture surface is shown in Fig. 58(a), where the possible failure initiation site is marked by the arrow and is completely internal. Examination at higher magnification of the same initiation site did not reveal the presence of any inclusion, void, and slow crack growth. Further evidence for failure initiations to originate internally (in volume) and surface associated flaws were observed in this series as discussed below.

TABLE 17

TENSILE STRESS RUPTURE RESULTS AT 1000°C, NC-132 Si_3N_4

Specimen No.	Applied Stress		Time to Failure
	PSI	~MN/m^2	
28	30,000	207	984* Hrs.
29	35,000	242	18 Hrs.
30	"	"	20 Hrs.
31	"	"	24 Hrs.
32	"	"	35 Hrs.
33	40,000	276	541 Hrs.
34	41,000	283	8 Hrs.
35	"	"	11 Hrs.
36	43,500	300	Failed on Loading
37	45,000	311	10 Min.
38	"	"	25 Min.
39	"	"	6.5 Hrs.
40	50,000	345	31 Hrs.
41	"	"	243 Hrs.

* Stepped Rupture Series

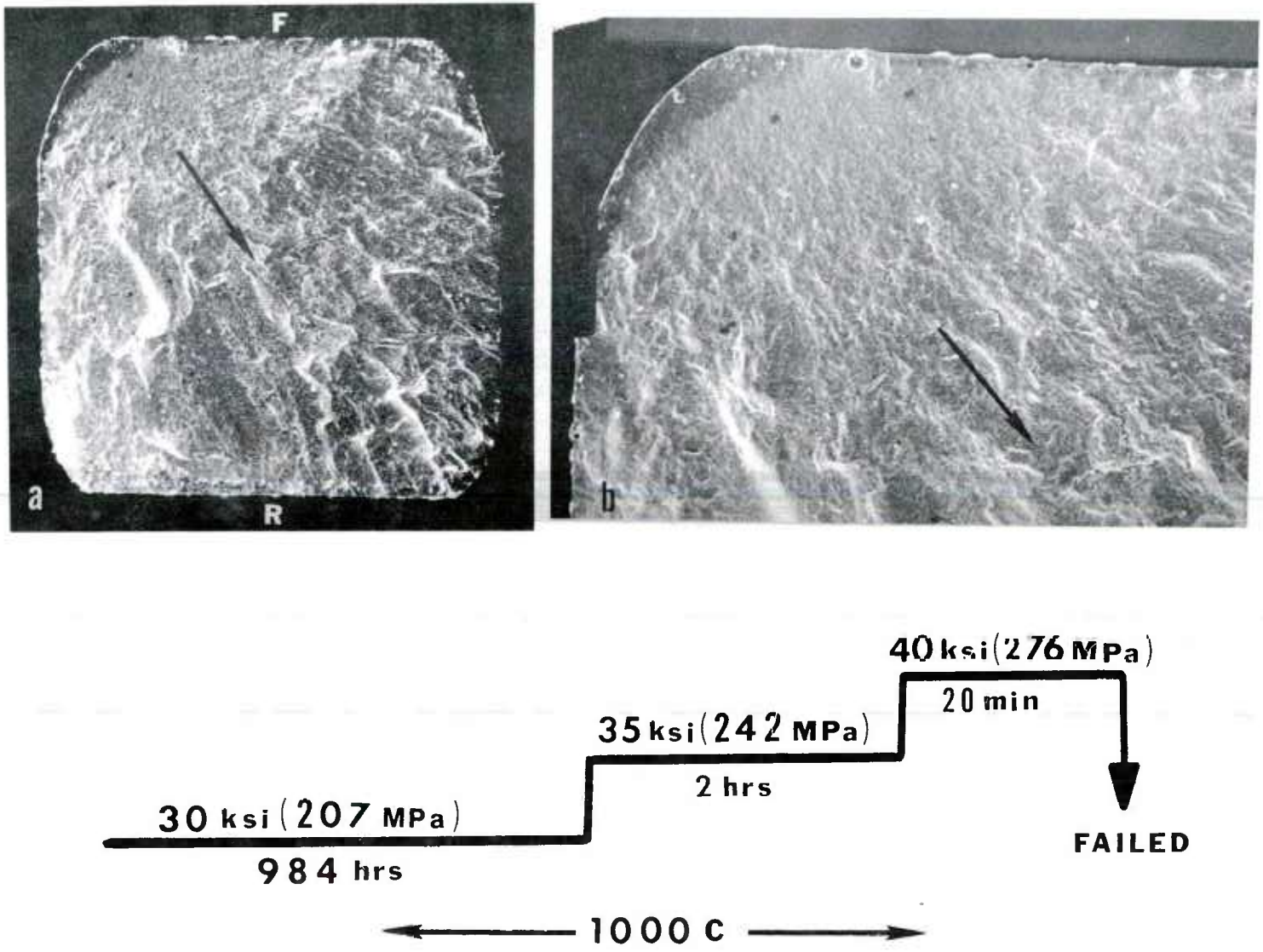

Fig. 55 NC-132 Si_3N_4 tensile stress rupture specimen (#28) tested at 1000°C in air in a stepped stress rupture series fashion. Fracture surfaces as seen in SEM are shown in (a) and (b). Arrow indicates the direction of crack propagation. This specimen did not show the presence of subcritical crack growth. Oxidation pits along the edges of the specimen are visible.

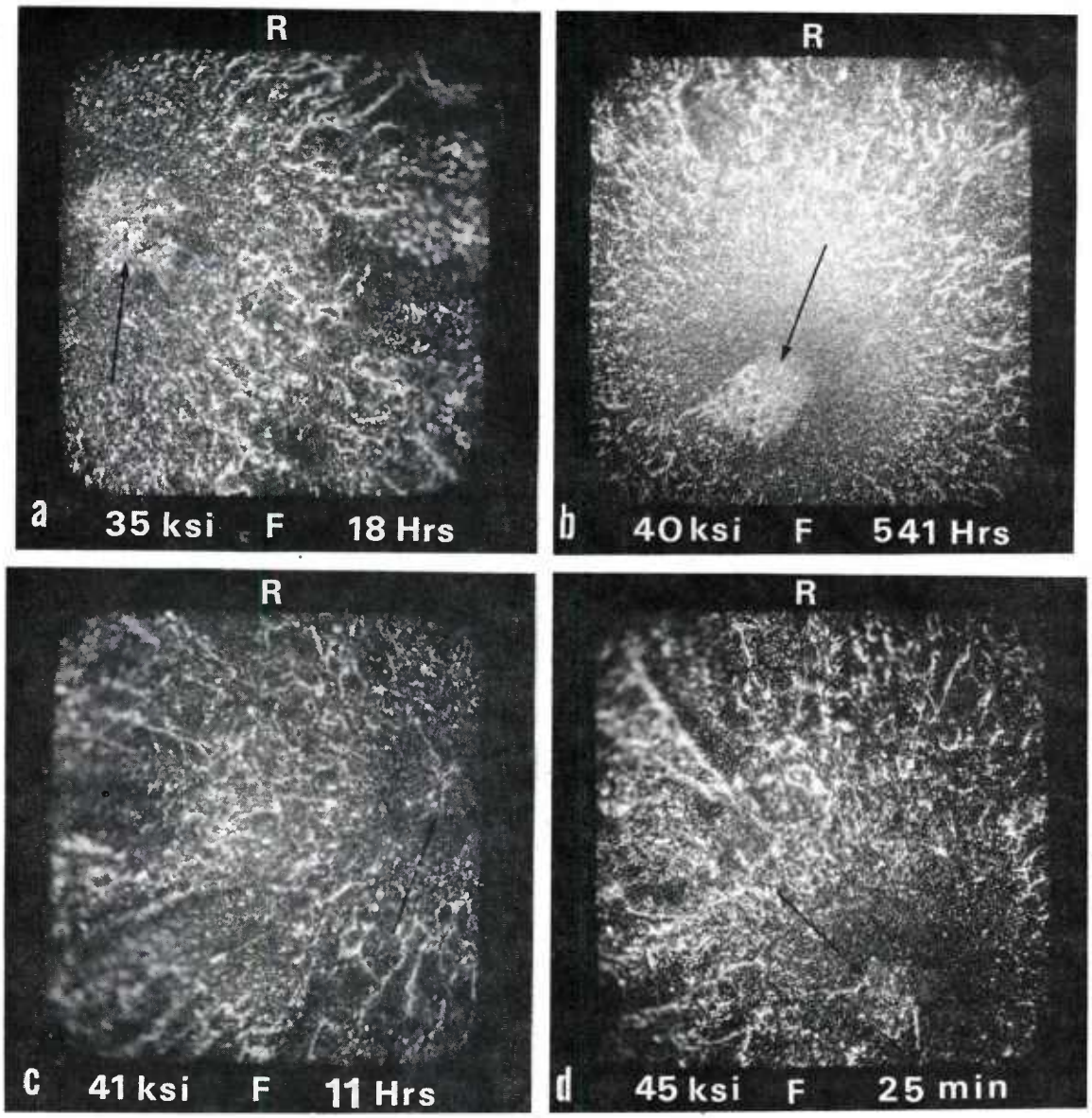

Fig. 56 Fracture surfaces for tensile stress rupture specimens of NC-132 Si_3N_4 (#29, #33 #35 and #38) tested at 1000°C in air at various applied stress levels. Micrographs taken in plane polarized light and arrows indicate the failure initiation site and possibly the associated slow crack growth region. Failure initiation sites in micrographs (a, c and d) are close to the edge or surface of the specimen and it is possible that failure orginated from surface flaw. Failure initiation site in micrograph (b) appears to be completely internal.

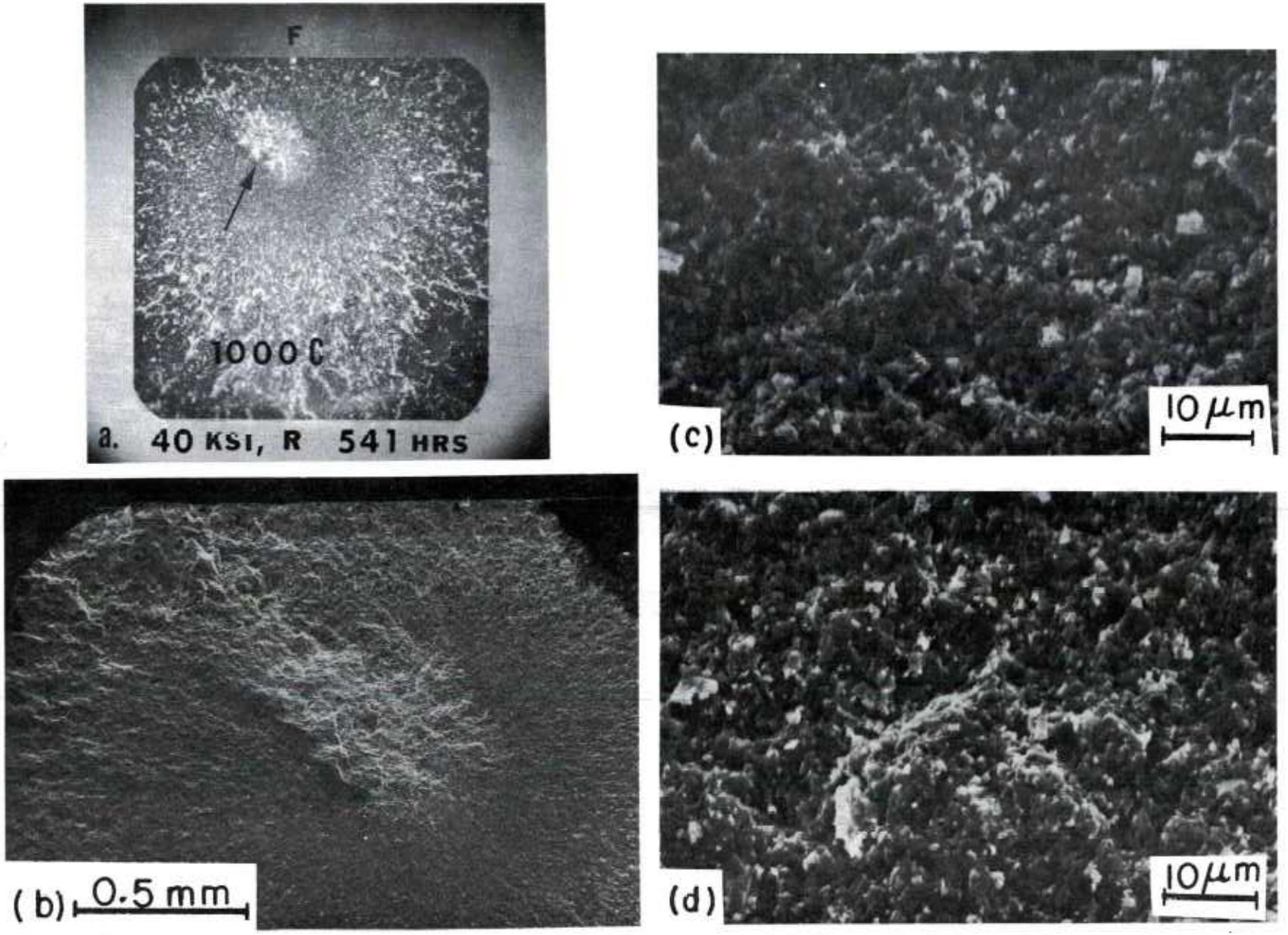

Fig. 57 Fracture surface of the other half of the specimen (#33) seen in Fig. 56(b). (a) Micrograph taken in plane polarized light and shows the failure initiation site. (b) SEM view of the failure initiation site seen in (a). Note the upper left edge is completely free from any cracks and failure originated internally. (c) SEM view taken inside the failure initiation region seen in (b). Crack propagation mode is primarily transgranular. (d) SEM view taken outside the failure initiation region seen in (b). Surface morphology is similar to that observed in (c).

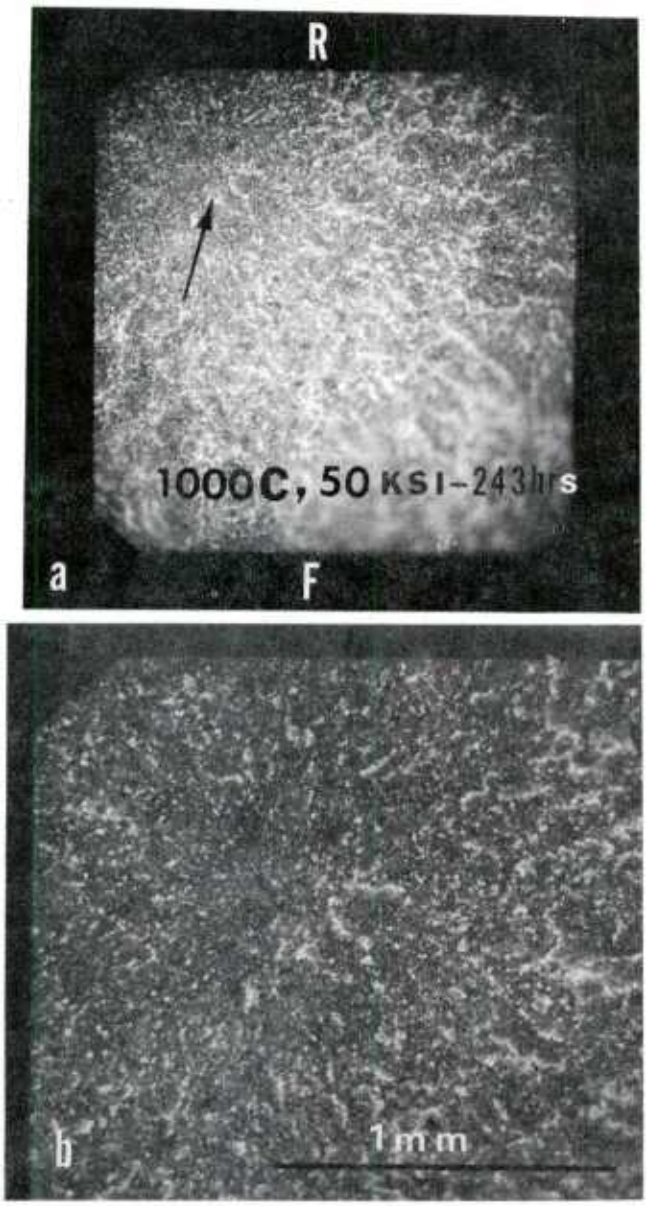

Fig. 58 Fracture surface for tensile stress rupture specimen of NC-132 Si_3N_4 (#41) tested at 1000°C in air. (a) Micrograph taken in plane polarized light. Arrow indicates the failure initiation site. (b) Enlarged view of failure initiation site as seen in polarized light. Note the edges are free from any surface cracks and failure initiation site appears to be completely internally originated. Specimen did not show the presence of slow crack growth.

A clear example of internal failure initiation was observed in specimen #39 tested at an applied stress of 45,000 psi at 1000°C and failed after 6.5 hrs. as shown in Fig. 59. Although the specimen survived over 6 hrs., examination of the fracture face in plane polarized light, Fig. 59(a), and in SEM, Figs. 59(b) and 59(c), revealed only the initiation site but without any evidence of SCG. SEM examination of the initiation site at higher manifications revealed an important fact that the mode of fracture at 1000°C was primarily transgranular, Fig. 59(d). No sign of any SCG similar to the type observed at 1300°C, was observed.

The outstanding feature of a failure initiation due to surface flaw in a uniaxial tensile test is that the growth of the flaw (SCG region) should occur from the edge of the test specimen and also be symmetrical due to uniform stress distribution provided bending stresses are minimal. Such incidence was found in specimen #30 subjected to a stress of 35,000 psi and 1000°C and failed after 20 hrs. Fracture surface of the specimen clearly showed the region of SCG in plane polarized light and in SEM, Figs. 60(a) and 60(b), respectively. Nature of crack propagation inside the SCG region consisted of primarily intergranular, Fig. 60(c).

It should be pointed out that there is considerable scatter in the time-to-failure at a given applied stress level and temperature due to surface machining flaws and inherent internal flaws in the test specimens. This is exemplified in results obtained at 1000°C, Table 17, such as the short life displayed by specimens at low stress levels of 35,000 psi (#29-32), 41,000 psi (#34 and 35), 45,000 psi (#37-39) and 50,000 psi (#40). This is further exemplified by the fact that the specimen #41 tested at a much higher stress level (50,000 psi) compared to specimens (#29-32) and showed a much longer life of 243 hrs. Furthermore, the specimen did not even show the presence of SCG which is critically dependent upon material composition. Of course time-to-failure is also dependent on applied stress and test temperature. If the applied stress is too high, failure will either occur instantly or in a short interval. If the test temperature is too high (e.g., 1400°C or above), the material's (under this study) strength decreases with increasing temperature because of weakening of atomic bonds from grain to grain and in addition the presence of SCG.

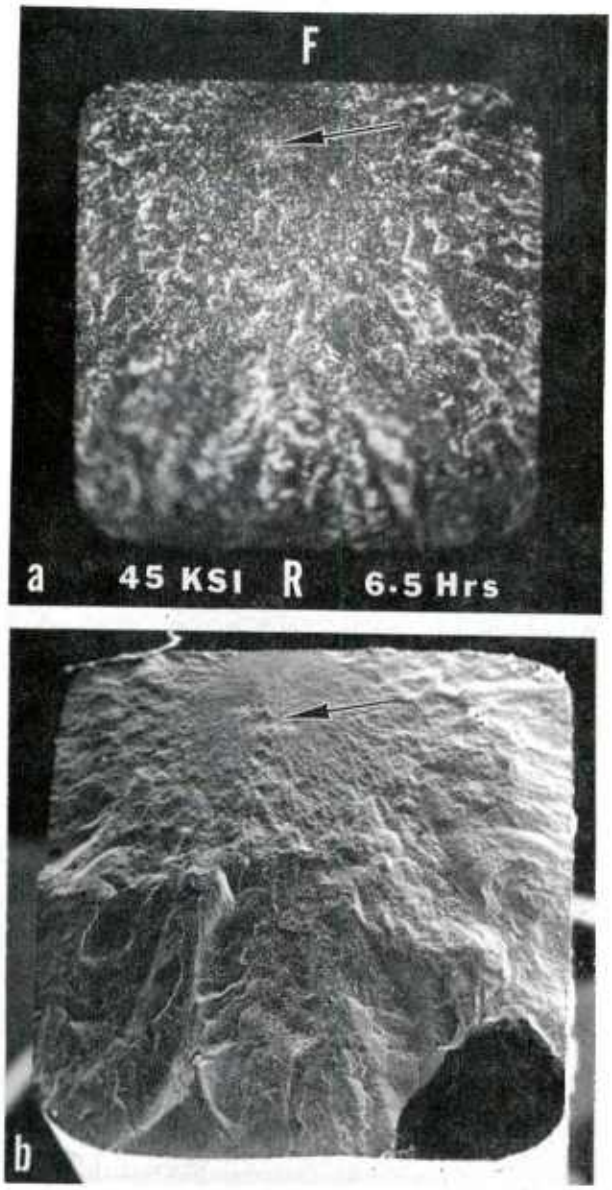

Fig. 59 Fracture surface for tensile stress rupture specimen of NC-132 Si_3N_4 (#39) tested at 1000°C in air. (a) Arrow indicates the failure initiation site as seen in polarized light which appears to be completely internal. Note the upper edge of the specimen is smooth and free from any surface cracks. (b) SEM view of the same fracture surface as seen in (a). Note the smooth area surrounding the failure initiation site (marked by arrow). Black mark at the bottom right corner is aquadag.

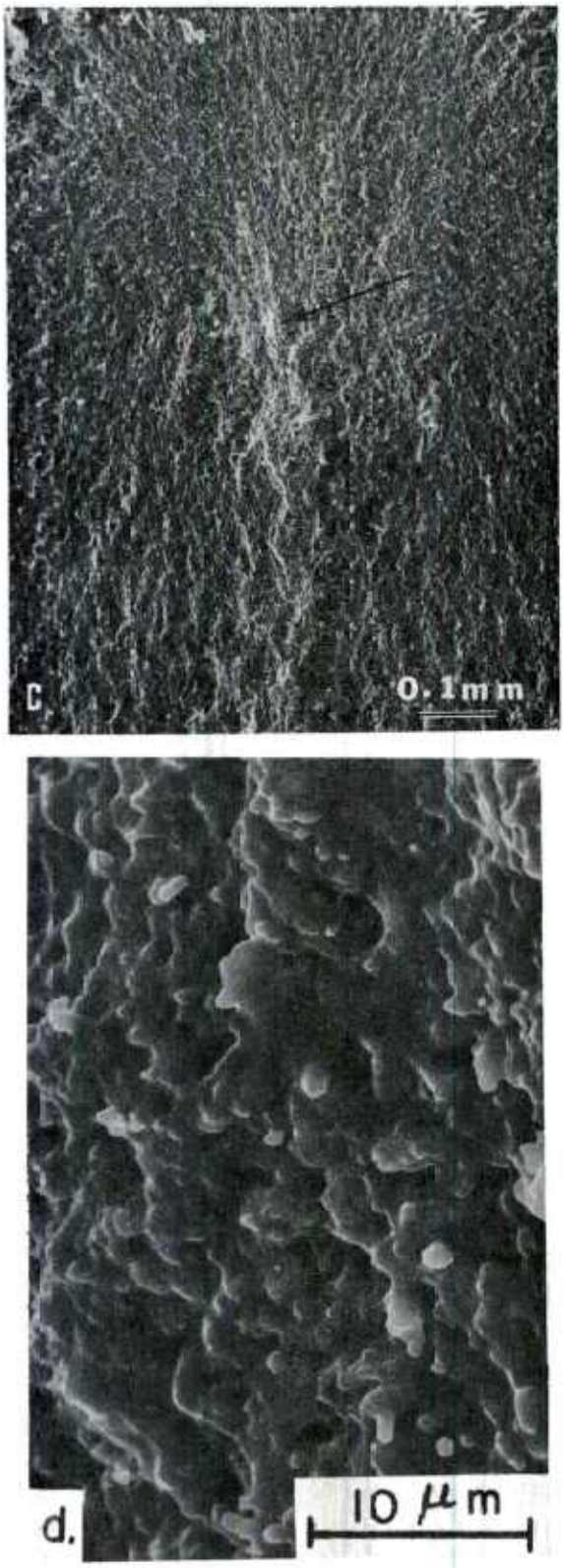

Fig. 59 (cont.) (c) Slightly enlarged view of the initiation site as seen in SEM. (d) High magnification view of the initiation site showing primarily transgranular fracture. No sign of slow crack growth is visible.

Fig. 60 Fracture surface for tensile stress rupture specimen of NC-132 Si_3N_4 (#30) tested at 1000°C in air showing evidence for failure initiation due to surface flaw. (a) Arrows point out the failure initiation site and the associated slow crack growth region. Micrograph taken in plane polarized light. (b) SEM view of the above fracture surface. The slow crack growth region (marked by arrows) is distinctly visible. Black mark at the bottom right corner is aquadag. (c) SEM view taken inside the slow crack growth region showing that the mode of crack propagation is primarily intergranular.

5.4 Tensile Stress Rupture Precracked Specimens

The introduction of a deliberate large flaw in a test specimen was thought to be one way of minimizing material scatter effects. Accordingly, a total of four (4) tensile specimens of NC-132 Si_3N_4 were tested in a precracked condition in a stepped stress rupture series fashion and the results are given in Table 18. Using the IIF method (Sec. 4), a crack of constant size (~100 micron depth) was introduced in the center of the gage length of these test specimens. The results are discussed as follows:

1300°C Tests

Two specimens in the precracked condition were tested at 1300°C in a stepped stress rupture series fashion and both of them failed away from the precrack site. Both specimens showed large regions of SCG. Typical fracture surface for specimen #42 which survived a total of 28.6 hrs. and finally failed in 15 mins. after being subjected to a stress of 10,000 psi is shown in Fig. 61. Figure 61(a) shows the fracture surface in plane polarized light while Fig. 61(b) is the SEM view from the other half of the fractured specimen (mirror image of Fig. 61(a). The SEM micrograph brings out the SCG region very clearly. Typical micrographs from regions inside and outside the SCG are shown in Fig. 61(c) and 61(d), respectively. Note that the mode of fracture during crack propagation in the SCG region is primarily intergranular. The extent of SCG which occurred in this specimen is comparable to that observed in test specimen #18 (Table 16, Fig. 54(a), an unindented specimen which failed after 27 hrs. at a stress of 9,600 psi. Therefore, we believe that the SCG region seen in Figs. 61(a-b), did not develop completely in 15 mins. at a stress of 10,000 psi at 1300°C. A possible reason for the specimen not failing at the precrack site is that the initial crack got 'blunted', possibly through oxidation or softening of the 'glassy phases' in the material thereby lowering the stress intensification at the precrack site and the test specimen behaved as an uncracked specimen. Other stress raisers such as sharp machine flaws could act as stress intensification sites and SCG could then start slowly from any one of them. Continuation of a propagating crack requires much less stress than to start a 'blunted crack'. As the higher stress was applied (10,000 psi for #42 and 8,000 psi for #43), the SCG region attained a critical crack size to satisfy the Griffith failure theory and resulted in catastrophic failure. This is why these specimens which underwent significant amount of SCG showed a very large region of fast fracture, Fig. 61(b). This was the case in all specimens observed in this study.

1200°C Tests

The first specimen tested at 1200°C in the precracked condition and subjected to a varying stress rupture cycle failed at the precracked site, Fig. 62. The specimen showed a large region of SCG surrounding

TABLE 18

UNIAXIAL TENSILE STRESS RUPTURE RESULTS FOR PRECRACKED
(4 Kg. VICKERS DIAMOND PYRAMID INDENTATION,~100 MICRON DEEP)
SPECIMENS OF NC-132 Si_3N_4
ALL SPECIMENS TESTED IN STEPPED STRESS RUPTURE SERIES

Specimen No.	Test Temp. °C	Applied Stress		Time, Hrs.	Remarks
		psi	~ MN/m^2		
42	1300	2,000 5,000 8,000 10,000	13.8 34.5 55.2 69.0	5.3 18.0 5.3 0.25 failed	Did not fail at the precrack site but failed 6mm away (below) from it and showed large region of of slow crack growth.
43	1300	2,000 4,000 6,000 8,000	13.8 27.6 41.4 55.2	20.0 20.0 72.0 1.0 failed	Failed 6.5 mm away (above) from the precrack site and showed large slow crack growth.
44	1200	8,000 10,000 12,000	55.2 69.0 82.8	20.0 3.0 0.75 failed	Failed at the precrack site and showed large slow crack growth.
45	1200	10,000 12,000	69.0 82.8	66.0 2.5 failed	Failed 6mm away (above) from the precrack site and showed large slow crack growth.

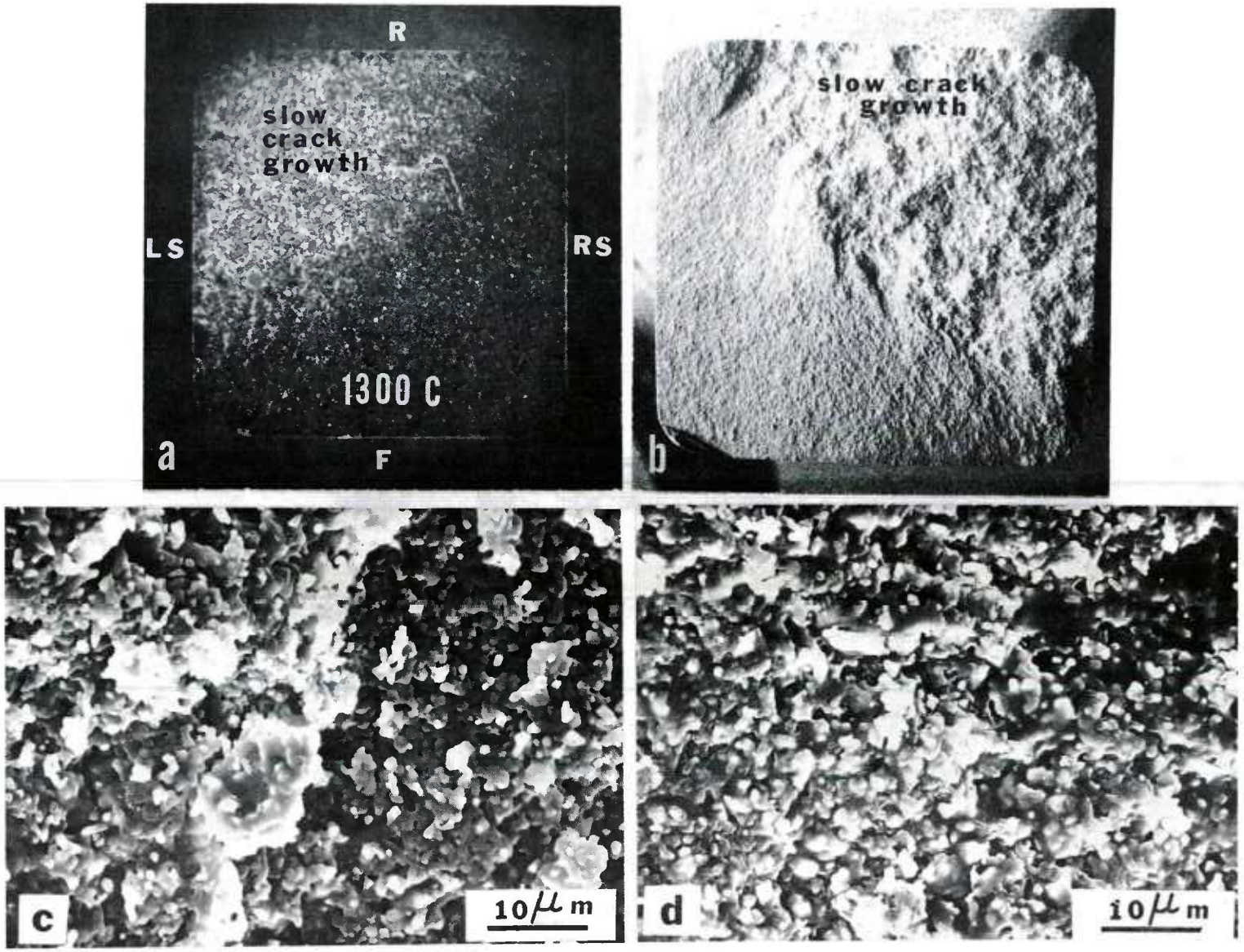

(110)

Fig. 61 Fracture surfaces for a tensile stress rupture specimen of NC-132 Si_3N_4 (#42) tested at 1300°C in air in a stepped stress rupture mode. This specimen contained a crack of 95-100 μm depth in the center of the gage length which was introduced using the indentation induced flaw technique. Precrack was blunted and specimen failed 6mm away (below) from it. (a) Micrograph taken in polarized light shows the extensive slow crack growth region and below it, the fast fracture region. (b) SEM view of the fracture surface (other half of the broken specimen seen in (a)) showing distinctly the slow crack growth and fast fracture regions. (c) SEM view taken inside the slow crack growth region (seen in (b)) showing intergranular crack propagation. (d) SEM view taken inside the fast fracture region (or outside the slow crack growth region seen in (b)).

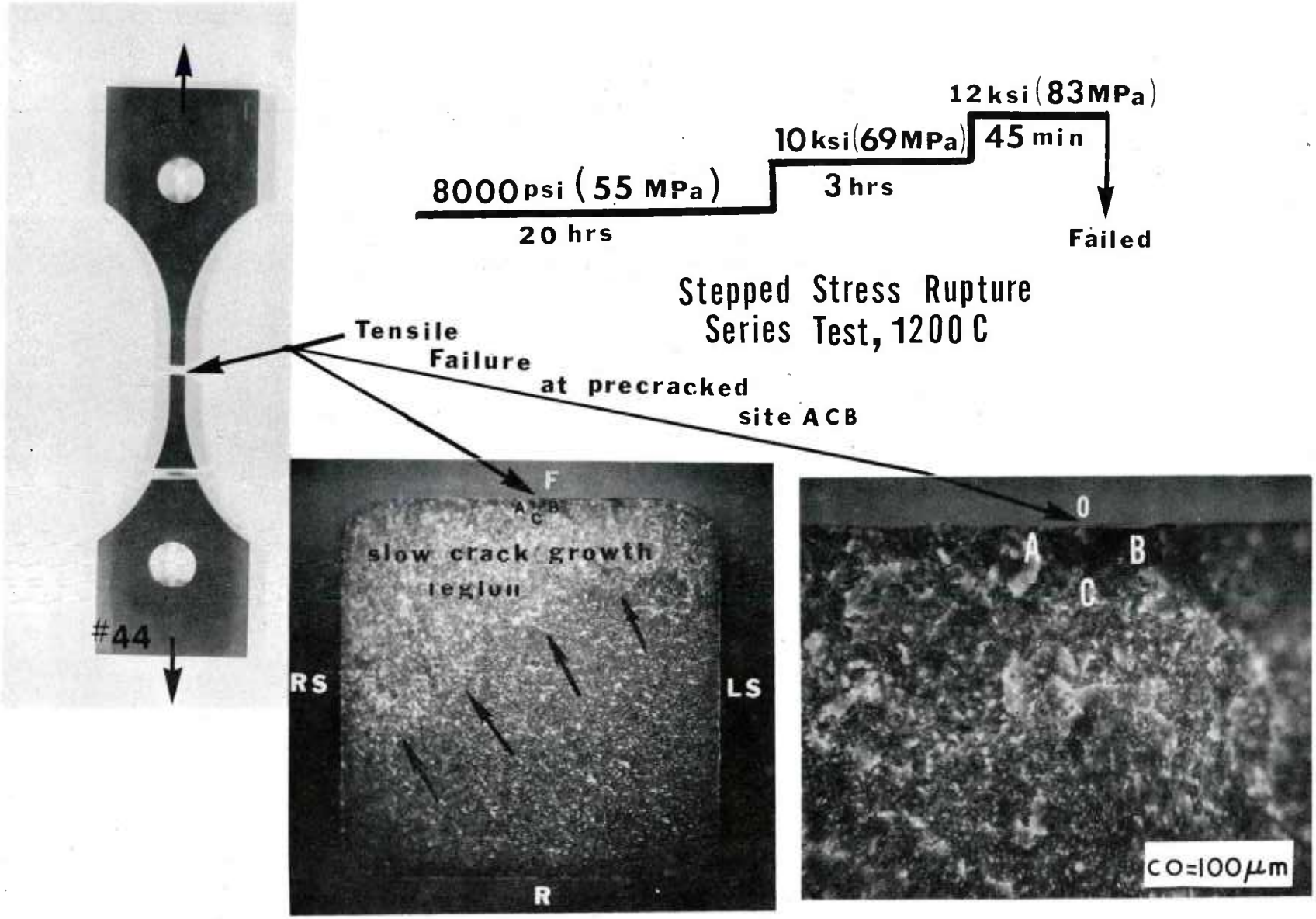

Fig. 62 Precracked (crack depth, CO=100 μm) NC-132 Si_3N_4 tensile stress rupture specimen (#44) tested at 1200°C in air in a stepped stress rupture series fashion. Specimen failed at the precrack site and showed extensive slow crack growth following the initial crack ACB. Fracture surface is seen in plane polarized light.

the initial crack ACB, Fig. 62. It appears that lowering the initial test temperature and increasing the applied stress possibly assisted in avoiding the crack blunting phenomenon as observed at 1300°C.

The second specimen in the precracked condition tested at 1200°C did not fail at the precrack site, and failed 6 mm away (above) from it, Fig. 63. Again, the fracture face showed a large region of SCG. Subsequently, the test specimen was broken at room temperature (20°C) at the precrack site to reveal the extent of any deformation. From the fracture face at 20°C, Fig. 63, it is clear that crack extension, region EDF, did occur from the initial crack ACB, but at some stage of deformation the propagating crack was blunted and so crack propagation occurred elsewhere at a sharper crack. Uniform extension of the SCG region surrounding the initial crack suggests the absence of bending stresses.

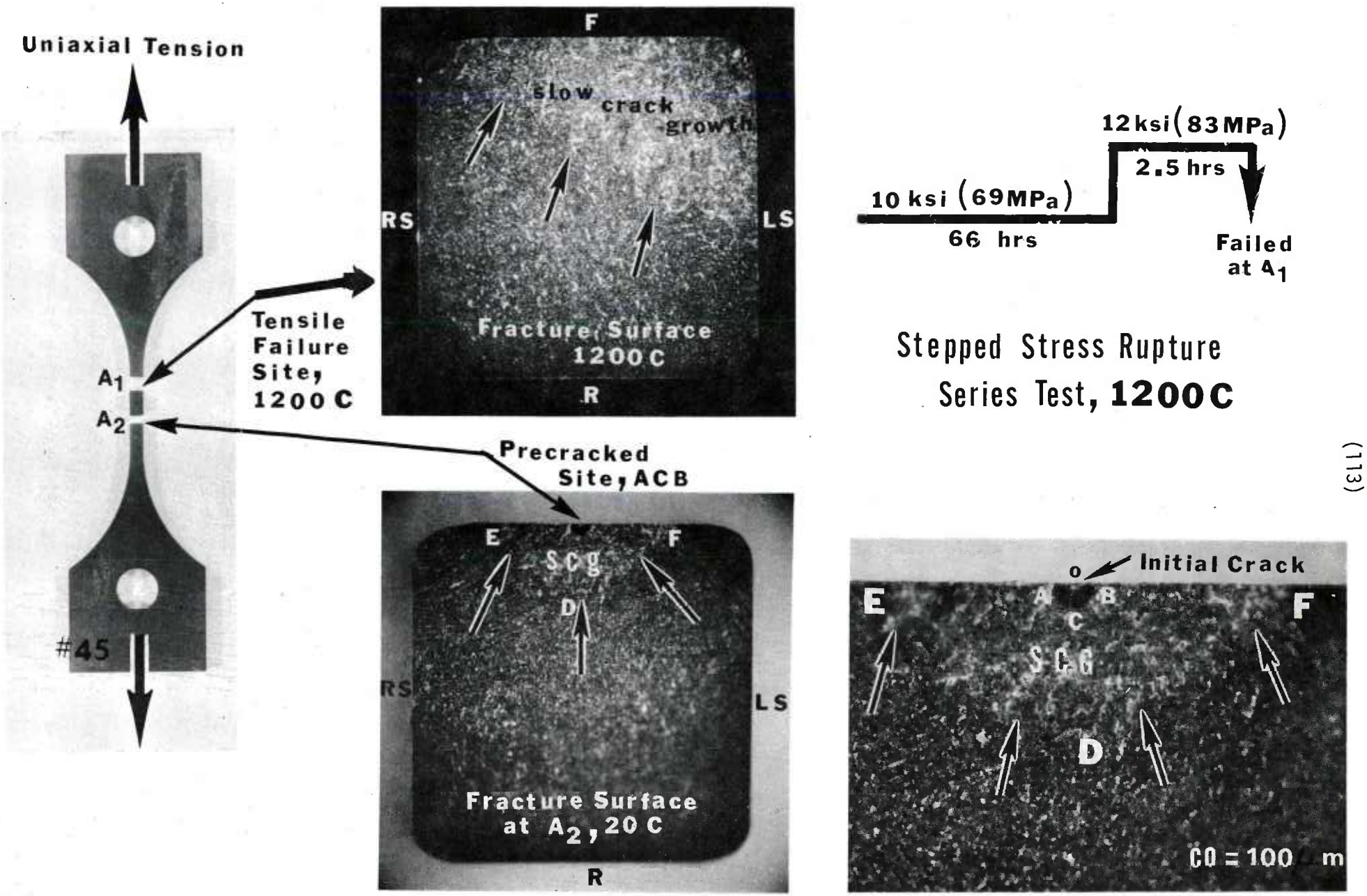

Fig. 63 Precracked (crack depth, CO=100 μm) NC-132 Si_3N_4 tensile stress rupture specimen (#45) tested at 1200°C in air in a stepped stress rupture series fashion. Specimen did not fail at the precrack site but failed 6mm away (above) at A_1. Fracture surface at the failure site, A_1, is shown in polarized light. Specimen was broken in flexure at the precrack site, A_2, to reveal the nature of deformation. Uniform extension of slow crack growth, EDF, following the initial crack ACB, occurred for small distance.

6. FAILURE PREDICTION ANALYSIS

The primary objective of this study has been to generate a statistical strength data base and material parameters for life prediction of NC-132 Si_3N_4 using various methods as reported herein. These parameters can now be used in confirmation studies of ceramic component life prediction using the following conventional analytical approach; the relationship between flaw size, a_o, applied stress, σ_A, and stress intensity factor, K_I, is simply given as:

$$K_I = \sigma_A Y \sqrt{a_o} \tag{17}$$

where Y is a constant depending on crack geometry. The crack velocity-stress intensity relationship as expressed earlier is given by:

$$V = \frac{da}{dt} = AK_I^n \tag{18}$$

Following the work of Evans and Wiederhorn [21,40] and combining the above two equations, the time to failure under a given applied stress is given by:

$$t_F \approx \frac{2}{\sigma_A^2 Y^2} \int_{K_{Ii}}^{K_{IC}} \left(\frac{K_I}{V}\right) dK_I$$

$$\approx \frac{2}{(n-2)A\sigma_A^2 Y^2} \left[K_{Ii}^{2-n} - K_{IC}^{2-n} \right]$$

$$\approx \frac{2}{(n-2)A\sigma_A^2 Y^2 K_{Ii}^{n-2}} \tag{19}$$

where K_{Ii} is the initial stress intensity factor at the most serious flaw in the test specimen. From Eq.(19), it is apparent that the theoretical time to failure or life prediction can be estimated if all the life prediction parameters such as a_o σ, n, and A are known.

The crack propagation data as shown in Fig. 42 and Table 14 can be used in determining a theoretical life prediction curve at a given applied stress and temperature (1300-1400°C) for a given environment (air) using Eq.(19). Presently efforts are being made to make analytical life predictions at 1300°C (and other temperatures as well) and compare with the results obtained from tersile stress rupture tests.

7. SUMMARY

This investigation has presented a cohesive experimental approach for determining the life prediction parameters in hot-pressed silicon nitride. Large statistical strength data bases for fast fracture and for subcritical crack growth have been generated for NC-132 Si_3N_4 (NORTON) and 3.5% MgO + Si_3N_4 (Ford material). The Weibull parameters (characteristic strength and modulus) have been determined and the strength-probability curves were established for NC-132 Si_3N_4.

Using the indentation induced flaw (IIF) method, the inherent flaw size, $a_o \approx 10\text{-}20$ μm deep, and the critical stress intensity factor (or nominal fracture toughness), $K_{IC} \approx 3.5$ MN/m$^{3/2}$ were determined for NC-132 at 20°C. The temperature for the onset of slow crack growth (SCG) is around 1200°C.

Using the double torsion (DT) method, $K_{IC} \approx 4.1$ MN/m$^{3/2}$ was measured at 20°C for NC-132 Si_3N_4. Curves for crack velocity V and the corresponding stress intensity K for SCG regime (1300°, 1350°, and 1400°C) were established for NC-132 Si_3N_4 and the parameters A and n in the relationship $V = AK_1^n$ were determined. The value of n at 1400°C is ≈ 5.25.

The subcritical crack growth parameter 'n' was determined for NC-132 Si_3N_4 using various methods: (1) $n \approx 19.1$ at 1204°C and $n = 17.2$ at 1371°C using stress rate method in as-received specimens. (2) $n = 9.5$ at 1204°C using flexural stress rupture method in as-received specimens. (3) $n = 10\text{-}12$ at 1400°C using flexural strain rate method in precracked (IIF) specimens. (4) $n = 7.6$ and 12.4 at 1300° and 1204°C respectively, using uniaxial tensile stress rupture method.

Detailed and careful uniaxial tensile stress rupture tests were made at high temperatures (1000°-1300°C) using NC-132 Si_3N_4 specimens in order to provide information related to the presence of subcritical crack growth. Results of this study have shown the importance of uniaxial tensile stress rupture testing in ceramic materials.

8. RECOMMENDATIONS

The ceramic life prediction parameters determined can be used for estimating the life (time-to-failure) of a ceramic component subjected to given stress, temperature and environment. This information can be used as a preliminary first confirmation of ceramic component life prediction experiments, e.g., the NC-132 Si_3N_4 hot-spin disk program now underway at Ford under AMMRC contract. Uniaxial tensile stress rupture testing should be carried out in both temperature regimes of fast fracture and slow crack growth for any potential ceramic component material if it is going to be used at high stresses (>30,000 psi) and temperatures ($\geq$1000 °C).

9. REFERENCES

[1.] A. F. McLean, and R. R. Baker, "Brittle Materials Design, High Temperature Gas Turbine, Vol. 2 Ceramic Turbine Rotor Technology," AMMRC-TR-78-14, Interim Report No. 12, March, 1978.

A. F. McLean, and E. A. Fisher, "Brittle Materials Design, High Temperature Gas Turbine," AMMRC-CTR-77-20, Interim Report No. 11, August, 1977.

[2.] R. J. Charles, "Static Fatigue in Glass: I," Appl. Phys. 29 [11] 1549-53 (1958); "II", ibid., pp. 1554-60.

R. J. Charles, "Dynamic Fatigue of Glass," ibid., [12] 1657-62.

[3.] F. F. Lange, "High-Temperature Strength Behavior of Hot-Pressed Si_3N_4: "Evidence for Subcritical Crack Growth," J. Am. Ceram. Soc., 57 [2], 84-87 (1974).

[4.] R. W. Davidge, J. R. McLaren, and G. Tappin, "Strength-Probability-Time (SPT) Relationships in Ceramics," J. Mater. Sci., 8 [12] 1699-1705 (1973).

[5.] G. D. Quinn, and R. N. Katz, "Stepped Temperature Stress Rupture Testing of Silicon-Based Ceramics," Am. Ceram. Soc. Bull., 57 [11] 1057-58 (1978).

[6.] D. G. S. Davies, "The Statistical Approach to Engineering Design in Ceramics," Proc. Brit. Ceram. Soc., 22, 429-452 (1973).

[7.] K. Trustrum, and A. D. Jayatilaka, "On Estimating the Weibull Modulus for a Brittle Material," J. Mater. Sci., 14 [5] 1080-1084 (1979).

[8.] A. G. Evans, and R. L. Jones, "Evaluation of a Fundamental Approach for the Statistical Analysis of Fracture," J. Am. Ceram. Soc., 61 [3-4] 156-160 (1978).

[9.] J. C. Uy, R. M. Williams, and L. R. Swank, "Design Properties of Silicon Nitride for High Temperature Gas Turbine Application," ASME Gas Turbine Conf., Philadelphia, Pa., March, 1977.

[10.] A. G. Evans, pp. 17-48 in Fracture Mechanics of Ceramics, Vol. 1. Plenum Press, New York, 1974.

[11.] R. K. Govila, in Ceramics for Structural Use, proceedings U.S. Army Research Office - Durham, September 9-10, 1969.

[12.] R. K. Govila, "Dislocation Etch Pits in Vanadium Carbide Monocrystals," Phil. Mag., 22 [8] 431-36 (1970).

[13.] R. K. Govila, "Cleavage Fracture of VC Monocrystals," Acta Met., 20 [3] 447-457 (1972).

[14.] P. Kenny, "The Application of Fracture Mechanics to Cemented Tungsten Carbides," Powder Met., 14 [27] 22-38 (1971).

[15.] N. Ingelstrom, and H. Nordberg, "The Fracture Toughness of Cemented Tungsten Carbides," Engr. Fract. Mech., 6 [3] 597-607 (1974).

[16.] J. J. Petrovic, L. A. Jacobson, P. K. Talty, and A. K. Vasudevan, "Controlled Surface Flaws in Hot-Pressed Si_3N_4," J. Am. Ceram. Soc., 58 [3-4] 113-16 (1975).

[17.] K. R. Kinsman, M. Yessik, P. Beardmore, and R. K. Govila, "On Techniques for Emplacing Small Cracks of Controlled Size in Brittle Solids, "Metalography, 8 [3] 351-57 (1975).

[18.] R. H. Keays, "Review of Stress Intensity Factors for Surface and Internal Cracks," Structures and Materials Report 343, Dept. of Supply, Australian Defense Scientific Service, Aeronautical Research Laboratories, April, 1973.

[19.] R. C. Shah,and A. S. Kobayashi; pp. 3-21 in Stress Analysis and Growth of Cracks. Am. Soc. Test. Mater., Spec. Tech. Publ., No. 513; 1972, 307 pp.

[20.] J. J. Petrovic,and L. A. Jacobson; pp. 397-414 in Ceramics for High Performance Applications. Edited by J. J. Burke, A. E. Gorum, and R. N. Katz, Brook Hill, Chestnut Hill, Mass., (1974).

[21.] A. G. Evans,and S. M. Wiederhorn, "Crack Propagation and Failure Prediction in Silicon Nitride at Elevated Temperatures," J. Mater. Sci., 9 [2] 270-78 (1974).

[22.] A. G. Evans, L. R. Russell, and D. W. Richerson, "Slow Crack Growth in Ceramic Materials at Elevated Temperatures," Met. Trans., 6A [4] 707-16 (1975).

[23.] J. A. Coppola, R. C. Bradt, D. W. Richerson,and R. A. Alliegro, "Fracture Energy of Silicon Nitrides," J. Am. Ceram. Soc. Bull., 51 [11] 847-51 (1972).

[24.] S. D. Hartline, R. C. Bradt, D. W. Richerson, and M. L. Torti, "Work-of-Fracture and Apparent Yield Correlation in Si_3N_4," J. Am. Ceram. Soc., 57 [4] 190-91 (1974).

[25.] M. G. Mendiratta, and J. J. Petrovic, "Slow Crack Growth from Controlled Surface Flaws in Hot-Pressed Si_3N_4," J. Am. Ceram. Soc., 61 [5-6] 226-30 (1978).

[26.] F. F. Lange, "Relation Between Strength, Fracture Energy, and Microstructure of Hot-Pressed Si_3N_4," J. Am. Ceram. Soc., 56 [10] 518-22 (1973).

[27.] J. J. Mecholsky, S. W. Freiman, and R. W. Rice, "Fracture Surface Analysis of Ceramics," J. Mater. Sci., 11 [7] 1310-19 (1976).

[28.] J. F. Neil, Ford Motor Company, Private Communication, 1980.

[29.] R. R. Wills, M. G. Mendiratta, and J. J. Petrovic, "Controlled Surface-Flaw-Initiated Fracture in Reaction Bonded Si_3N_4", J. Mater. Sci., 11 [7] 1330-34 (1976).

[30.] A. J. Moulson, "Reaction-bonded Silicon Nitride: its Formation and Properties," J. Mater. Sci., 14 [5] 1017-1051 (1979).

[31.] R. K. Govila, K. R. Kinsman, and P. Beardmore, "Phenomenology of Fracture in Hot-Pressed Silicon Nitride," J. Mater. Sci., 14 [5] 1095-1102 (1979).

[32.] D. W. Richerson, "Effect of Impurities on the High Temperature Properties of Hot-Pressed Silicon Nitride," Am. Ceram. Soc. Bull., 52 [7] 560-62, 569 (1973).

[33.] D. R. Clarke, and G. Thomas, "Grain Boundary Phases in a Hot-Pressed MgO Fluxed Silicon Nitride," J. Am. Ceram. Soc., 60 [11-12] 491-95 (1977).

[34.] R. K. Govila, P. Beardmore, and K. R. Kinsman, "High Temperature Annealing Effects in Precracked Ceramics," to be published, 1980.

[35.] G. G. Trantina, "Stress Analysis of the Double-Torsion Specimen, J. Am. Ceram. Soc., 60 [7-8] 338-41 (1977).

[36.] A. G. Evans, "A Method for Evaluating the Time-Dependent Failure Characteristics of Brittle Materials and Its Application to Polycrystalline Alumina," J. Mater. Sci., 7 [10] 1137-46 (1972).

[37.] D. P. Williams, and A. G. Evans, "Simple Method for Studying Slow Crack Growth," J. Test. Eval., 1 [4] 264-70 (1973).

[38.] P. H. Hodkinson, and J. S. Nadeau, "Slow Crack Growth in Graphite," J. Mater. Sci., 10 [5] 846-56 (1975).

[39.] P. W. R. Beaumont, and R. J. Young, "Failure of Brittle Polymers by Slow-Crack Growth, " J. Mater. Sci., 10 [8] 1334-42 (1975; "II," ibid., pp. 1343-50.

[40.] A. G. Evans, and S. M. Wiederhorn, "Proof Testing of Ceramic Materials: Analytical Basis for Failure Prediction," Int. J. Fract. Mech., 10 [3] 379-92 (1974).

APPENDICES

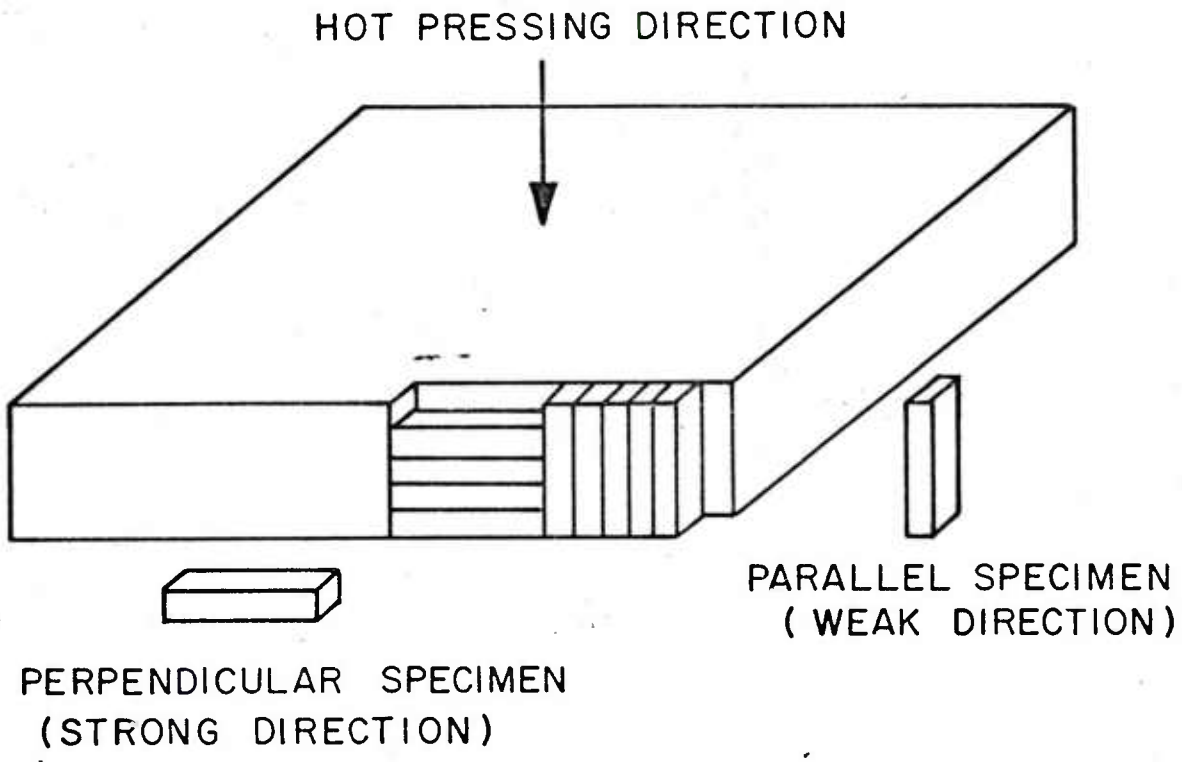

Fig. A_1 Schematic representation of specimen layout from the hot pressed silicon nitride billet showing strong and weak directions.

TABLE A-1

Standard Bar Preparation Procedure

Slicing

Wheel Spec.	Resin 120 grit
Wheel Speed	5000 - 6000 SFPM
Downfeed	.0005" - .001"
Table Speed	100 - 140 inches/min

Rough Grind (when there is enough material allowed)

Wheel Spec.	Resin 100 grit
Wheel Speed	5000 - 6000 SFPM
Downfeed	.0015" - .002" inches/pass
Crossfeed	1/8 - 1/4 inches/pass
Table Feed	300 - 400 inches/pass

Intermediate Grind

Wheel Spec.	Resin 150 grit
Wheel Speed	5000 - 6000 SFPM
Downfeed	.008" - .0015"
Crossfeed	1/8 - 1/4
Table Speed	200 inches/min

Finish Grind

Wheel Spec.	Resin 280 grit
Wheel Speed	5000 - 6000 SFPM
Downfeed	.0003" - .0005"
Table Speed	100 - 140 inches/min

All final grinding done parallel to the long axis of the specimen.

All edges bevelled .005" - .010" by lapping in longitudinal direction.

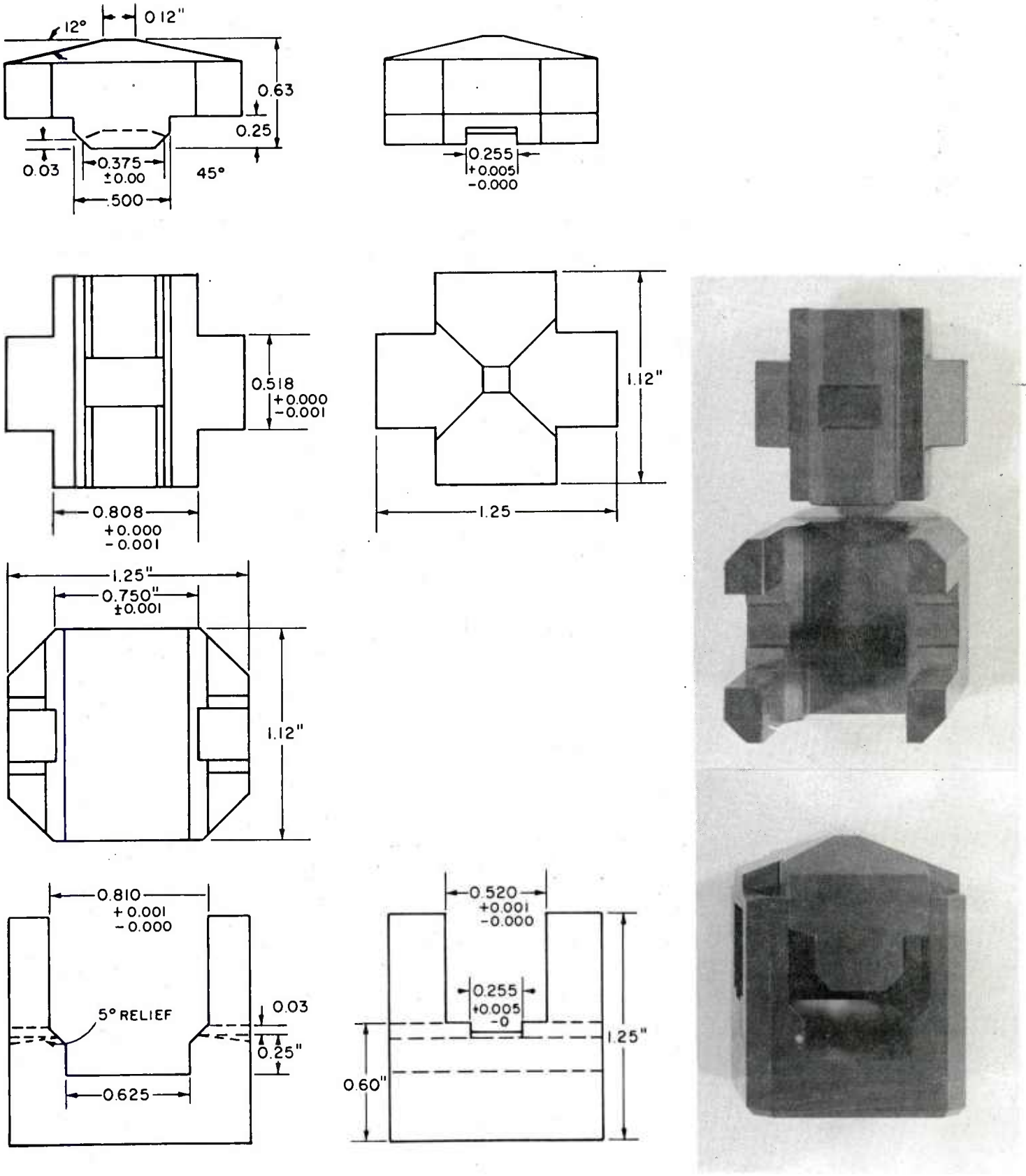

Fig. A_2 Details of the self aligning ceramic fixture used in high temperature bend tests.

TABLE A-2

FOUR-POINT BEND STRENGTH DATA FOR NC-132 Si_3N_4

Test Temp. °C	Machine Head Speed mm/min.	Stress Rate, MPa/min.	Billet No.	Individual Fracture Strength, MPa									
20	0.5	1900	N	696	722	800	821	834	841	876	896	924	993
	"	1860	A	513	529	536	542	574	614	652	687	754	833
	"	1860	B	667	679	692	703	723	745	786	797	817	819
704	0.5	2030	N	620	626	639	670	725					
	"	2000	A	619	658	714	716	870					
	"	2250	B	602	665	681	783	819					
	0.0005	--	N	-	-	-							
	"	1.9	A	569	610	747							
	"	1.7	B	702	823	-							
871	5.0	19,040	N	575	640	657	665	672	684	689	694	737	749
		20,940	A	598	618	647	647	650	661	705	730	745	792
		19,230	B	604	679	683	745	752	761	788	790	805	808
	0.5	2140	N	640	660	670	681	696	707	737	741	766	771
		1910	A	522	629	632	712	730	748	759	768	781	826
		1960	B	658	676	696	696	721	735	761	828	875	917
	0.005	24.8	N	486	513	513	551	556	603	615	642	680	722
		20.0	A	632	643	652	687	696	701	759	786	837	862
		21.0	B	679	687	708	719	725	748	772	781	786	828

TABLE A-2 (Cont.)

FOUR-POINT BEND STRENGTH DATA FOR NC-132 Si_3N_4

Test Temp. °C	Machine Head Speed mm/min.	Stress Rate, MPa/min.	Billet No.	Individual Fracture Strength, MPa									
871	0.0005	-	N	-	-	-	-	-					
	"	1.9	A	769	781	902							
	"	1.6	B	718	772	-							
1038	5.0	19,230	N	594	632	645	651	775					
		16,570	A	654	665	681	692	737					
		15,500	B	701	732	763	772	781					
	0.5	1970	N	630	660	670	695	695	696	702	714	769	774
		1840	A	596	641	676	696	703	705	714	719	750	799
		1830	B	672	685	696	701	701	723	723	725	754	772
	0.005	23.0	N	570	603	615	630	657	657	657	660	684	712
		22.2	A	496	620	636	643	643	661	676	681	699	770
		22.2	B	643	650	661	661	670	670	687	692	703	732
	0.0005	-	N	-	-	-							
		1.5	A	649	692	707							
		1.6	B	562	597	-							
1204	5.0	18,670	N	625	645	652	655	665	690	690	696	699	704
		18,440	A	509	545	562	587	620	620	623	641	663	748
		17,240	B	540	594	596	605	641	643	669	686	692	716

TABLE A-2 (Cont.)

FOUR-POINT BEND STRENGTH DATA FOR NC-132 Si_3N_4

Test Temp. °C	Machine Head Speed mm/min.	Stress Rate, MPa/min.	Billet No.	Individual Fracture Strength, MPa									
1204	0.5	1920	N	672	682	685	689	696	702	702	712	722	722
		1780	A	620	620	625	636	638	662	665	676	694	703
		1810	B	603	661	661	663	663	676	687	692	699	705
	0.05	155	N	508	533	551	553	600	608	627	645	654	690
		162	A	415	516	551	576	580	591	598	607	634	650
		171	B	545	552	569	575	591	591	603	603	603	670
	0.005	19.3	N	466	486	536	538	541	563	573	575	590	598
		23.0	A	478	484	491	493	522	522	533	536	551	569
		21.1	B	502	502	502	509	516	520	529	542	547	550
	0.0005	-	N	-	-	-							
		0.8	A	397	509	522							
		0.8	B	435	450	-							
1371	5.0	11,580	N	397	404	417	419	421	422	424	441	449	453
		12,330	A	346	366	379	384	396	402	408	408	417	417
		11,820	B	330	334	341	359	366	391	393	406	408	417
	0.5	924	N	337	342	350	355	360	365	365	366	372	384
		993	A	306	312	315	319	330	333	339	373	453	475
		960	B	290	297	299	304	306	321	326	328	346	359

TABLE A -2 (Cont.)

FOUR-POINT BEND STRENGTH DATA FOR NC-132 Si_3N_4

Test Temp. °C	Machine Head Speed mm/min.	Stress Rate, MPa/min.	Billet No.	Individual Fracture Strength, MPa									
1371	0.05	86.5	N	292	305	310	310	323					
		85.5	A	275	290	297	297	306					
		101.0	B	283	286	295	307	363					

TABLE A-3

FOUR-POINT BEND STRENGTH DATA FOR 3.5% MgO + Si_3N_4 (FHPSN)

Test Temp. °C	Machine Head Speed mm/min.	Stress Rate, MPa/min.	Hub No.	Individual Fracture Strength, MPa									
20	0.5	1973	1180, 1181	589	596	596	636	670	484	496	565	618	620
			1215, 1216	629	634	647	694	790	674	681	690	703	725
			1234, 1269	522	614	656	656	685	585	598	661	679	745
704	0.5	1857	1180, 1181	442	455	462	533	699	578	714	725	729	809
			1215, 1216	614	634	752	775	799	627	718	730	752	853
			1234, 1269	547	607	629	696	795	491	491	549	585	695
871	0.5	1766	1180, 1183	326	344	446	496	558	619	627	629	634	708
			1215, 1216	614	629	656	661	730	424	451	529	658	810
			1234, 1269	408	451	480	520	565	350	420	424	540	587
	0.05	207	1181, 1215	560	594	661	670	687	462	549	618	641	652
			1216	435	435	435	453	554					
	0.005	20	1180, 1183	355	368	391	451	500	536	603	629	658	663
			1215, 1216	473	500	589	603	609	620	661	703	714	728
			1234, 1269	393	437	446	507	585	408	429	487	498	498
1038	0.5	1708	1180, 1183	453	498	498	518	580	453	471	487	491	507
			1215, 1216	516	529	567	591	594	417	462	509	522	654
			1234, 1269	455	529	531	574	591	464	487	525	591	616

TABLE A-3 (continued)

FOUR-POINT BEND STRENGTH DATA FOR 3.5% MgO + Si_3N_4 (FHPSN)

Test Temp. °C	Machine Head Speed mm/min.	Stress Rate, MPa/min.	Hub No.	Individual Fracture Strength, MPa									
1038	0.05	198	1215	504	551	596	623	629					
			1216	558	567	569	571	620					
	0.005	19	1180, 1183	402	408	417	469	520	473	473	502	518	547
			1215, 1216	480	529	558	562	562	460	520	554	565	585
			1234, 1269	453	520	529	551	558	462	480	518	547	565
1204	0.5	1576	1180, 1181	353	362	382	386	402	442	520	520	531	545
			1183, 1215	395	431	449	449	464	478	487	549	634	674
			1216, 1234	335	375	395	462	486	397	417	440	458	458
			1269	368	379	413	413	449					
	0.05	172	1180, 1181	345	348	354	357	383	417	420	451	460	496
			1183, 1215	368	384	391	396	446	397	415	591	598	629
			1216, 1234	371	379	395	406	426	368	368	379	399	431
			1269	308	312	335	346	373					

TABLE A-3 (continued)

FOUR-POINT BEND STRENGTH DATA FOR 3.5% MgO + Si_3N_4 (FHPSN)

Test Temp. °C	Machine Head Speed mm/min.	Stress Rate, MPa/min.	Hub No.	Individual Fracture Strength, MPa									
1204	0.005	17.5	1180, 1181	281	290	305	308	317	256	412	415	421	440
			1183, 1215	344	350	355	359	378	341	341	352	357	379
			1216, 1234	373	379	384	391	397	310	328	344	346	348
			1269	317	321	335	335	346					
1371	5.0	7224	1215	283	321								
			1216	275	363								
			1308	303									
	0.5	558	1180, 1181	218	220	222	223	249	139	278	285	296	-
			1215, 1216	223	225	225	237	250	230	270	286	290	295
			1234, 1269	205	217	239	248	251	212	217	237	239	246
	0.05	43	1215	211	217								
			1216	224	-								
			1308	199	-								
			1390	179	-								

Load Train Instrumentation Details

The load applied to the specimen is transferred to an Interface* load cell with a 0-1000 lb. sensitivity and a 1% possible error. The applied load is then converted into a millivolt signal which is received by a Daytronic** strain gage conditioner Model number 9171. The conditioner converts the millivolt signal into the actual load (in lbs.) applied to the specimen. This load value is indicated on a Daytronic digital indicator Model number 9530. The MV signal is then relayed to a Doric Digitrend*** 200 Strip Chart recorder, which subsequently records the load in pounds. The Doric recorder can be programmed to record continuously or at specific intervals. In addition to recording the load, the temperature is also recorded by the Doric, which receives a signal from a Pt-Rhodium thermocouple placed in close proximity to the sample. Figure A_3 is a block diagram of the load sensing and recording instruments.

* Interface, Scottsdale, Arizona 85260
** Daytronic, Miamisburg, Ohio 45342
*** Doric, San Diego, California 92123

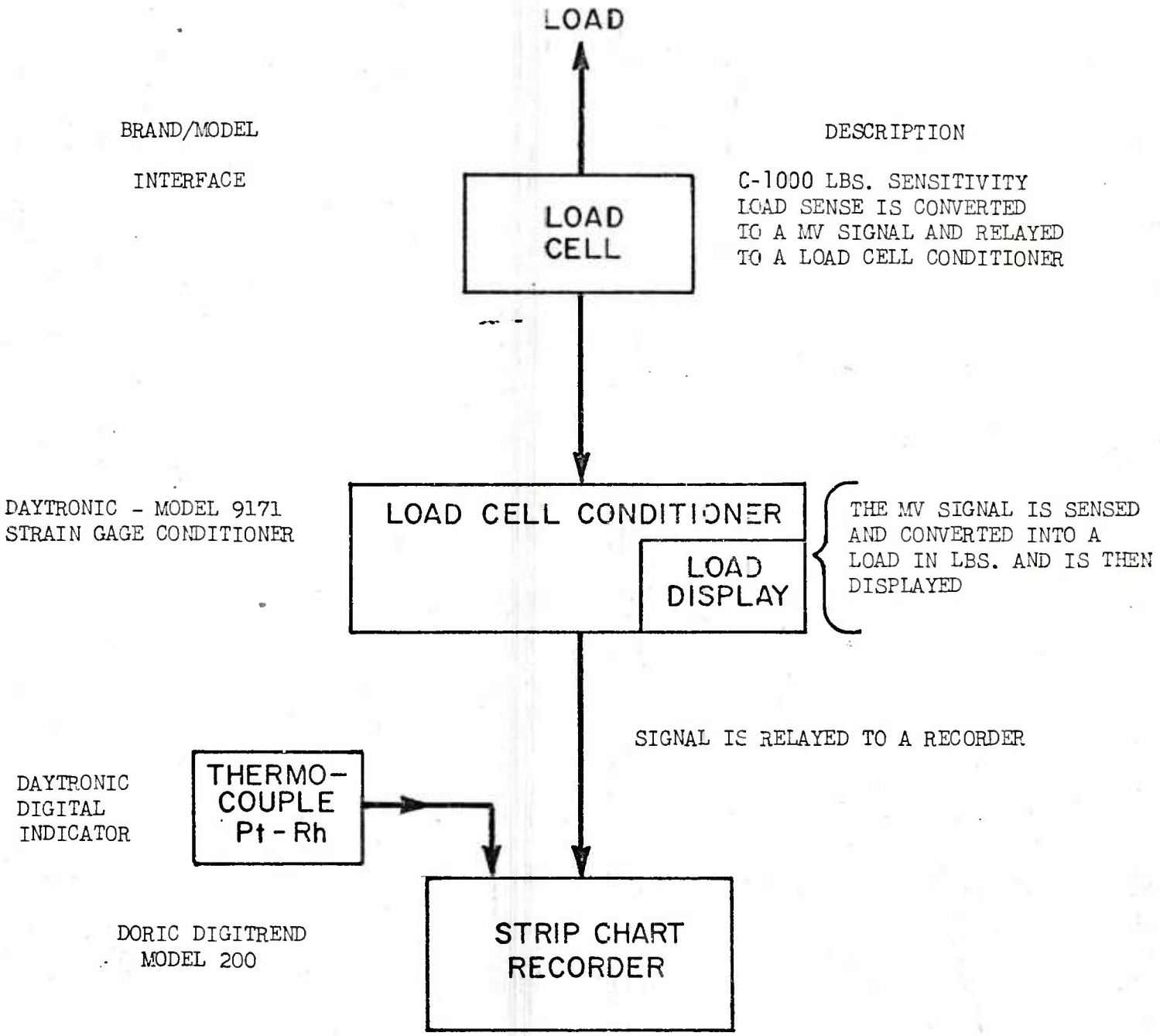

Fig. A_3 A block diagram view of the load sensing and recording equipment associated with load train assembly.

UNCLASSIFIED

SECURITY CLASSIFICATION OF THIS PAGE (When Date Entered)

REPORT DOCUMENTATION PAGE		READ INSTRUCTIONS BEFORE COMPLETING FORM
1. REPORT NUMBER AMMRC TR 80-18	2. GOVT ACCESSION NO. -	3. RECIPIENT'S CATALOG NUMBER -
4. TITLE (and Subtitle) Ceramic Life Prediction Parameters		5. TYPE OF REPORT & PERIOD COVERED Report - Phase I Jan. 1, 1977 - March, 1980 6. PERFORMING ORG. REPORT NUMBER
7. AUTHOR(s) R. K. Govila		8. CONTRACT OR GRANT NUMBER(s) DAAG-46-77-C-0028
9. PERFORMING ORGANIZATION NAME AND ADDRESS Ford Motor Co. - Scientific Research Lab. P. O. Box 2052 - Room E-3172 - Cer. Matls. Dept. Dearborn, Michigan 48121		10. PROGRAM ELEMENT, PROJECT, TASK AREA & WORK UNIT NUMBERS D/A Project: - AMCMS Code: - Agency Accession: -
11. CONTROLLING OFFICE NAME AND ADDRESS Army Materials and Mechanics Research Center Watertown, Massachusetts 02172		12. REPORT DATE May, 1980 13. NUMBER OF PAGES 132
14. MONITORING AGENCY NAME & ADDRESS(if different from Controlling Office) -		15. SECURITY CLASS. (of this report) Unclassified 15a. DECLASSIFICATION/DOWNGRADING SCHEDULE -

16. DISTRIBUTION STATEMENT (of this Report)

Approved for public release; distribution unlimited.

17. DISTRIBUTION STATEMENT (of the abstract entered in Block 20, if different from Report)

-

18. SUPPLEMENTARY NOTES

-

19. KEY WORDS (Continue on reverse side if necessary and identify by block number)

Ceramic Life Prediction, Subcritical Crack Growth
Fracture Silicon Nitride
Indentation Induced Flaw Method
Double Torsion
Statistical Strength Evaluation

20. ABSTRACT (Continue on reverse side if necessary and identify by block number)

See next page

DD FORM 1 JAN 73 1473 EDITION OF 1 NOV 65 IS OBSOLETE

UNCLASSIFIED

SECURITY CLASSIFICATION OF THIS PAGE (When Data Entered)

20. Abstract

This program consisted of a basic study using two potential high temperature ceramic materials, hot-pressed silicon nitride, NC-132 (NORTON), and hot-presses silicon nitride made with 3.5 wt. percent MgO (Ford material) to establish a statistical strength data base for fast fracture as well as for the presence of subcritical crack growth. The Weibull characteristic strength and modulus were determined. Among the fracture mechanics approach, the primary experimental techniques were double-torsion and indentation-induced flaw methods to determine the relationship between crack velocity, V, and stress intensity, K, during subcritical crack growth for NC-132 Si_3N_4.

The subcritical crack growth exponent 'n' was determined using flexural stress and strain rate methods and stress rupture methods, and showed a wide scatter in magnitude. When all the relevant life prediction parameters such as inherent flaw size, strength, critical stress intensity factor, and K-V relationship for slow crack growth are known, an estimate of time-to-failure for a given applied stress, temperature and environment can be made using the numerical relationships outlined by Evans and Wiederhorn earlier. Care should be taken in selecting the appropriate parameters since these parameters are a function of evaluation technique, otherwise the predicted time-to-failure will show a large variation.

Uniaxial tensile stress-rupture testing of NC-132 Si_3N_4 was investigated at 1000°, 1200°, and 1300°C, in air at various applied stress levels and the corresponding times-to-failure were measured. All of these data are used to assess parameters for use in confirmation studies of ceramic component life prediction experiments.